



Robots with

11. Robots with Flexible Elements

Alessandro De Luca, Wayne J. Book

Design issues, dynamic modeling, trajectory planning, and feedback control problems are presented for robot manipulators having components with mechanical flexibility, either concentrated at the joints or distributed along the links. The chapter is divided accordingly into two main parts. Similarities or differences between the two types of flexibility are pointed out wherever appropriate.

For robots with flexible joints, the dynamic model is derived in detail by following a Lagrangian approach and possible simplified versions are discussed. The problem of computing the nominal torques that produce a desired robot motion is then solved. Regulation and trajectory tracking tasks are addressed by means of linear and nonlinear feedback control designs.

For robots with flexible links, relevant factors that lead to the consideration of distributed flexibility are analyzed. Dynamic models are presented, based on the treatment of flexibility through lumped elements, transfer matrices, or assumed modes. Several specific issues are then highlighted, including the selection of sensors, the model order

11.1 Robots with Flexible Joints	244
11.1.1 Dynamic Modeling.....	245
11.1.2 Inverse Dynamics	249
11.1.3 Regulation Control.....	252
11.1.4 Trajectory Tracking.....	257
11.1.5 Further Reading	261
11.2 Robots with Flexible Links	263
11.2.1 Design Issues	263
11.2.2 Modeling of Flexible Link Arms	265
11.2.3 Control	269
11.2.4 Further Reading	278
Video-References	279
References	279

used for control design, and the generation of effective commands that reduce or eliminate residual vibrations in rest-to-rest maneuvers. Feedback control alternatives are finally discussed.

In each of the two parts of this chapter, a section is devoted to the illustration of the original references and to further readings on the subject.

The standard assumption underlying robot kinematics, dynamics, and control design is that manipulators consist only of rigid bodies (links and motion transmission components). This is, however, an ideal situation that may be considered valid only for slow motion and small interacting forces. In practice, mechanical flexibility in robot manipulators is present for two main reasons: the use of compliant transmission elements and the reduction of the mass of the moving links through the use of lightweight material and slender design. These two kinds of flexibility introduce static and dynamic deflections between the position of the driving actuators and the position of the manipulator end-effector. If flexibil-

ity is not taken into account when considering robot design and control, a degradation of the overall expected performance of the robot typically occurs.

From a modeling point of view, flexibility can be assumed as concentrated at the robot joints or distributed (in different ways) along the robot links. The dynamic modeling steps are similar, with the need to introduce additional generalized coordinates besides those used to describe the rigid motion of the robot arm. However, the properties of the resulting models are quite different from a control point of view. Therefore, the case of *robots with flexible joints* and of *robots with flexible links* are presented in this chapter mostly as

separate items, pointing out similarities or structural differences wherever appropriate. For both classes of flexible robots, the relevant design issues, dynamic modeling, inverse dynamics algorithms, and control laws for set-point regulation and trajectory tracking will be discussed. Indeed, joint and link flexibilities may

be present (and dynamically interact) at the same time. Many of the presented results can be extended to this case as well.

In the following, it is assumed that the reader is already familiar with basic issues on kinematics, dynamics, and control of rigid robots (Chaps. 2, 3, 8).

11.1 Robots with Flexible Joints

The presence of joint flexibility is common in current industrial robots, when motion transmission/reduction elements such as belts – (as in the selective compliant assembly robot arm (SCARA) family), long shafts (as in the forearm of the Unimation Puma arm), cables, harmonic drives, or cycloidal gears are used. The purpose of these components is to allow relocation of the actuators next to the robot base, thus improving dynamic efficiency, or to guarantee high reduction ratios with power-efficient compact inline devices.

However, when subject to the forces/torques arising in normal robot operation, these components are intrinsically flexible (e.g., the flexspline in harmonic drives; Fig. 11.1) and introduce a time-varying displacement between the position of the actuators and that of the driven links. Without a specific control action, an oscillatory behavior, typically of small magnitude but at a relatively high frequency, is observed at the robot end-effector level during free motion. Moreover, some form of instability (e.g., chattering) may occur in tasks involving contact with the environment.

Recently, flexible actuation/transmission elements have been deliberately selected in soft robots (such as those driven by serial elastic actuation (SEA) or variable stiffness actuation (VSA), Chap. 21) intended for physical human–robot interaction and for achieving more natural motion characteristics. In fact, this form of mechanical compliance guarantees an iner-

tial decoupling between the actuator and the (possibly, lightweight) link, thus reducing the kinetic energy involved in undesired collisions with humans. Such a safety-oriented mechanical design should be traded-off with a more complex control design aimed at preserving the same performance of rigid robots in terms of speed and accuracy of the end-effector motion (Chap. 69).

Figures 11.2 and 11.3 show two examples of robot manipulators with flexible joints, the 8R robot *Dex-*

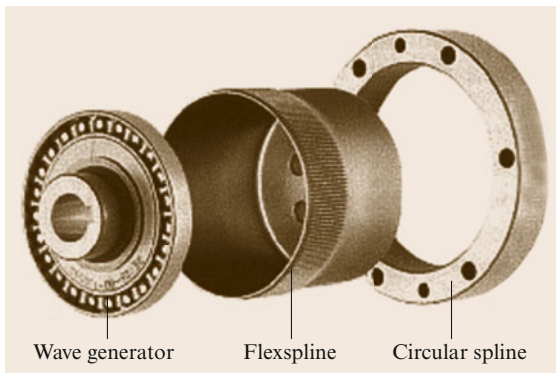


Fig. 11.1 The components of a harmonic drive

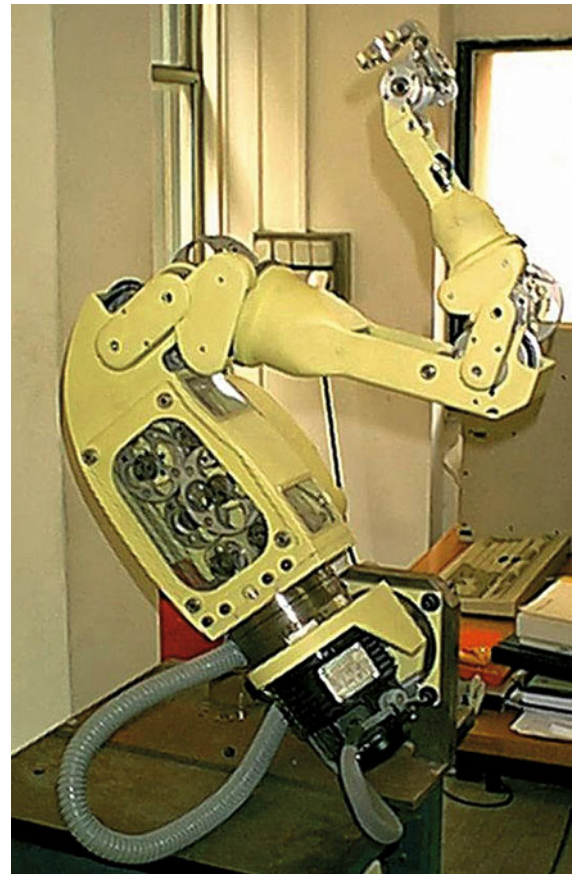


Fig. 11.2 The cable-driven robot *Dexter* by Scienza Machinale

ter and the 7R lightweight manipulator *DLR LWR-III*. The first robot has motors 3–8 located inside the second link, with motion transmitted to the distal links through steel cables and pulleys; the second robot has a modular structure, with each motor integrated in the associated joint and using an harmonic drive as reduction element. The joint stiffnesses of the *Dexter* robot vary between 120 and 6300 N m/rad depending on the joint, while for the *DLR LWR-III* manipulator, the range is 6000–15 000 N m/rad. These numerical values refer to deflections and associated torques evaluated after the reduction gears.

Deflection of the flexible transmission elements can be modeled as being *concentrated at the joints* of the robot, thus limiting the complexity of the associated equations of motion. When compared to the rigid case, the dynamic model of robots with flexible joints (and rigid links) requires *twice* the number of generalized coordinates to completely characterize the configuration of all rigid bodies (motors and links) constituting the arm.

As a result, the case of flexible joint robots is one example in which the number of control inputs is strictly less than the number of mechanical degrees of freedom. This suggests that the design of control schemes re-

alizing standard motion tasks is expected to be more difficult than for rigid robots. Moreover, the implementation of a full state feedback law will require twice the number of sensors, measuring quantities that are *before* and *after* (or across) the joint deformation. On the other hand, the motor torques used to command the robot as well as the disturbance torques due to joint flexibility perform work on the same joint axes (they are *physically collocated*). It should be noted that this is one relevant difference with respect to the case of flexibility distributed along the links. This characteristic is very helpful for rejecting vibrations and controlling the overall robot motion. Roughly speaking, we will be able to use input commands acting before the source of flexibility to ensure that output variables defined beyond the flexibility behave in a desired way.

11.1.1 Dynamic Modeling

Dynamic models that explicitly include joint flexibility are used to evaluate quantitatively vibratory effects superposed on the rigid motion, verify whether the control laws obtained under the assumption of joint rigidity can still work in practice (or to what extent they should be modified), and enable the design of new model-based feedforward and feedback controllers.

We consider a robot with flexible joints as an open kinematic chain having $N + 1$ rigid bodies, the base and the N links, interconnected by N (rotary or prismatic) joints undergoing deflection, and actuated by N electrical drives. From a mechanical point of view, each motor (with its stator and rotor) is an additional rigid body with its inertial properties. All joints are considered to be flexible, though mixed situations may be encountered due to the use of different transmission devices. When reduction gearings are present, they are modeled as being placed *before* the joint deflection occurs.

The following standard assumptions are made:

- A1** Joint deflections are small, so that flexibility effects are limited to the domain of linear elasticity.
- A2** The actuators' rotors are modeled as uniform bodies having their center of mass on the rotation axis.
- A3** Each motor is located on the robot arm in a position preceding the driven link. (This can be generalized to the case of multiple motors simultaneously driving multiple distal links.)

The first assumption supports the terminology of robots with *elastic* joints often used in the literature. The elasticity at joint i is modeled by a spring of stiff-



Fig. 11.3 The lightweight manipulator *DLR LWR-III* by the German Aerospace Center

ness $K_i > 0$, which is torsional for rotational joints and linear for translational ones. Figure 11.4 shows a single link driven by a motor through a rotational elastic joint. Nonlinear stiffness characteristics for the flexible joint can also be considered, provided that the map from deflection to force is smooth and invertible. Assumption A2 is a basic requirement for the long life of an electrical drive, and thus very reasonable. As we will see, it implies that the inertia matrix and the gravity term in the robot dynamic model will be independent of the angular position of the motors. A typical arrangement of motors satisfying assumption A3 is shown in Fig. 11.5. The simplest situation is when the i -th motor moves link i and is mounted on link $i - 1$ with its rotation axis aligned with the i -th joint. This is, for instance, the case for the *LWR-III* manipulator. The dislocation of the actuating motors along the structure has a great influence on the structure of the dynamic equations of motion.

For kinematic and dynamic analysis, $2N$ frames are attached to the $2N$ moving rigid bodies (links and motors) in the robot chain: the link frames L_i and the motor frames R_i , for $i = 1, \dots, N$ (Fig. 11.5). For the definition of the link frames L_i , the standard Denavit–Hartenberg convention can be used. The frames R_i are attached to the motor stators, aligned with the axes of

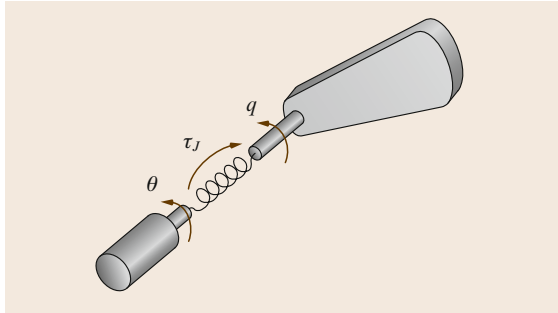


Fig. 11.4 Schematic representation of an elastic joint

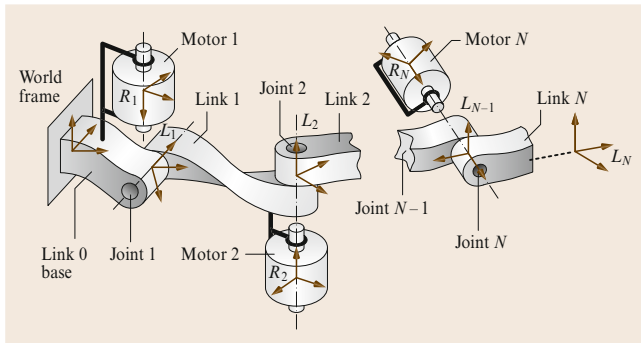


Fig. 11.5 Arrangement of motors and links in an open kinematic chain

symmetry of the motors and with the z -axis along the spinning direction of the rotor.

Accordingly, $2N$ generalized coordinates will be needed. A possible set of coordinates is given by

$$\Theta = \begin{pmatrix} \mathbf{q} \\ \boldsymbol{\theta} \end{pmatrix} \in \mathbb{R}^{2N},$$

where \mathbf{q} is the N -vector of link positions and $\boldsymbol{\theta}$ is the N -vector of motor (i.e., rotor) positions, as reflected through the transmission/reduction gears. This choice of variables is quite convenient because:

1. The model will be formally independent of the reduction ratios.
2. These position variables will have a similar dynamic range.
3. The kinematics of the robot will be a function of the link variables \mathbf{q} only (these variables are already *beyond* the joint flexibility) so that all issues related to direct/inverse kinematics will be identical to the case of fully rigid robots.

For some considerations, it is also useful to define the variable $\boldsymbol{\theta}_m$, namely the N -vector of motor positions before reduction, which are the quantities directly measured by encoders mounted on the motors. In the case of a motor directly placed on the i -th joint axis, one has $\dot{\theta}_{m,i} = n_i \dot{\theta}_i$, where $n_i \geq 1$ is the reduction ratio at the i -th joint. In addition, for $i = 1, \dots, N$, the difference

$$\delta_i = q_i - \theta_i$$

is the deflection at the i -th joint, while

$$\tau_{J,i} = K_i(\theta_i - q_i)$$

is the torque transmitted to the i -th link through the associated elastic spring (Fig. 11.4) – the quantity measured by a joint torque sensor, whenever present. Note that for robots with flexible links, the set $(\boldsymbol{\theta}, \boldsymbol{\delta})$ is typically used in the dynamic modeling, where $\boldsymbol{\delta}$ is the vector of link deflection coordinates.

Following a Lagrangian approach, the single energy contributions to the Lagrangian

$$\mathcal{L} = \mathcal{T}(\boldsymbol{\Theta}, \dot{\boldsymbol{\Theta}}) - \mathcal{U}(\boldsymbol{\Theta})$$

will be derived next.

The *potential energy* of the robot is due to gravity and joint elasticity. The gravity part is related to the position of the barycenter of the links (each of mass m_i) and of the motors (of mass m_{r_i}). Because of assumption A2, the latter will be independent of $\boldsymbol{\theta}$. Thus,

$$\mathcal{U}_{\text{grav}} = \mathcal{U}_{\text{grav,link}}(\mathbf{q}) + \mathcal{U}_{\text{grav,motor}}(\mathbf{q}).$$

For the elastic part of the potential, because of assumption **A1**, we have

$$\mathcal{U}_{\text{elas}} = \frac{1}{2} (\mathbf{q} - \boldsymbol{\theta})^T \mathbf{K} (\mathbf{q} - \boldsymbol{\theta}),$$

$$\mathbf{K} = \text{diag}(K_1, \dots, K_N).$$

As a result,

$$\mathcal{U}(\boldsymbol{\Theta}) = \mathcal{U}_{\text{grav}}(\mathbf{q}) + \mathcal{U}_{\text{elas}}(\mathbf{q} - \boldsymbol{\theta}).$$

The *kinetic energy* of the robot is the sum of the link and rotor contributions. For the links, there is no difference with respect to the standard rigid robot case and it will be sufficient to write in general

$$\mathcal{T}_{\text{link}} = \frac{1}{2} \dot{\mathbf{q}}^T \mathbf{M}_L(\mathbf{q}) \dot{\mathbf{q}}, \quad (11.1)$$

with the positive-definite symmetric link inertia matrix $\mathbf{M}_L(\mathbf{q})$. For the rotors, some more details are needed

$$\begin{aligned} \mathcal{T}_{\text{rotor}} &= \sum_{i=1}^N \mathcal{T}_{\text{rotor}_i} \\ &= \sum_{i=1}^N \left(\frac{1}{2} m_{r_i} \mathbf{v}_{r_i}^T \mathbf{v}_{r_i} + \frac{1}{2} {}^{R_i} \boldsymbol{\omega}_{r_i}^T \mathbf{I}_{r_i} {}^{R_i} \boldsymbol{\omega}_{r_i} \right), \end{aligned} \quad (11.2)$$

where \mathbf{v}_{r_i} is the linear velocity of the center of mass of the i -th rotor and $\boldsymbol{\omega}_{r_i}$ is the angular velocity of the i -th rotor body. All quantities in the angular contributions in (11.2) are conveniently expressed in the local frame R_i . According to assumption **A2**, the rotor inertia matrix is then diagonal

$${}^{R_i} \mathbf{I}_{r_i} = \text{diag}(I_{r_{ixx}}, I_{r_{iyy}}, I_{r_{izz}}),$$

with $I_{r_{ixx}} = I_{r_{iyy}}$, while \mathbf{v}_{r_i} can be expressed as a function of \mathbf{q} and $\dot{\mathbf{q}}$ only. Moreover, due to assumption **A3**, the angular velocity of the i -th rotor has the general expression

$${}^{R_i} \boldsymbol{\omega}_{r_i} = \sum_{j=1}^{i-1} \mathbf{J}_{r_{i,j}}(\mathbf{q}) \dot{q}_j + \begin{pmatrix} 0 \\ 0 \\ \dot{\theta}_{m,i} \end{pmatrix}, \quad (11.3)$$

where $\mathbf{J}_{r_{i,j}}(\mathbf{q})$ is the j -th column of the Jacobian relating the link velocities $\dot{\mathbf{q}}$ to the angular velocity of the i -th rotor in the robot chain. By substituting (11.3) into (11.2) and expressing $\dot{\theta}_m$ in terms of $\dot{\boldsymbol{\theta}}$, it can be shown that

$$\begin{aligned} \mathcal{T}_{\text{rotor}} &= \frac{1}{2} \dot{\mathbf{q}}^T [\mathbf{M}_R(\mathbf{q}) + \mathbf{S}(\mathbf{q}) \mathbf{B}^{-1} \mathbf{S}^T(\mathbf{q})] \dot{\mathbf{q}} \\ &\quad + \dot{\mathbf{q}}^T \mathbf{S}(\mathbf{q}) \dot{\boldsymbol{\theta}} + \frac{1}{2} \dot{\boldsymbol{\theta}}^T \mathbf{B} \dot{\boldsymbol{\theta}}, \end{aligned} \quad (11.4)$$

where \mathbf{B} is the constant diagonal inertia matrix collecting the rotors inertial components $I_{r_{izz}}$ around their spinning axes, as reflected through the reduction ratios, $\mathbf{M}_R(\mathbf{q})$ contains the rotor masses (and, possibly, the rotor inertial components along the other principal axes), and the square matrix $\mathbf{S}(\mathbf{q})$ expresses the inertial couplings between the rotors and the previous links in the robot chain.

A simple example illustrates the derivation and the actual expressions of the terms in (11.4). We also include the reduction elements to show how the rotor inertial component around the spinning axis will appear in the kinetic energy, weighted by different powers of the reduction ratios. Consider a planar robot with two rotational elastic joints, a first link of length ℓ_1 , and motors mounted directly on the joint axes. The kinetic energies of the two rotors are

$$\begin{aligned} \mathcal{T}_{\text{rotor}_1} &= \frac{1}{2} I_{r_{1zz}} \dot{\theta}_{m,1}^2 = \frac{1}{2} I_{r_{1zz}} n_1^2 \dot{\theta}_1^2 \\ \mathcal{T}_{\text{rotor}_2} &= \frac{1}{2} m_{r_2} \ell_1^2 \dot{q}_1^2 + \frac{1}{2} I_{r_{2zz}} (\dot{q}_1 + \dot{\theta}_{m,2})^2 \\ &= \frac{1}{2} m_{r_2} \ell_1^2 \dot{q}_1^2 + \frac{1}{2} I_{r_{2zz}} (\dot{q}_1^2 + 2n_2 \dot{q}_1 \dot{\theta}_2 + n_2^2 \dot{\theta}_2^2), \end{aligned}$$

leading to

$$\begin{aligned} \mathbf{B} &= \begin{pmatrix} I_{r_{1zz}} n_1^2 & 0 \\ 0 & I_{r_{2zz}} n_2^2 \end{pmatrix}, \quad \mathbf{S} = \begin{pmatrix} 0 & I_{r_{2zz}} n_2 \\ 0 & 0 \end{pmatrix}, \\ \mathbf{M}_R &= \begin{pmatrix} m_{r_2} \ell_1^2 & 0 \\ 0 & 0 \end{pmatrix}, \quad \mathbf{S} \mathbf{B}^{-1} \mathbf{S}^T = \begin{pmatrix} I_{r_{2zz}} & 0 \\ 0 & 0 \end{pmatrix}. \end{aligned}$$

In this specific case, the matrix \mathbf{S} (as well as \mathbf{M}_R) is constant. Note that for large reduction ratios n_i , the dominant inertial effect due to the rotors is given by the matrix \mathbf{B} . Also, if the second motor was mounted remotely on the first joint (as it is often the case in the class of SCARA arms), or still close to the second joint but with the spinning axis orthogonal to the axis of this joint, then the matrix \mathbf{S} would be zero.

In general, as a consequence of assumption **A3**, the matrix $\mathbf{S}(\mathbf{q})$ has always a strictly upper triangular structure with a cascaded dependence of its nonzero elements

$$\begin{aligned} \mathbf{S}(\mathbf{q}) &= \\ &\begin{pmatrix} 0 & S_{12} & S_{13}(q_2) & S_{14}(q_2, q_3) & \dots & \dots & S_{1N}(q_2, \dots, q_{N-1}) \\ 0 & 0 & S_{23} & S_{24}(q_3) & \dots & \dots & S_{2N}(q_3, \dots, q_{N-1}) \\ 0 & 0 & 0 & S_{34} & \dots & \dots & S_{3N}(q_4, \dots, q_{N-1}) \\ \vdots & \vdots & \vdots & \ddots & \ddots & \vdots & \vdots \\ 0 & 0 & 0 & \dots & 0 & S_{N-2,N-1} & S_{N-2,N}(q_{N-1}) \\ 0 & 0 & 0 & \dots & 0 & 0 & S_{N-1,N} \\ 0 & 0 & 0 & \dots & 0 & 0 & 0 \end{pmatrix}. \end{aligned} \quad (11.5)$$

Summing up, the total kinetic energy of the robot is

$$\begin{aligned}\mathcal{T} &= \frac{1}{2} \dot{\Theta}^T \mathcal{M}(\Theta) \dot{\Theta} \\ &= \frac{1}{2} \begin{pmatrix} \dot{q}^T & \dot{\theta}^T \end{pmatrix} \begin{pmatrix} \mathbf{M}(q) & \mathbf{S}(q) \\ \mathbf{S}^T(q) & \mathbf{B} \end{pmatrix} \begin{pmatrix} \dot{q} \\ \dot{\theta} \end{pmatrix},\end{aligned}$$

with

$$\mathbf{M}(q) = \mathbf{M}_L(q) + \mathbf{M}_R(q) + \mathbf{S}(q)\mathbf{B}^{-1}\mathbf{S}^T(q). \quad (11.6)$$

As anticipated, the total inertia matrix \mathcal{M} of the robot depends only on q .

Using the Lagrange equations, finally yields the complete dynamic model

$$\begin{aligned}\begin{pmatrix} \mathbf{M}(q) & \mathbf{S}(q) \\ \mathbf{S}^T(q) & \mathbf{B} \end{pmatrix} \begin{pmatrix} \ddot{q} \\ \ddot{\theta} \end{pmatrix} + \begin{pmatrix} c(q, \dot{q}) + c_1(q, \dot{q}, \dot{\theta}) \\ c_2(q, \dot{q}) \end{pmatrix} \\ + \begin{pmatrix} g(q) + \mathbf{K}(q - \theta) \\ \mathbf{K}(\theta - q) \end{pmatrix} = \begin{pmatrix} 0 \\ \tau \end{pmatrix},\end{aligned} \quad (11.7)$$

where the inertial terms (related to the total inertia matrix $\mathcal{M}(q)$), the Coriolis and centrifugal terms (collectively denoted by $c_{\text{tot}}(\Theta, \dot{\Theta})$), and the potential terms $(\partial \mathcal{U}(\Theta)/\partial \Theta)^T$ have been written separately. In particular, $g(q) = (\partial \mathcal{U}_{\text{grav}}(q)/\partial q)^T$ while $\tau_J = \mathbf{K}(\theta - q)$ is the elastic torque transmitted through the joints.

The first N and the last N equations of the dynamic model (11.7) are referred to as the *link* and the *motor* equations, respectively.

On the right-hand side of (11.7), all nonconservative generalized forces should appear. When dissipative effects are not considered, only the motor torque τ producing work on the θ variable is present (i.e., the torques on the motor output shafts, amplified by the reduction ratios) in the motor equations. If the robot end-effector is in contact with the environment, the zero on the right-hand side of the link equations should be replaced by $\tau_{\text{ext}} = \mathbf{J}^T(q)\mathbf{F}$, where $\mathbf{J}(q)$ is the robot Jacobian and \mathbf{F} the forces/torques acting from the environment on the robot.

In the presence of energy-dissipating effects, additional terms appear on the right-hand side of (11.7). For instance, viscous friction at both sides of the transmissions and spring damping of the (visco)elastic joints give rise to the vector term

$$\begin{pmatrix} -\mathbf{F}_q \dot{q} - \mathbf{D}(\dot{q} - \dot{\theta}) \\ -\mathbf{F}_\theta \dot{\theta} - \mathbf{D}(\dot{\theta} - \dot{q}) \end{pmatrix}, \quad (11.8)$$

where the diagonal, positive-definite matrices \mathbf{F}_q , \mathbf{F}_θ , and \mathbf{D} contain, respectively, the viscous coefficients on

the link side and on the motor side, and the damping of the elastic springs at the joints. More general forms of nonlinear friction τ_F can be considered. Note that, in principle, friction acting on the motor side can be fully compensated by a suitable choice of the control torque τ , while this is not true for friction acting on the link side, due to the noncollocation.

Model Properties

All elements in the $2N$ -vector $c_{\text{tot}}(\Theta, \dot{\Theta})$ of velocity-dependent terms in (11.7) are independent of the motor position θ . The specific dependence of the N -vectors c , c_1 , and c_2 follows from the general expression of the components of c_{tot} based on Christoffel symbols

$$c_{\text{tot},i}(\Theta, \dot{\Theta}) = \frac{1}{2} \dot{\Theta}^T \left[\frac{\partial \mathcal{M}_i}{\partial \Theta} + \left(\frac{\partial \mathcal{M}_i}{\partial \Theta} \right)^T - \frac{\partial \mathcal{M}}{\partial \Theta_i} \right] \dot{\Theta},$$

for $i = 1, \dots, 2N$, where \mathcal{M}_i is the i -th column of the total inertia matrix $\mathcal{M}(\Theta)$. In particular, the velocity vectors c_1 and c_2 arise only in the presence of a configuration-dependent $\mathbf{S}(q)$ matrix. Performing calculations, it can be shown that:

1. The vector c_1 does not contain quadratic velocity terms in \dot{q} or $\dot{\theta}$, but only mixed quadratic terms $\dot{\theta}_i \dot{q}_j$.
2. When the matrix \mathbf{S} is constant (in particular, zero), both c_1 and c_2 vanish.

The dynamic model (11.7) also shares some properties of the rigid case, such as:

- The model equations admit a linear parametrization in terms of a suitable set of dynamic coefficients, including joint stiffnesses and motor inertias, which is useful for model identification and adaptive control.
- The Coriolis and centrifugal terms can always be factorized as $c_{\text{tot}}(\Theta, \dot{\Theta}) = \mathcal{C}(\Theta, \dot{\Theta})\dot{\Theta}$, in such a way that matrix $\mathcal{M} - 2\mathcal{C}$ is skew-symmetric – a property used in control analysis.
- For robots having only rotational joints, the gradient of the gravity vector $g(q)$ is globally bounded in norm by a constant.

Finally, when the joint stiffness is extremely large ($\mathbf{K} \rightarrow \infty$), then $\theta \rightarrow q$ while $\tau_J \rightarrow \tau$. It is easy to check that the dynamic model (11.7) collapses in the limit into the standard model of fully rigid robots (including links and motors).

Reduced Model

In general, the link and motor equations in (11.7) are dynamically coupled through the elastic torque τ_J at the joints, but also (at the acceleration level) via the inertial components of matrix $\mathbf{S}(q)$ – usually a path of low energy transfer. The presence and actual relevance

of these inertial couplings depend on the kinematic arrangement of the manipulator and, in particular, on the specific placement of the motors and transmission devices. There are cases in which the matrix \mathbf{S} is constant (e.g., the planar case, as in the previous example, with any number of links) or zero (e.g., for a single link with elastic joint or for a robot with $N = 2$ links having the two joint axes orthogonal and the motors mounted at the joints). As a result, the dynamic equations will simplify considerably.

For a generic robot with elastic joints, one can take advantage of the presence of large reduction ratios (with the n_i 's of the order of 100–150) and simply neglect energy contributions due to the inertial couplings between the motors and the links (see again the 2R planar example). This is equivalent to considering the following simplifying assumption:

A4 The angular velocity of the rotors is due only to their own spinning, i. e.,

$${}^{R_i}\boldsymbol{\omega}_{r_i} = \begin{pmatrix} 0 & 0 & \dot{\theta}_{m,i} \end{pmatrix}^T, \quad i = 1, \dots, N,$$

instead of the complete expression (11.3).

As a result, the total angular kinetic energy of the rotors is just $\frac{1}{2} \dot{\boldsymbol{\theta}}^T \mathbf{B} \dot{\boldsymbol{\theta}}$ (or $\mathbf{S} \equiv \mathbf{0}$), and the dynamic model (11.7) reduces to

$$\begin{aligned} \mathbf{M}(\mathbf{q})\ddot{\mathbf{q}} + \mathbf{c}(\mathbf{q}, \dot{\mathbf{q}}) + \mathbf{g}(\mathbf{q}) + \mathbf{K}(\mathbf{q} - \boldsymbol{\theta}) &= \mathbf{0} \\ \mathbf{B}\ddot{\boldsymbol{\theta}} + \mathbf{K}(\boldsymbol{\theta} - \mathbf{q}) &= \boldsymbol{\tau}, \end{aligned} \quad (11.9)$$

with $\mathbf{M}(\mathbf{q}) = \mathbf{M}_L(\mathbf{q}) + \mathbf{M}_R(\mathbf{q})$. The main feature of this model is that the link and motor equations are dynamically coupled only through the elastic torque $\boldsymbol{\tau}_J$. In addition, the motor equations are now fully linear.

We note that the complete model (11.7) and the reduced model (11.9) display different characteristics with respect to certain control problems. In fact, the reduced model is always feedback linearizable by *static* state feedback, whereas this is never the case for the complete model as soon as a coupling $\mathbf{S} \neq \mathbf{0}$ is present.

Singular Perturbation Model

It is interesting to show the *two-time-scale* dynamic behavior that it is induced in robots with elastic joints when the joint stiffness \mathbf{K} is relatively large, but still finite. This behavior can be made explicit by a simple linear change of coordinates, namely replacing $\boldsymbol{\theta}$ with the joint torque $\boldsymbol{\tau}_J$. For the sake of simplicity, this is illustrated on the reduced model only (without dissipation).

Since the diagonal joint stiffness matrix is assumed to have large but similar elements, a common scalar fac-

tor $1/\epsilon^2 \gg 1$ can be extracted as

$$\mathbf{K} = \frac{1}{\epsilon^2} \hat{\mathbf{K}} = \frac{1}{\epsilon^2} \text{diag}(\hat{K}_1, \dots, \hat{K}_N).$$

The *slow* subsystem is then given by the link equations, once they are rewritten as

$$\mathbf{M}(\mathbf{q})\ddot{\mathbf{q}} + \mathbf{c}(\mathbf{q}, \dot{\mathbf{q}}) + \mathbf{g}(\mathbf{q}) = \boldsymbol{\tau}_J. \quad (11.10)$$

To obtain the dynamics of the *fast* subsystem, the joint torque is differentiated twice, the motor and link accelerations are replaced from (11.9), and the above definition of $\hat{\mathbf{K}}$ is used. This leads to

$$\begin{aligned} \epsilon^2 \ddot{\boldsymbol{\tau}}_J &= \hat{\mathbf{K}} \{ \mathbf{B}^{-1} \boldsymbol{\tau} - [\mathbf{B}^{-1} + \mathbf{M}^{-1}(\mathbf{q})] \boldsymbol{\tau}_J \\ &\quad + \mathbf{M}^{-1}(\mathbf{q})[\mathbf{c}(\mathbf{q}, \dot{\mathbf{q}}) + \mathbf{g}(\mathbf{q})] \}. \end{aligned} \quad (11.11)$$

For small ϵ , (11.10) and (11.11) represent a singularly perturbed system. The two separate time scales governing the slow and fast dynamics are t and $\sigma = t/\epsilon$, since

$$\epsilon^2 \ddot{\boldsymbol{\tau}}_J = \epsilon^2 \frac{d^2 \boldsymbol{\tau}_J}{dt^2} = \frac{d^2 \boldsymbol{\tau}_J}{d\sigma^2}.$$

This model serves as a basis for composite control schemes, where the control torque has the general form

$$\boldsymbol{\tau} = \boldsymbol{\tau}_s(\mathbf{q}, \dot{\mathbf{q}}, t) + \epsilon \boldsymbol{\tau}_f(\mathbf{q}, \dot{\mathbf{q}}, \boldsymbol{\tau}_J, \dot{\boldsymbol{\tau}}_J). \quad (11.12)$$

This includes a slow action $\boldsymbol{\tau}_s$, designed when neglecting joint elasticity, and an additional action $\boldsymbol{\tau}_f$ for locally stabilizing the fast flexible dynamics around a suitable manifold in the state space. It can be verified that, when setting $\epsilon = 0$ in (11.10)–(11.12), the equivalent rigid robot model is recovered as

$$[\mathbf{M}(\mathbf{q}) + \mathbf{B}]\ddot{\mathbf{q}} + \mathbf{c}(\mathbf{q}, \dot{\mathbf{q}}) + \mathbf{g}(\mathbf{q}) = \boldsymbol{\tau}_s.$$

A similar singular perturbation model (and control design) can also be derived for robot manipulators with flexible links.

11.1.2 Inverse Dynamics

Given a desired motion of a robot, we wish to compute the nominal torque needed to reproduce this motion in ideal conditions (the inverse dynamics problem). Such nominal torque can be used as the feedforward term in a trajectory-tracking control law.

For rigid robots, the inverse dynamics is a straightforward algebraic computation obtained by replacing the desired motion of the generalized coordinates in the dynamic model. The minimum requirement for exact

reproduction is that the planned motion has a continuously differentiable desired velocity. For robots with elastic joints, a motion task can be conveniently expressed in terms of a desired link trajectory $\mathbf{q} = \mathbf{q}_d(t)$ (possibly obtained from the kinematic inversion of a desired motion in Cartesian space). The additional complexity lies in the fact that not all robot coordinates are directly assigned in this way, so that additional derivations should be performed. This will require some higher degree of smoothness of the desired trajectory $\mathbf{q}_d(t) \in [0, T]$, where the final time T may or may not be finite.

Reduced Model

Consider first the case of the reduced model (11.7) and set $\mathbf{n}(\mathbf{q}, \dot{\mathbf{q}}) = \mathbf{c}(\mathbf{q}, \dot{\mathbf{q}}) + \mathbf{g}(\mathbf{q})$ for compactness. By evaluating the link equations on the desired link motion

$$\mathbf{M}(\mathbf{q}_d)\ddot{\mathbf{q}}_d + \mathbf{n}(\mathbf{q}_d, \dot{\mathbf{q}}_d) + \mathbf{K}\mathbf{q}_d = \mathbf{K}\boldsymbol{\theta}_d, \quad (11.13)$$

the nominal position $\boldsymbol{\theta}_d$ of the motors associated with the desired link motion is readily obtained. The nominal elastic torque at the joints is $\boldsymbol{\tau}_{J,d} = \mathbf{K}(\boldsymbol{\theta}_d - \mathbf{q}_d)$; note that, from (11.13), this quantity can be expressed as a function of \mathbf{q}_d , $\dot{\mathbf{q}}_d$, and $\ddot{\mathbf{q}}_d$, which is independent of \mathbf{K} . Differentiating (11.13) leads to the expression for the nominal motor velocity $\dot{\boldsymbol{\theta}}_d$,

$$\mathbf{M}(\mathbf{q}_d)\mathbf{q}_d^{[3]} + \dot{\mathbf{M}}(\mathbf{q}_d)\ddot{\mathbf{q}}_d + \dot{\mathbf{n}}(\mathbf{q}_d, \dot{\mathbf{q}}_d) + \mathbf{K}\dot{\mathbf{q}}_d = \mathbf{K}\dot{\boldsymbol{\theta}}_d, \quad (11.14)$$

where the notation $\mathbf{y}^{[i]} = d^i\mathbf{y}/dt^i$ is used. Differentiating once more, we obtain

$$\begin{aligned} &\mathbf{M}(\mathbf{q}_d)\mathbf{q}_d^{[4]} + 2\dot{\mathbf{M}}(\mathbf{q}_d)\mathbf{q}_d^{[3]} + \ddot{\mathbf{n}}(\mathbf{q}_d, \dot{\mathbf{q}}_d) \\ &+ [\dot{\mathbf{M}}(\mathbf{q}_d) + \mathbf{K}]\ddot{\mathbf{q}}_d = \mathbf{K}\ddot{\boldsymbol{\theta}}_d, \end{aligned} \quad (11.15)$$

to be used in the motor equations evaluated along the desired motion. After simplifications, the nominal torque is obtained as

$$\begin{aligned} \boldsymbol{\tau}_d = &[\mathbf{M}(\mathbf{q}_d) + \mathbf{B}]\ddot{\mathbf{q}}_d + \mathbf{n}(\mathbf{q}_d, \dot{\mathbf{q}}_d) \\ &+ \mathbf{BK}^{-1} \left[\mathbf{M}(\mathbf{q}_d)\mathbf{q}_d^{[4]} + 2\dot{\mathbf{M}}(\mathbf{q}_d)\mathbf{q}_d^{[3]} \right. \\ &\left. + \ddot{\mathbf{M}}(\mathbf{q}_d)\ddot{\mathbf{q}}_d + \ddot{\mathbf{n}}(\mathbf{q}_d, \dot{\mathbf{q}}_d) \right], \end{aligned} \quad (11.16)$$

where the extra contributions to the nominal torque of the rigid case due to joint elasticity can be clearly recognized. The evaluation of $\boldsymbol{\tau}_d$ involves the computation of first- and second-order partial derivatives of the dynamic model terms. For instance, one needs to compute

$$\dot{\mathbf{M}}[\mathbf{q}_d(t)] = \sum_{i=1}^N \frac{\partial \mathbf{M}_i(\mathbf{q})}{\partial \mathbf{q}} \bigg|_{\mathbf{q}=\mathbf{q}_d(t)} \dot{\mathbf{q}}_d(t) \mathbf{e}_i^T,$$

where \mathbf{e}_i is the i -th unit vector and \mathbf{M}_i is the i -th column of matrix $\mathbf{M}(\mathbf{q})$. This and other similar expressions can be obtained by symbolic manipulation software. From (11.16), it follows that the minimum requirement for the exact reproducibility of the desired motion is that $\mathbf{q}_d(t)$ admits a continuously differentiable jerk (i. e., that $\mathbf{q}_d^{[4]}(t)$ exists in the time interval $[0, T]$). Such a smoother requirement should not come unexpected, in view of the flexible nature of the system.

Similarly to the rigid case, a recursive numerical Newton–Euler algorithm can be defined, which computes efficiently the inverse dynamics torque (11.16) in $O(N)$ asymptotic complexity. For the reduced model of robots with elastic joints, the algorithm involves forward recursion of motion variables up to the fourth differential order and backward recursion of second time derivatives of forces and torques.

Complete Model

Some more analysis is needed for the model (11.9). For ease of exposition, and without loss of generality, the case of a constant matrix \mathbf{S} is considered. When evaluating the link equations on the desired link motion

$$\mathbf{M}(\mathbf{q}_d)\ddot{\mathbf{q}}_d + \mathbf{S}\ddot{\boldsymbol{\theta}}_d + \mathbf{n}(\mathbf{q}_d, \dot{\mathbf{q}}_d) + \mathbf{K}\mathbf{q}_d = \mathbf{K}\boldsymbol{\theta}_d, \quad (11.17)$$

the additional presence of the motor acceleration on the left-hand side does not allow solving directly for the motor position $\boldsymbol{\theta}_d$ as a function of $(\mathbf{q}_d, \dot{\mathbf{q}}_d, \ddot{\mathbf{q}}_d)$ only. However, the strictly upper triangular structure (11.5) of \mathbf{S} allows one to define $\boldsymbol{\theta}_d$ componentwise, using the scalar equations in (11.17) recursively. The N -th equation is in fact independent of $\ddot{\boldsymbol{\theta}}_d$,

$$\mathbf{M}_N^T(\mathbf{q}_d)\ddot{\mathbf{q}}_d + \mathbf{0}^T\ddot{\boldsymbol{\theta}}_d + n_N(\mathbf{q}_d, \dot{\mathbf{q}}_d) + K_N q_{d,N} = K_N \theta_{d,N},$$

so that this equation can be used to define

$$\theta_{d,N} = f_N(\mathbf{q}_d, \dot{\mathbf{q}}_d, \ddot{\mathbf{q}}_d)$$

and, after double differentiation, its second time derivative

$$\ddot{\theta}_{d,N} = f_N''(\mathbf{q}_d, \dot{\mathbf{q}}_d, \ddot{\mathbf{q}}_d).$$

In the $(N-1)$ -th equation,

$$\begin{aligned} &\mathbf{M}_{N-1}^T(\mathbf{q}_d)\ddot{\mathbf{q}}_d + S_{N-1,N}\ddot{\theta}_{d,N} \\ &+ n_{N-1}(\mathbf{q}_d, \dot{\mathbf{q}}_d) + K_{N-1}q_{d,N-1} = K_{N-1}\theta_{d,N-1}, \end{aligned}$$

the acceleration $\ddot{\theta}_{d,N}$ has already been determined in the previous step. Therefore, this equation can be used similarly to define

$$\theta_{d,N-1} = f_{N-1}(\mathbf{q}_d, \dot{\mathbf{q}}_d, \ddot{\mathbf{q}}_d)$$

and, after two time differentiations, also

$$\ddot{\theta}_{d,N-1} = f''_{N-1}(\mathbf{q}_d, \dot{\mathbf{q}}_d, \dots, \mathbf{q}_d^{[6]}).$$

Note that whenever $S_{N-1,N} = 0$, there will be no increase in the degree of the highest order derivatives of \mathbf{q}_d within the functional dependence of $\theta_{d,N-1}$. This argument also applies recursively to the following steps. Proceeding backward through the link equations, the scalar computations end up with the definition of

$$\theta_{d,1} = f_1(\mathbf{q}_d, \dot{\mathbf{q}}_d, \dots, \mathbf{q}_d^{[2N]})$$

and

$$\ddot{\theta}_{d,1} = f''_1(\mathbf{q}_d, \dot{\mathbf{q}}_d, \dots, \mathbf{q}_d^{[2(N+1)]}),$$

where the dependence on the highest possible differential degree of \mathbf{q}_d is shown. With $\ddot{\theta}_d = f''(\cdot)$ made available in this way, the nominal torque is finally computed from the motor equations, again evaluated along the desired motion. Using (11.17) to substitute for $\mathbf{K}(\theta_d - \mathbf{q}_d)$ yields

$$\begin{aligned} \tau_d &= [\mathbf{M}(\mathbf{q}_d) + \mathbf{S}^T] \ddot{\mathbf{q}}_d + \mathbf{n}(\mathbf{q}_d, \dot{\mathbf{q}}_d) \\ &\quad + (\mathbf{B} + \mathbf{S}) \ddot{\theta}_d(\mathbf{q}_d, \dot{\mathbf{q}}_d, \dots, \mathbf{q}_d^{[2(N+1)]}). \end{aligned} \quad (11.18)$$

As a result, the presence of inertial motor-link couplings considerably increases the complexity of the solution to the inverse dynamics problem. The exact reproduction of a desired link trajectory by the nominal torque in (11.18) requires that $\mathbf{q}_d(t)$ has a continuously differentiable $(2N+1)$ -th time derivative (i.e., that $\mathbf{q}_d^{[2(N+1)]}(t)$ exists in the time interval $[0, T]$). For rest-to-rest motions, this implies a trajectory plan that imposes a very slow start and ending phases.

We finally remark that the possibility of expressing the evolution of the state and input of a system algebraically in terms of the evolution of an output variable (in our case \mathbf{q}) and a finite number of its derivatives is sometimes referred to as the *flatness* property. The above inverse dynamics analysis shows that \mathbf{q} is a flat output for robots with elastic joints modeled either by (11.7) or (11.9).

Note also that, when a *constant* \mathbf{q}_d is considered, these computations all provide the same condition for the associated motor position

$$\theta_d = \mathbf{q}_d + \mathbf{K}^{-1} \mathbf{g}(\mathbf{q}_d) \quad (11.19)$$

and nominal static torque

$$\tau_d = \mathbf{g}(\mathbf{q}_d). \quad (11.20)$$

Presence of Dissipative Terms

Inclusion of dissipative terms in the inverse dynamics deserves some additional comments. Any model of frictional effects acting on the motor side of the transmissions can be included in the computation without extra requirements. Friction at the link side should instead be described by a smooth model, because of the need to differentiate the link equations. Thus, some functional approximations may be needed (e.g., replacing discontinuous *sign* functions with hyperbolic tangents) before including this term in (11.13) or (11.17).

On the other hand, the presence of a nonnegligible spring damping \mathbf{D} in (11.8) changes the structure of the computations. While this reduces the order of the derivatives of \mathbf{q}_d involved, the problem itself will become nonalgebraic; in fact, the inverse system will require the use of the solution of a dynamical system, albeit a simple one.

Consider for instance the model (11.9), including now all the dissipative terms given in (11.8). When evaluating the link equations,

$$\begin{aligned} \mathbf{M}(\mathbf{q}_d) \ddot{\mathbf{q}}_d + \mathbf{n}(\mathbf{q}_d, \dot{\mathbf{q}}_d) + (\mathbf{D} + \mathbf{F}_q) \dot{\mathbf{q}}_d + \mathbf{K} \mathbf{q}_d \\ = \mathbf{D} \ddot{\theta}_d + \mathbf{K} \theta_d, \end{aligned} \quad (11.21)$$

the motor velocity $\dot{\theta}_d$ additionally appears on the right-hand side. Differentiating (11.21) leads to

$$\mathbf{D} \ddot{\theta}_d + \mathbf{K} \dot{\theta}_d = \mathbf{w}_d, \quad (11.22)$$

with

$$\begin{aligned} \mathbf{w}_d &= \mathbf{M}(\mathbf{q}_d) \mathbf{q}_d^{[3]} + [\dot{\mathbf{M}}(\mathbf{q}_d) + \mathbf{D} + \mathbf{F}_q] \ddot{\mathbf{q}}_d \\ &\quad + \dot{\mathbf{n}}(\mathbf{q}_d, \dot{\mathbf{q}}_d) + \mathbf{K} \dot{\mathbf{q}}_d. \end{aligned}$$

Equation (11.22) represents a first-order linear *asymptotically stable* dynamical system (internal dynamics), with state θ_d and forcing signal $\mathbf{w}_d(t)$. For a given $\dot{\theta}_d(0)$, its solution $\dot{\theta}_d(t)$ and the associated solution derivative $\ddot{\theta}_d(t)$ are needed to evaluate the nominal torque in the motor equations. This yields

$$\tau_d = \mathbf{M}(\mathbf{q}_d) \ddot{\mathbf{q}}_d + \mathbf{n}(\mathbf{q}_d, \dot{\mathbf{q}}_d) + \mathbf{F}_q \dot{\mathbf{q}}_d + \mathbf{B} \ddot{\theta}_d + \mathbf{F}_\theta \dot{\theta}_d,$$

where (11.21) has been used to replace the term $\mathbf{D}(\dot{\theta}_d - \dot{\mathbf{q}}_d) + \mathbf{K}(\theta_d - \mathbf{q}_d)$. In this case, the desired link trajectory $\mathbf{q}_d(t)$ should have a continuously differentiable acceleration ($\mathbf{q}_d^{[3]}$ should exist, since it is used in the definition of \mathbf{w}_d). Note that any initialization $\dot{\theta}_d(0)$ of the internal dynamics (11.22) is feasible (i.e., it produces a specific torque profile $\tau_d(t)$ yielding the same link

motion $\mathbf{q}_d(t)$, with the associated motor position $\theta_d(0)$ initialized from (11.21). Indeed, we should match the actual initial state of the robot. For instance, starting from an equilibrium state implies the unique choice $\theta_d(0) = 0$.

A similar procedure can also be applied to the complete model (11.7) in the presence of spring damping. Again a dynamical inverse system will be needed, while the smoothness requirement on $\mathbf{q}_d(t)$ would be even more dramatically reduced in that case.

We finally remark that, for robots with flexible links, the inverse dynamics problem gives also rise to an internal dynamics, independently of the presence of modal damping. Moreover, when specifying a desired motion for the tip of the flexible arm, the associated internal dynamics will be *unstable* and this critical issue has to be tackled to determine a feasible solution.

11.1.3 Regulation Control

We now consider the problem of controlling the motion of a robot with joint elasticity to a *constant* configuration. In this problem, no trajectory planning is involved and a feedback law should be found that achieves asymptotic stabilization of a desired closed-loop equilibrium. Global solutions (i. e., those valid when starting from any initial state) are indeed preferred.

From the analysis in the previous section, it should be clear that one needs to define only a constant reference \mathbf{q}_d (with $\dot{\mathbf{q}}_d(t) \equiv \mathbf{0}$) for the link coordinates.

From (11.19), a unique reference θ_d for the motor variables is in fact associated with the desired \mathbf{q}_d (which, in turn, may result from a desired pose of the robot end-effector). Furthermore, (11.20) provides the needed static torque to be applied at steady state by any feasible controller.

A major aspect of the presence of joint elasticity is that the feedback part of the control law can depend in general on *four* variables for each joint: the motor and link position, and the motor and link velocity. However, in most robots where joint elasticity is not explicitly considered in the system design, at most two sensors are available for measurement at the joints: a position sensor (e.g., an encoder) and, in some cases, a tachometer as a velocity sensor. When no velocity sensors are present, velocity is typically reconstructed by suitable numerical differentiation of high-resolution position measurements. Due to the presence of joint elasticity, the position/velocity quantities that are actually measured depend on where these sensors are mounted in the motor/transmission assembly.

A single link driven through an elastic joint is introduced as a paradigmatic case study to show what can be achieved using different sets of partial state measurements. This simple situation provides indications on how to handle the general multilink case.

In the absence of gravity, it will be shown that a proportional–derivative (PD) controller based only on motor measurements is sufficient to achieve the desired regulation task. In the presence of gravity, various gravity compensation schemes can be added to the PD feedback controller. These control results mimic the situation of robots with rigid joints, once the convenient quantities for use in the feedback have been identified.

Single Elastic Joint Example

Consider a single link rotating on a horizontal plane (thus, without gravity) and actuated with a motor through an elastic joint coupling (Fig. 11.4). When viscous friction on motor and link side as well as damping across the spring are included, the dynamic model is

$$M\ddot{q} + D(\dot{q} - \dot{\theta}) + K(q - \theta) + F_q\dot{q} = 0,$$

$$B\ddot{\theta} + D(\dot{\theta} - \dot{q}) + K(\theta - q) + F_\theta\dot{\theta} = \tau,$$

where the same, now scalar, notation of Sect. 11.1.1 has been used. Since this system is described by linear equations, Laplace transforms are used to derive the transfer functions of interest, namely from input torque to motor position

$$\frac{\theta(s)}{\tau(s)} = \frac{Ms^2 + (D + F_q)s + K}{\text{den}(s)},$$

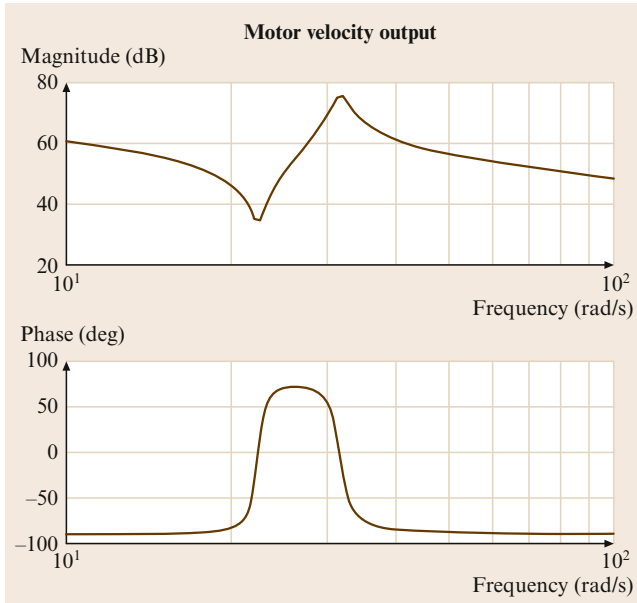


Fig. 11.6 Bode diagrams of the torque to motor velocity transfer function

and from input torque to link position

$$\frac{q(s)}{\tau(s)} = \frac{Ds + K}{\text{den}(s)},$$

with the common denominator $\text{den}(s)$ given by

$$\begin{aligned} \text{den}(s) = & \left\{ MBs^3 + [M(D + F_\theta) + B(D + F_q)]s^2 \right. \\ & + [(M + B)K + (F_q + F_\theta)D + F_q F_\theta]s \\ & \left. + (F_q + F_\theta)K \right\} s. \end{aligned}$$

In the case of link position output, the transfer function has a larger relative degree (or pole-zero excess). Figures 11.6 and 11.7 show typical frequency responses in the two cases. For clarity, the outputs have been chosen at the velocity level. In the Bode diagram of the magnitude for the motor velocity output, note the presence of an antiresonance/resonance behavior. Similarly, there is a pure resonance (more pronounced for weak or zero spring damping D) for the link velocity output. The phase profile in Fig. 11.7, with a high-frequency lag of 270° , indicates the greater control difficulty encountered when closing the feedback loop on link quantities. In experimental tests on a robot joint, such plots are quite characteristic of the presence of concentrated joint elasticity and can be used to assess the relevance of this phenomenon and for identifying model parameters.

For the analysis of the stabilizing properties of different feedback arrangements, all dissipative effects will be neglected in the following ($D = F_q = F_\theta = 0$ is anyway the worst case). Consider first the transfer function relative to the motor position output

$$\left. \frac{\theta(s)}{\tau(s)} \right|_{\text{no diss}} = \frac{Ms^2 + K}{[MBs^2 + (M + B)K]s^2}. \quad (11.23)$$

Apart from a double pole at the origin, this transfer function has a pair of imaginary zeros and poles, with the zero pair occurring at the so-called locked frequency

$$\omega_1 = \sqrt{\frac{K}{M}},$$

which characterizes the oscillations occurring when the motor is locked ($\theta \equiv 0$), e.g., by a high-gain positional feedback. This frequency is used to assess the performance limit of a simple PD control for the motor variables. In order to achieve enough damping in the closed-loop system, the bandwidth should be limited, as a rule of thumb, to one-third of ω_1 . Faster transients can be achieved only by taking into account the fourth-order dynamics of the elastic joint assembly. Note also

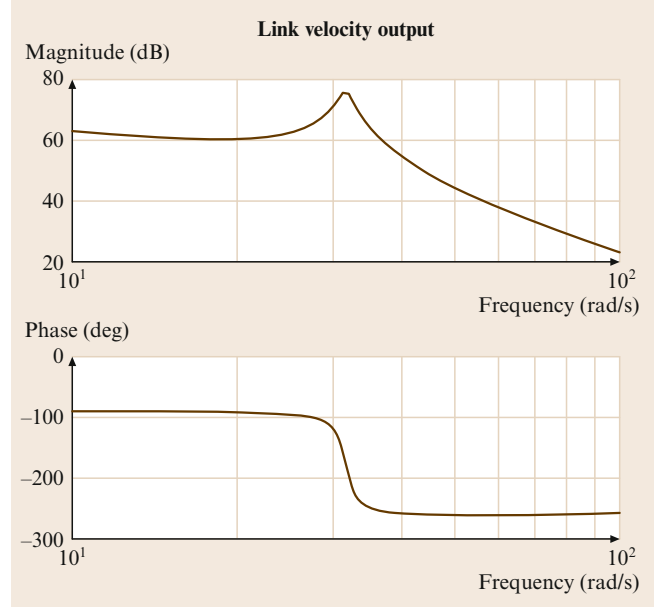


Fig. 11.7 Bode diagrams of the torque to link velocity transfer function

that the frequency of the zero pair is always *lower* than that of the pole pair in (11.23). This is related to the *passivity* of the mapping from torque to motor velocity, a property useful for stability and robust or adaptive control design.

Since the control objective is to regulate the link position output, we are also interested in the open-loop transfer function

$$\left. \frac{q(s)}{\tau(s)} \right|_{\text{no diss}} = \frac{K}{[MBs^2 + (M + B)K]s^2}. \quad (11.24)$$

This transfer function has *no zeros* (in fact, for this to happen it is sufficient that $D = 0$) so that the relative degree is now four, the maximum possible. We shall see that the nonlinear counterpart of the absence of zeros in (11.24) will play a relevant role also for trajectory control in the multilink case of robots with elastic joints.

It is worth mentioning that this situation is completely different from the case in which the elastic spring would be moved out of the joint and placed anywhere along the link – a simple one-mode approximate model of link flexibility. In that case, the analogous transfer function will possess a negative and a positive real zero, symmetrically placed w.r.t. the origin (a *non-minimum-phase* system). This indicates the criticality of a direct inversion of the system input–output map for the execution of a desired link trajectory.

With the desired position given in terms of the link variable q_d , the most natural choice for the design of

a linear stabilizing feedback using one position and one velocity variable, is to close a PD loop from the link variables,

$$\tau = u_q - (K_{P,q}q + K_{D,q}\dot{q}) , \quad (11.25)$$

with position and velocity gains $K_{P,q}$ and $K_{D,q}$, and with $u_q = K_{P,q}q_d$ being the external input used for defining the set point. It is easy to verify that the closed-loop poles will be unstable no matter how the gains are chosen, so that error feedback from link variables alone should be avoided. In a similar way, also the combination of motor position and link velocity feedback is always unstable.

Another mixed feedback strategy is to use link position and motor velocity

$$\tau = u_q - (K_{P,q}q + K_{D,m}\dot{\theta}) . \quad (11.26)$$

This combination corresponds, e.g., to the case of a tachometer integrated in a direct-current (DC) motor and of an optical encoder placed on the load shaft for sensing its position (without any knowledge about the relevance of joint elasticity). Use of (11.26) leads to the closed-loop characteristic equation

$$BMs^4 + MK_{D,m}s^3 + (B + M)Ks^2 + KK_{D,m}s + KK_{P,q} = 0 .$$

Using Routh's criterion, asymptotic stability occurs if and only if the motor velocity gain $K_{D,m} > 0$ and the link position gain satisfies $0 < K_{P,q} < K$, i.e., the proportional feedback should not *override* the spring stiffness. The existence of such an upper bound limits the usefulness of this scheme.

Finally, consider performing feedback from the motor variables

$$\tau = u_\theta - (K_{P,m}\theta + K_{D,m}\dot{\theta}) , \quad (11.27)$$

with $u_\theta = K_{P,m}\theta_d = K_{P,m}q_d$ (due to the absence of gravity). The closed-loop system will be asymptotically stable provided that both $K_{P,m}$ and $K_{D,m}$ are strictly positive (and otherwise arbitrarily large). This favorable situation lends itself to a convenient generalization in the multilink case.

Note that other partial state feedback combinations would be possible, depending on the available sensing devices. For instance, mounting a strain gauge on the transmission shaft provides a direct measure of the elastic torque $\tau_j = K(\theta - q)$ for control use. Strain gauges are also useful sensors for flexible links. Indeed, full-state feedback may be designed so as to guarantee

asymptotic stability and improve the transient behavior considerably; however, this would be obtained at the cost of additional sensors and requires proper tuning of the four gains.

PD Control Using only Motor Variables

For the general multilink case in the absence of gravity, consider the PD control law based on motor position and velocity feedback

$$\tau = \mathbf{K}_P(\boldsymbol{\theta}_d - \boldsymbol{\theta}) - \mathbf{K}_D\dot{\boldsymbol{\theta}} , \quad (11.28)$$

with symmetric (typically, diagonal) positive-definite gain matrices \mathbf{K}_P and \mathbf{K}_D . Since $\mathbf{g}(\mathbf{q}) \equiv \mathbf{0}$, it follows from (11.19) that the reference value for the motor position is $\boldsymbol{\theta}_d = \mathbf{q}_d$ (neither a joint deflection is present nor an input torque is needed at steady state).

The control law (11.28) globally asymptotically stabilizes the desired equilibrium state $\mathbf{q} = \boldsymbol{\theta} = \mathbf{q}_d$, $\dot{\mathbf{q}} = \dot{\boldsymbol{\theta}} = \mathbf{0}$. This can be shown through a Lyapunov argument, completed by the application of La Salle's theorem. In fact, a candidate Lyapunov function is given by the sum of the total energy of the system (kinetic plus elastic potential) and of the control energy due to the proportional term (a virtual elastic potential energy)

$$V = \frac{1}{2} \dot{\boldsymbol{\theta}}^T \mathcal{M}(\boldsymbol{\theta}) \dot{\boldsymbol{\theta}} + \frac{1}{2} (\mathbf{q} - \boldsymbol{\theta})^T \mathbf{K} (\mathbf{q} - \boldsymbol{\theta}) + \frac{1}{2} (\boldsymbol{\theta}_d - \boldsymbol{\theta})^T \mathbf{K}_P (\boldsymbol{\theta}_d - \boldsymbol{\theta}) \geq 0 . \quad (11.29)$$

Computing the time derivative of V along the trajectories of the closed-loop system given by (11.7) (or (11.9)) and (11.28), and taking into account the skew-symmetry of $\dot{\mathcal{M}} - 2\mathbf{C}$, leads to

$$\dot{V} = -\dot{\boldsymbol{\theta}}^T \mathbf{K}_D \dot{\boldsymbol{\theta}} \leq 0 .$$

The inclusion of dissipative terms (viscous friction and spring damping) would render \dot{V} even more negative-semidefinite. The analysis is completed by verifying that the maximum invariant set contained in the set of states such that $\dot{V} = 0$ (i.e., those with $\dot{\boldsymbol{\theta}} = \mathbf{0}$) collapses into the desired unique equilibrium state.

We point out that an identical control law is able to globally regulate, in the absence of gravity, robots with flexible links to a desired joint configuration. In that case, $\boldsymbol{\theta}$ in (11.28) would be the rigid coordinates at the base of the flexible links of the robot.

PD with Constant Gravity Compensation

The presence of gravity requires the addition of some form of gravity compensation to the PD action (11.28).

Moreover, this will typically need an additional structural assumption and may demand some caution in the selection of the control gains.

Before proceeding, we recall a basic property of the gravity vector $\mathbf{g}(\mathbf{q})$ (under assumption **A2**, the gravity vector in (11.7) is the same appearing in the dynamics of the equivalent rigid robot). For robots with rotational joints, elastic or not, a positive constant α exists such that

$$\left\| \frac{\partial \mathbf{g}(\mathbf{q})}{\partial \mathbf{q}} \right\| \leq \alpha, \quad \forall \mathbf{q} \in \mathbb{R}^N. \quad (11.30)$$

The norm of a matrix $\mathbf{A}(\mathbf{q})$ is that induced by the Euclidean norm for vectors, i.e.,

$$\|\mathbf{A}\| = \sqrt{\lambda_{\max}(\mathbf{A}^T \mathbf{A})}.$$

Inequality (11.30) implies that

$$\|\mathbf{g}(\mathbf{q}_1) - \mathbf{g}(\mathbf{q}_2)\| \leq \alpha \|\mathbf{q}_1 - \mathbf{q}_2\|, \quad \forall \mathbf{q}_1, \mathbf{q}_2 \in \mathbb{R}^N. \quad (11.31)$$

In common practice, robot joints are never unrealistically soft. More precisely, they are stiff enough to have, under the load of the robot's own weight, a *unique* equilibrium link position \mathbf{q}_e associated with any assigned motor position $\boldsymbol{\theta}_e$ – the reverse of the relationship expressed by (11.19). This situation is by no means restrictive, but will be stated for clarity as a further modeling assumption:

A5 The lowest joint stiffness is larger than the upper bound on the gradient of gravity forces acting on the robot, or

$$\min_{i=1, \dots, N} K_i > \alpha.$$

The simplest modification for handling the presence of gravity is to consider the addition of a constant term that compensates exactly the gravity load at the desired steady state. According to (11.19) and (11.20), the control law (11.28) is then modified to

$$\boldsymbol{\tau} = \mathbf{K}_P(\boldsymbol{\theta}_d - \boldsymbol{\theta}) - \mathbf{K}_D \dot{\boldsymbol{\theta}} + \mathbf{g}(\mathbf{q}_d), \quad (11.32)$$

with symmetric, typically diagonal, $\mathbf{K}_P > \mathbf{0}$ (as a minimum) and $\mathbf{K}_D > \mathbf{0}$, and with the motor reference given by $\boldsymbol{\theta}_d = \mathbf{q}_d + \mathbf{K}^{-1} \mathbf{g}(\mathbf{q}_d)$.

A sufficient condition guaranteeing that $\mathbf{q} = \mathbf{q}_d$, $\boldsymbol{\theta} = \boldsymbol{\theta}_d$, $\dot{\mathbf{q}} = \dot{\boldsymbol{\theta}} = \mathbf{0}$ will be the unique globally asymptotically stable equilibrium for the system (11.7) under the control law (11.32) is that

$$\lambda_{\min} \left[\begin{pmatrix} \mathbf{K} & -\mathbf{K} \\ -\mathbf{K} & \mathbf{K} + \mathbf{K}_P \end{pmatrix} \right] > \alpha, \quad (11.33)$$

with α defined in (11.30). Taking into account the diagonal structure of \mathbf{K} and \mathbf{K}_P , and thanks to assumption **A5**, it is always possible to fulfill this condition by increasing the smallest proportional gain in the controller (or, the smallest eigenvalue of \mathbf{K}_P if this matrix has not been chosen diagonal).

In the following, we sketch the motivation for this condition and the associated proof of asymptotic stability. The equilibrium configurations of the closed-loop system are the solutions of

$$\begin{aligned} \mathbf{K}(\mathbf{q} - \boldsymbol{\theta}) + \mathbf{g}(\mathbf{q}) &= \mathbf{0}, \\ \mathbf{K}(\boldsymbol{\theta} - \mathbf{q}) - \mathbf{K}_P(\boldsymbol{\theta}_d - \boldsymbol{\theta}) - \mathbf{g}(\mathbf{q}_d) &= \mathbf{0}. \end{aligned}$$

Indeed, the pair $(\mathbf{q}_d, \boldsymbol{\theta}_d)$ satisfies these equations. However, in order to obtain a global result one should guarantee that this pair is the unique solution. Therefore, recalling (11.19), the null term $\mathbf{K}(\boldsymbol{\theta}_d - \mathbf{q}_d) - \mathbf{g}(\mathbf{q}_d)$ can be added/subtracted to both equations to obtain

$$\begin{aligned} \mathbf{K}(\mathbf{q} - \mathbf{q}_d) - \mathbf{K}(\boldsymbol{\theta} - \boldsymbol{\theta}_d) &= \mathbf{g}(\mathbf{q}_d) - \mathbf{g}(\mathbf{q}) \\ -\mathbf{K}(\mathbf{q} - \mathbf{q}_d) + (\mathbf{K} + \mathbf{K}_P)(\boldsymbol{\theta} - \boldsymbol{\theta}_d) &= \mathbf{0}, \end{aligned}$$

where the matrix in condition (11.33) can be clearly recognized. Taking the norms of terms on both sides and bounding gravity terms using (11.31), the introduced condition (11.33) implies that the pair $(\mathbf{q}_d, \boldsymbol{\theta}_d)$ is in fact the unique equilibrium. To show asymptotic stability, a candidate Lyapunov function is built based on the one introduced in (11.29) in the absence of gravity

$$\begin{aligned} V_{g1} &= V + \mathcal{U}_{\text{grav}}(\mathbf{q}) - \mathcal{U}_{\text{grav}}(\mathbf{q}_d) - (\mathbf{q} - \mathbf{q}_d)^T \mathbf{g}(\mathbf{q}_d) \\ &\quad - \frac{1}{2} \mathbf{g}^T(\mathbf{q}_d) \mathbf{K}^{-1} \mathbf{g}(\mathbf{q}_d) \geq 0. \end{aligned} \quad (11.34)$$

The positive-definiteness of V_{g1} and the fact that its unique minimum is at the desired state are again implied by condition (11.33). (The last constant term in (11.34) is used to set to zero the minimum value of V_{g1} at the equilibrium.). By the usual computations, it follows that $\dot{V}_{g1} = -\dot{\boldsymbol{\theta}}^T \mathbf{K}_D \dot{\boldsymbol{\theta}} \leq 0$ and the result is obtained applying La Salle's theorem.

The control law (11.32) is based only on the knowledge of the gravity term $\mathbf{g}(\mathbf{q}_d)$ and of the joint stiffness \mathbf{K} . The latter appears in fact in the definition of the motor position reference $\boldsymbol{\theta}_d$. Uncertainties in the gravitational term $\mathbf{g}(\mathbf{q}_d)$ and in the joint stiffness \mathbf{K} affect the performance of the controller. Still, the existence of a unique closed-loop equilibrium and its asymptotic stability are preserved when the gravity bound by α is still correct and condition (11.33) holds for the true stiffness

values. Indeed, the robot will converge to an equilibrium that is different from the desired one – the better the estimates $\hat{\mathbf{K}}$ and $\hat{\mathbf{g}}(\mathbf{q}_d)$ used, the closer the actual equilibrium will be to the desired one.

PD with Online Gravity Compensation

Similarly to the rigid robot case, a better transient behavior is expected if gravity compensation (or, more precisely, its perfect cancellation) is performed at all configurations during motion. However, the gravity vector in (11.7) depends on the link variables \mathbf{q} , which are assumed not to be measurable at this stage. It is easy to see that using $\mathbf{g}(\boldsymbol{\theta})$, with the measured motor positions in place of the link positions, leads in general to an incorrect closed-loop equilibrium. Moreover, even if \mathbf{q} were available, adding $\mathbf{g}(\mathbf{q})$ to a motor PD error feedback has no guarantee of success because this compensation, which appears in the motor equation, does not instantaneously cancel the gravity load acting on the links.

With this in mind, a PD control with *online* gravity compensation can be introduced as follows. Define the variable

$$\tilde{\boldsymbol{\theta}} = \boldsymbol{\theta} - \mathbf{K}^{-1}\mathbf{g}(\mathbf{q}_d), \quad (11.35)$$

which is a *gravity-biased* modification of the measured motor position $\boldsymbol{\theta}$, and let

$$\boldsymbol{\tau} = \mathbf{K}_P(\boldsymbol{\theta}_d - \boldsymbol{\theta}) - \mathbf{K}_D\dot{\boldsymbol{\theta}} + \mathbf{g}(\tilde{\boldsymbol{\theta}}), \quad (11.36)$$

where $\mathbf{K}_P > \mathbf{0}$ and $\mathbf{K}_D > \mathbf{0}$ are both symmetric (and typically diagonal) matrices. The control law (11.36) can still be implemented using only motor variables. The term $\mathbf{g}(\tilde{\boldsymbol{\theta}})$ provides only an approximate cancellation (though, of a large part) of gravity during motion, but leads to the correct gravity compensation at steady state. In fact, by using (11.19) and (11.35), it follows that

$$\tilde{\boldsymbol{\theta}}_d := \boldsymbol{\theta}_d - \mathbf{K}^{-1}\mathbf{g}(\mathbf{q}_d) = \mathbf{q}_d,$$

so that $\mathbf{g}(\tilde{\boldsymbol{\theta}}_d) = \mathbf{g}(\mathbf{q}_d)$.

Global asymptotic stability of the desired equilibrium can be guaranteed under the same condition (11.33) used for the constant gravity compensation case. A slightly different Lyapunov candidate is defined, starting again from the one in (11.29), as

$$\begin{aligned} V_{g2} &= V + \mathcal{U}_{\text{grav}}(\mathbf{q}) - \mathcal{U}_{\text{grav}}(\tilde{\boldsymbol{\theta}}) \\ &\quad - \frac{1}{2} \mathbf{g}^T(\mathbf{q}_d) \mathbf{K}^{-1} \mathbf{g}(\mathbf{q}_d) \geq 0, \end{aligned}$$

to be compared with (11.34).

The use of an online gravity compensation scheme typically provides a smoother time course and a noticeable reduction of the positional transient errors, with no additional control effort in terms of peak and average torques. We note that choices of low position gains, even when largely violating the sufficient condition (11.33) for stability, may still work, contrary to the case of constant gravity compensation. However even for increasing values of joint stiffness, in the limit for $\mathbf{K} \rightarrow \infty$, the range of feasible values of \mathbf{K}_P that guarantee exact regulation does not extend down to zero.

A possibility to refine the previous online gravity compensation scheme, again based only on motor position measurement, is offered by the use of a fast iterative algorithm that elaborates the measure $\boldsymbol{\theta}$ in order to generate a quasistatic estimate $\bar{\mathbf{q}}(\boldsymbol{\theta})$ of the current (unmeasured) \mathbf{q} . In fact, in any steady-state configuration $(\mathbf{q}_s, \boldsymbol{\theta}_s)$, a direct mapping is defined from \mathbf{q}_s to $\boldsymbol{\theta}_s$

$$\boldsymbol{\theta}_s = \mathbf{h}_g(\mathbf{q}_s) := \mathbf{q}_s + \mathbf{K}^{-1}\mathbf{g}(\mathbf{q}_s).$$

Assumption A5 is sufficient to guarantee the existence and uniqueness also of the inverse mapping $\mathbf{q}_s = \mathbf{h}_g^{-1}(\boldsymbol{\theta}_s)$. For a measured $\boldsymbol{\theta}$, the function

$$\mathbf{q} = \mathbf{T}(\boldsymbol{\theta}) := \boldsymbol{\theta} - \mathbf{K}^{-1}\mathbf{g}(\boldsymbol{\theta})$$

is then a *contraction mapping* and the iteration

$$\mathbf{q}_{i+1} = \mathbf{T}(\mathbf{q}_i), \quad i = 0, 1, 2, \dots$$

will converge to the unique fixed point of this mapping, which is exactly the value $\bar{\mathbf{q}}(\boldsymbol{\theta}) = \mathbf{h}_g^{-1}(\boldsymbol{\theta})$. A suitable initialization for \mathbf{q}_0 is either the measured $\boldsymbol{\theta}$ or the value $\bar{\mathbf{q}}$ computed at the previous sampling instant. In this way, just two or three iterations are needed to obtain sufficient accuracy and this is fast enough to be implemented within a sensing/control sampling interval of a digital robot controller. With this iterative scheme running in the background, the regulation control law becomes

$$\boldsymbol{\tau} = \mathbf{K}_P(\boldsymbol{\theta}_d - \boldsymbol{\theta}) - \mathbf{K}_D\dot{\boldsymbol{\theta}} + \mathbf{g}(\bar{\mathbf{q}}(\boldsymbol{\theta})), \quad (11.37)$$



with symmetric (diagonal) $\mathbf{K}_P > \mathbf{0}$ and $\mathbf{K}_D > \mathbf{0}$. A proof of the global asymptotic stability of this control scheme can be given by further modifying the previous Lyapunov candidates. The advantage of (11.37) is that any positive value of the feedback gain \mathbf{K}_P is allowed, thus recovering in full the operative working conditions of the rigid case with exact gravity cancellation.

With reference to the reduced model (11.9), a further improvement can be obtained via a nonlinear PD-like controller that removes completely the gravity from

the actual motion of the robot links. For this, consider the control law

$$\begin{aligned} \tau = & \mathbf{K}_P[\mathbf{q}_d - \boldsymbol{\theta} + \mathbf{K}^{-1}\mathbf{g}(\mathbf{q})] - \mathbf{K}_D(\dot{\boldsymbol{\theta}} - \mathbf{K}^{-1}\dot{\mathbf{g}}(\mathbf{q})) \\ & + \mathbf{g}(\mathbf{q}) + \mathbf{B}\mathbf{K}^{-1}\ddot{\mathbf{g}}(\mathbf{q}) \end{aligned} \quad (11.38)$$

with symmetric (diagonal) $\mathbf{K}_P > 0$ and $\mathbf{K}_D > 0$. The last two terms are those needed to cancel both static and dynamic effects due to gravity. Even when assumption **A5** does not hold, the control law (11.38) guarantees global asymptotic stability of the desired equilibrium state. This result is a byproduct of feedback linearization design (Sect. 11.1.4), though much simpler than the complete one, and can be proven using again a Lyapunov analysis. Since a lower bound on the joint stiffness is not required (the joints may be arbitrarily soft), the same approach can be used also for robots using variable stiffness actuation (VSA). The price to pay is that an estimate of the link acceleration $\ddot{\mathbf{q}}$ is needed when computing the term $\ddot{\mathbf{g}}$ in (11.38).

The two online gravity compensation schemes (11.36) and (11.37) realize a *compliance control* in the joint space with only motor measurements. The same idea can also be extended to the case of Cartesian compliance control by evaluating the direct kinematics and the Jacobian (transpose) of the robot arm with $\boldsymbol{\theta}$ or, respectively, $\bar{\mathbf{q}}(\boldsymbol{\theta})$ in place of \mathbf{q} . The role of a damping action within a compliance/impedance control scheme can be clearly understood when looking at  VIDEO 133 and  VIDEO 134.

Full-State Feedback

When the feedback law is based on a full set of measurements of the robot state, the transient performance of regulation control laws can be improved. Taking advantage of the availability of a joint torque sensor, we present a convenient design for the reduced model (11.9) of robots with elastic joints, including spring damping as a dissipation effect. Full-state feedback can be obtained in two phases, by combining a preliminary torque feedback with the motor feedback law in (11.28).

Using $\tau_J = \mathbf{K}(\boldsymbol{\theta} - \mathbf{q})$, the motor equation can be rewritten as

$$\mathbf{B}\ddot{\boldsymbol{\theta}} + \tau_J + \mathbf{D}\mathbf{K}^{-1}\dot{\tau}_J = \tau.$$

The joint torque feedback

$$\tau = \mathbf{B}\mathbf{B}_\theta^{-1}\mathbf{u} + (\mathbf{I} - \mathbf{B}\mathbf{B}_\theta^{-1})(\tau_J + \mathbf{D}\mathbf{K}^{-1}\dot{\tau}_J), \quad (11.39)$$

where \mathbf{u} is an auxiliary input to be designed, transforms the motor equations into

$$\mathbf{B}_\theta\ddot{\boldsymbol{\theta}} + \tau_J + \mathbf{D}\mathbf{K}^{-1}\dot{\tau}_J = \mathbf{u}.$$

In this way, the apparent motor inertia can be reduced to a desired, arbitrary small value \mathbf{B}_θ , with clear benefits in terms of vibration damping. For instance in the linear and scalar case, a very small B shifts the pair of complex poles in (11.23) to a very high frequency, with the joint behaving almost as a rigid one.

Setting now

$$\mathbf{u} = \mathbf{K}_{P,\theta}(\boldsymbol{\theta}_d - \boldsymbol{\theta}) - \mathbf{K}_{D,\theta}\dot{\boldsymbol{\theta}} + \mathbf{g}(\mathbf{q}_d)$$

in (11.39) leads to the state feedback controller

$$\begin{aligned} \tau = & \mathbf{K}_P(\boldsymbol{\theta}_d - \boldsymbol{\theta}) - \mathbf{K}_D\dot{\boldsymbol{\theta}} + \mathbf{K}_T[\mathbf{g}(\mathbf{q}_d) - \tau_J] \\ & - \mathbf{K}_S\dot{\tau}_J + \mathbf{g}(\mathbf{q}_d), \end{aligned} \quad (11.40)$$

with gains

$$\begin{aligned} \mathbf{K}_P &= \mathbf{B}\mathbf{B}_\theta^{-1}\mathbf{K}_{P,\theta}, \\ \mathbf{K}_D &= \mathbf{B}\mathbf{B}_\theta^{-1}\mathbf{K}_{D,\theta}, \\ \mathbf{K}_T &= \mathbf{B}\mathbf{B}_\theta^{-1} - \mathbf{I} \\ \mathbf{K}_S &= (\mathbf{B}\mathbf{B}_\theta^{-1} - \mathbf{I})\mathbf{D}\mathbf{K}^{-1}. \end{aligned}$$

Indeed, the law (11.40) can also be rewritten in terms of $(\boldsymbol{\theta}, \mathbf{q}, \dot{\boldsymbol{\theta}}, \dot{\mathbf{q}})$, if the torque sensor is not available. However, keeping this structure of the gains preserves the interesting physical interpretation of what the full-state feedback controller is able to achieve.

11.1.4 Trajectory Tracking

As for rigid robots, the problem of tracking desired time-varying trajectories for robots with elastic joints is harder than that of achieving constant regulation. In general, solving this problem requires the use of full-state feedback and knowledge of all the terms in the dynamic model.

Under these conditions, we shall focus on the *feedback linearization* approach, namely a nonlinear state feedback law that leads to a closed-loop system with decoupled and exactly linear behavior for all the N joints of the robot (in fact, the link variables \mathbf{q}). The tracking errors along the reference trajectory are forced to be *globally exponentially stable*, with a decaying rate that can be directly specified through the choice of the scalar feedback gains in the controller. This fundamental result is the direct extension of the well-known *computed torque* method for rigid robots. Because of its relevant properties, the feedback linearization approach

can be used as a reference to assess the performance of any other trajectory tracking control law, which may possibly be designed using less/approximate model information and/or only partial-state feedback.

However, in the presence of joint elasticity, the design of a feedback linearization law is not straightforward. Furthermore, as soon as $\mathbf{S} \neq \mathbf{0}$, the dynamic model (11.7) will not satisfy the necessary conditions for exact linearization (nor those for input–output decoupling) when only a *static* (or, instantaneous) feedback law from the full state is allowed. Therefore, we will restrict our attention to the more tractable case of the reduced dynamic model (11.9) and sketch only briefly the more general picture.

As a second much simpler approach to trajectory tracking problems, we also present a *linear control design* that makes use of a model-based feedforward command and a precomputed state reference trajectory, as obtained from the inverse dynamics in Sect. 11.1.2, with the addition of a linear feedback from the full state. In this case, convergence to the desired trajectory is only locally guaranteed, i. e., the tracking errors should be small enough, but the control implementation is straightforward and the real-time computational burden is considerably reduced.

Feedback Linearization

Consider the reduced model (11.9) and let the desired motion be specified by a smooth reference trajectory $\mathbf{q}_d(t)$ for the robot links. The control design will proceed by system inversion, in a similar way to the inverse dynamics computations of Sect. 11.1.2 but using now the current measures of the state variables $(\mathbf{q}, \boldsymbol{\theta}, \dot{\mathbf{q}}, \dot{\boldsymbol{\theta}})$ instead of the reference state evolution $(\mathbf{q}_d, \boldsymbol{\theta}_d, \dot{\mathbf{q}}_d, \dot{\boldsymbol{\theta}}_d)$. Notably, there is no need to transform the robot equations into their state-space description, which is the standard form used in control design for general nonlinear systems; we will use the robot model directly in its second-order differential form (typical of mechanical systems).

The outcome of the inversion procedure will be the definition of a torque $\boldsymbol{\tau}$, in the form of a static state feedback control law, which cancels the original robot dynamics and replaces it with a desired linear and decoupled one of suitable differential order. In this sense, the control law *stiffens* the dynamics of the robot with elastic joints, irrespective of the fact that \mathbf{K} is already relatively large (stiff joint) or small (soft joint). The feasibility of inverting the system from the chosen output \mathbf{q} without causing instability problems (related to the presence of unobservable dynamics in the closed-loop system, after cancellation) is a relevant property of robots with elastic joints. In fact, this is the direct generalization to the nonlinear multiple-input multiple-

output (MIMO) case of the possibility of inverting a scalar transfer function in the absence of zeros (see also the considerations made on (11.24)).

Rewrite the link equation in the compact form

$$\mathbf{M}(\mathbf{q})\ddot{\mathbf{q}} + \mathbf{n}(\mathbf{q}, \dot{\mathbf{q}}) + \mathbf{K}(\mathbf{q} - \boldsymbol{\theta}) = \mathbf{0}. \quad (11.41)$$

None of the above quantities depends instantaneously on the input torque $\boldsymbol{\tau}$. Therefore, we can differentiate once w.r.t. time and obtain

$$\mathbf{M}(\mathbf{q})\dot{\mathbf{q}}^{[3]} + \dot{\mathbf{M}}(\mathbf{q})\ddot{\mathbf{q}} + \dot{\mathbf{n}}(\mathbf{q}, \dot{\mathbf{q}}) + \mathbf{K}(\dot{\mathbf{q}} - \dot{\boldsymbol{\theta}}) = \mathbf{0}. \quad (11.42)$$

Proceeding one step further leads to

$$\begin{aligned} \mathbf{M}(\mathbf{q})\mathbf{q}^{[4]} + 2\dot{\mathbf{M}}(\mathbf{q})\dot{\mathbf{q}}^{[3]} + \ddot{\mathbf{M}}(\mathbf{q})\ddot{\mathbf{q}} \\ + \ddot{\mathbf{n}}(\mathbf{q}, \dot{\mathbf{q}}) + \mathbf{K}(\ddot{\mathbf{q}} - \ddot{\boldsymbol{\theta}}) = \mathbf{0}, \end{aligned} \quad (11.43)$$

where $\ddot{\boldsymbol{\theta}}$ now appears. The motor acceleration is at the same differential level of $\boldsymbol{\tau}$ in the motor equation

$$\mathbf{B}\ddot{\boldsymbol{\theta}} + \mathbf{K}(\boldsymbol{\theta} - \mathbf{q}) = \boldsymbol{\tau}, \quad (11.44)$$

and thus, replacing $\ddot{\boldsymbol{\theta}}$ from (11.44), we get

$$\begin{aligned} \mathbf{M}(\mathbf{q})\mathbf{q}^{[4]} + 2\dot{\mathbf{M}}(\mathbf{q})\dot{\mathbf{q}}^{[3]} + \ddot{\mathbf{M}}(\mathbf{q})\ddot{\mathbf{q}} + \ddot{\mathbf{n}}(\mathbf{q}, \dot{\mathbf{q}}) + \mathbf{K}\ddot{\mathbf{q}} \\ = \mathbf{KB}^{-1} [\boldsymbol{\tau} - \mathbf{K}(\boldsymbol{\theta} - \mathbf{q})]. \end{aligned} \quad (11.45)$$

We note that, using (11.41), the last term $\mathbf{K}(\boldsymbol{\theta} - \mathbf{q})$ in (11.45) may also be replaced by $\mathbf{M}(\mathbf{q})\ddot{\mathbf{q}} + \mathbf{n}(\mathbf{q}, \dot{\mathbf{q}})$.

Since the matrix $\mathbf{A}(\mathbf{q}) = \mathbf{M}^{-1}(\mathbf{q})\mathbf{KB}^{-1}$ is always nonsingular, an arbitrary value \mathbf{v} can be assigned to the fourth derivative of \mathbf{q} by a suitable choice of the input torque $\boldsymbol{\tau}$. The matrix $\mathbf{A}(\mathbf{q})$ is the so-called decoupling matrix of the system and its nonsingularity is a necessary and sufficient condition for imposing a decoupled input–output behavior by nonlinear static state feedback. Moreover, (11.45) indicates that each component q_i of \mathbf{q} needs to be differentiated $r_i = 4$ times in order to be algebraically related to the input torque $\boldsymbol{\tau}$ (r_i is the *relative degree* of q_i , when this is chosen as a system output). Since there are N link variables, the total sum of the relative degrees is $4N$, equal to the dimension of the state of a robot with elastic joints. All these facts taken together lead to the conclusion that, when inverting (11.45) to determine the input $\boldsymbol{\tau}$ that imposes $\mathbf{q}^{[4]} = \mathbf{v}$, there will be no dynamics left other than the one appearing in the closed-loop input–output map.

Therefore, choose

$$\begin{aligned} \boldsymbol{\tau} = \mathbf{BK}^{-1} [\mathbf{M}(\mathbf{q})\mathbf{v} + \boldsymbol{\alpha}(\mathbf{q}, \dot{\mathbf{q}}, \ddot{\mathbf{q}}, \mathbf{q}^{[3]})] \\ + [\mathbf{M}(\mathbf{q}) + \mathbf{B}]\ddot{\mathbf{q}} + \mathbf{n}(\mathbf{q}, \dot{\mathbf{q}}), \end{aligned} \quad (11.46)$$

with

$$\alpha(q, \dot{q}, \ddot{q}, q^{[3]}) = \ddot{M}(q)\ddot{q} + 2\dot{M}(q)\dot{q}^{[3]} + \ddot{n}(q, \dot{q}),$$

where the terms in α have been ordered according to the dependence on increasing orders of derivatives of q . It is easy to verify that the control law (11.46) leads to a closed-loop system fully described by

$$q^{[4]} = v, \quad (11.47)$$

i.e., chains of four input–output integrators from each auxiliary input v_i to each link position output q_i , for $i = 1, \dots, N$. Thus, the robot system has been exactly linearized and decoupled by the nonlinear feedback law (11.46). The improvement in performance can be appreciated in a comparative way by looking at VIDEO 135 and VIDEO 770.

The complete control law (11.46) is expressed as a function of the so-called *linearizing* coordinates $(q, \dot{q}, \ddot{q}, q^{[3]})$ only. This has led to some misunderstandings in the past, as it seemed that the feedback linearization approach for robots with elastic joints would need direct measures of the link acceleration \ddot{q} and jerk $q^{[3]}$, which are impossible to obtain with currently available sensors (or would require multiple numerical differentiations of position measures in real time, with critical noise problems).

When considering the latest technology in the field, it is now feasible to have a set of sensors for elastic joints measuring in a reliable and accurate way the motor position θ (and, possibly, also its velocity $\dot{\theta}$), the joint torque $\tau_J = K(\theta - q)$, as well as the link position q . For instance, this is the arrangement of sensors available at each joint of the *LWR-III* lightweight manipulator, where expressly designed high-resolution incremental encoders of the magneto-resistive type are used for the motor position, joint torque sensing is based on a full bridge of strain gauges, and a high-end capacitive potentiometer is used for the absolute link position (Fig. 11.8). Therefore, only one numerical differentiation is needed in order to obtain a good estimate of \dot{q} and/or $\dot{\tau}_J$ as well. Note that, depending on the specific sensor resolution, it may also be convenient to evaluate q using the measures of θ and τ_J as $\theta - K^{-1}\tau_J$.

With this in mind, it is easy to see that the following three sets of $4N$ variables

$$(q, \dot{q}, \ddot{q}, q^{[3]}), \quad (q, \theta, \dot{q}, \dot{\theta}), \quad (q, \tau_J, \dot{q}, \dot{\tau}_J)$$

are all equivalent state variables for a robot with elastic joints, related by globally invertible transformations. Therefore, under the assumption that the dynamic

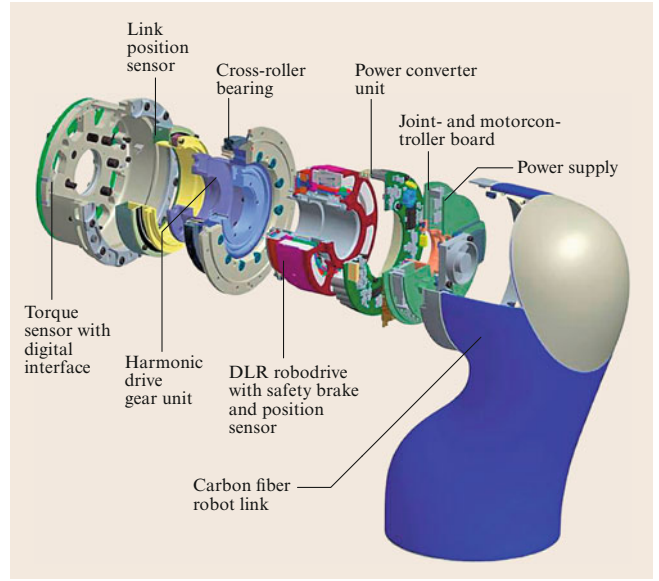


Fig. 11.8 Exploded view of a joint of the *DLR LWR-III* lightweight manipulator and its sensor suite

model is available, we can completely rewrite the feedback linearizing control law (11.46) in terms of the more *conventional* state $(q, \theta, \dot{q}, \dot{\theta})$ or, taking advantage of a joint torque sensor, in terms of $(q, \tau_J, \dot{q}, \dot{\tau}_J)$. In particular, as a byproduct of (11.41) and (11.42), we have

$$\begin{aligned} \ddot{q} &= M^{-1}(q) [K(\theta - q) - n(q, \dot{q})] \\ &= M^{-1}(q) [\tau_J - n(q, \dot{q})], \end{aligned} \quad (11.48)$$

and

$$\begin{aligned} q^{[3]} &= M^{-1}(q) [K(\dot{\theta} - \dot{q}) - \dot{M}(q)\ddot{q} - \dot{n}(q, \dot{q})] \\ &= M^{-1}(q) [\dot{\tau}_J - \dot{M}(q)\ddot{q} - \dot{n}(q, \dot{q})], \end{aligned} \quad (11.49)$$

where the acceleration \ddot{q} appearing in (11.49) has already been computed through (11.48). Therefore, the exact linearizing and decoupling control law can be rewritten in terms of a static state feedback law of the form $\tau = \tau(q, \theta, \dot{q}, \dot{\theta}, v)$ or $\tau = \tau(q, \tau_J, \dot{q}, \dot{\tau}_J, v)$. Indeed, the evaluation of the various derivatives of the dynamic model terms that are present in these expressions should be properly organized or customized in order to optimize computations.

Based on the resulting (11.47), the trajectory-tracking problem is solved by setting

$$\begin{aligned} v &= q_d^{[4]} + K_3 (q_d^{[3]} - q^{[3]}) + K_2 (\ddot{q}_d - \ddot{q}) \\ &\quad + K_1 (\dot{q}_d - \dot{q}) + K_0 (q_d - q), \end{aligned} \quad (11.50)$$

where it is assumed that the reference trajectory $q_d(t)$ is (at least) three times continuously differentiable (i.e., the fourth derivative $q_d^{[4]}$ exists), and the *diagonal* matrices K_0, \dots, K_3 have scalar elements $K_{.,i}$ such that

$$s^4 + K_{3,i}s^3 + K_{2,i}s^2 + K_{1,i}s + K_{0,i}, \quad i = 1, \dots, N,$$

are Hurwitz polynomials. In view of the obtained decoupling, the trajectory error

$$e_i(t) = q_{d,i}(t) - q_i(t)$$

for the i -th link satisfies then

$$e_i^{[4]} + K_{3,i}e_i^{[3]} + K_{2,i}\ddot{e}_i + K_{1,i}\dot{e}_i + K_{0,i}e_i = 0;$$

yielding $e_i(t) \rightarrow 0$ in a global exponential way, for any initial state. A series of remarks are in order:

- When the initial state $(q(0), \theta(0), \dot{q}(0), \dot{\theta}(0))$ is matched with the reference trajectory and its first three derivatives at time $t=0$ (for this check, (11.48) and (11.49) are to be used), exact reproduction of the reference trajectory is achieved at all times.
- In the case of a discontinuity of the reference position trajectory, or of any of its first three derivatives, at a time $t^* \in [0, T]$, a trajectory error occurs at $t = t^*$ that will again decay to zero, independently for each link and with the prescribed exponential rate.
- The choice of the gains $K_{3,i}, \dots, K_{0,i}$ can be made by a pole placement technique (equivalent in this case to an eigenvalue assignment). Let $\lambda_1, \dots, \lambda_4$ be four poles with negative real parts, possibly given in complex pairs and/or coincident, specifying the desired transient of the trajectory error. These closed-loop poles will be assigned by the unique choice of real and positive gains

$$\begin{aligned} K_{3,i} &= -(\lambda_1 + \lambda_2 + \lambda_3 + \lambda_4), \\ K_{2,i} &= \lambda_1(\lambda_2 + \lambda_3 + \lambda_4) + \lambda_2(\lambda_3 + \lambda_4) + \lambda_3\lambda_4, \\ K_{1,i} &= -[\lambda_1\lambda_2(\lambda_3 + \lambda_4) + \lambda_3\lambda_4(\lambda_1 + \lambda_2)], \\ K_{0,i} &= \lambda_1\lambda_2\lambda_3\lambda_4. \end{aligned}$$

When the values of link and motor inertias are very different from each other, or when the joint stiffness is very large, the above fixed choice of gains has the drawback of generating too large control efforts. In those cases, a more tailored set of eigenvalues can be assigned scheduling their placement as a function of the physical data of robot inertias and joint stiffnesses.

- When compared to the *computed torque* method for rigid robots, the feedback linearization control

for trajectory tracking given by (11.46)–(11.50) requires the inversion of the inertia matrix $M(q)$ and the additional evaluation of derivatives of the inertia matrix and of other terms in the dynamic model.

- The feedback linearization approach can also be applied without any changes in the presence of viscous (or otherwise smooth) friction at the motor and link side. The inclusion of spring damping leads instead to a third-order decoupled differential relation between the auxiliary input v and q , leaving thus a N -dimensional unobservable dynamics in the closed-loop system, which is, however, still asymptotically stable. In this case, only input–output (and not full-state) linearization and decoupling is achieved.

We conclude with some considerations on exact linearization/decoupling by feedback for the general model (11.7) of robots with elastic joints. Unfortunately, due to the presence of the inertial coupling matrix $S(q)$ between links and rotors, the above control design can no longer be applied. Consider as an illustration the case of a constant S in (11.7), with the associated model simplifications. Solving for $\ddot{\theta}$ from the motor equations, $\ddot{\theta} = B^{-1}(\tau - \tau_J - S^T\ddot{q})$, and substituting into the link equations leads to

$$\begin{aligned} [M(q) - SB^{-1}S^T]\ddot{q} + n(q, \dot{q}) - (I + SB^{-1})\tau_J \\ = -SB^{-1}\tau. \end{aligned}$$

In this case, the input torque τ appears already in the expression for the link acceleration \ddot{q} . Using (11.6), the expression of the decoupling matrix is then

$$A(q) = -[M_L(q) + M_R(q)]^{-1}SB^{-1},$$

which is never full rank in view of the structure (11.5) of S . As a consequence, the necessary condition for obtaining (at least) input–output linearization and decoupling by static state feedback fails to hold.

However, by resorting to the use of a larger class of control laws, it is still possible to obtain an exact linearization and decoupling result. For this purpose, consider a *dynamic* state feedback controller of the form

$$\begin{aligned} \tau &= \alpha(q, \dot{q}, \theta, \dot{\theta}, \xi) + \beta(q, \dot{q}, \theta, \dot{\theta}, \xi)v, \\ \dot{\xi} &= \gamma(q, \dot{q}, \theta, \dot{\theta}, \xi) + \delta(q, \dot{q}, \theta, \dot{\theta}, \xi)v, \end{aligned} \quad (11.51)$$

where $\xi \in \mathbb{R}^p$ is the state of the dynamic compensator, α , β , γ , and δ are suitable nonlinear vector functions, and $v \in \mathbb{R}^N$ is (as before) an external input used for trajectory-tracking purposes. It is possible to show in general that a dynamic compensator (11.51) of order

at most $v = 2N(N-1)$ can be designed so as to yield a closed-loop system that is globally described by

$$\mathbf{q}^{[2(N+1)]} = \mathbf{v}, \quad (11.52)$$

in place of (11.47). Note the coincidence of this differential order with the one found for exact reproducibility of a desired trajectory $\mathbf{q}_d(t)$ in Sect. 11.1.2. The tracking problem is then solved by working on (11.52), with a direct generalization of the linear stabilization design in (11.50).

It is interesting to give a physical interpretation for this control result. The structural obstruction to input–output decoupling of the model (11.7) is related to the fact that the motion of a link attached to an elastic joint is affected *too soon* (at the second differential level) by torques originating at other elastic joints. This is due to the inertial couplings present between motors and links. The addition of dynamics (i.e., of integrators) in the controller slows down these low-energy paths and allows for the high-energy effects of the elastic torque at the local joint (a fourth-order differential path) to come into play. This dynamic balancing allows both input–output decoupling and exact linearization of the extended system (having the robot and the controller states).

Linear Control Design

The feedback linearization approach to trajectory tracking gives rise to a rather complex nonlinear control law. Its main advantage of globally enforcing a linear and decoupled behavior to the trajectory error dynamics should be traded-off with a control design that achieves only local stability around the reference trajectory, but is much simpler to implement (and may run at higher sampling rates).

For this, the inverse dynamics results of Sect. 11.1.2 can be used, assuming either the reduced or the complete robot model, with and without dissipative terms. Given a sufficiently smooth desired link trajectory $\mathbf{q}_d(t)$, we have seen that it is always possible to associate:

1. The nominal torque $\boldsymbol{\tau}_d(t)$ needed for its exact reproduction.
2. The reference evolution of all other state variables (e.g., $\boldsymbol{\theta}_d(t)$, as given by (11.13), or $\boldsymbol{\tau}_{J,d}(t)$).

These signals define a sort of steady-state (though, time-varying) operation for the system.

A simpler tracking controller combines a model-based feedforward term with a linear feedback term using the trajectory error. The linear feedback locally stabilizes the system around the reference state trajectory, whereas the feedforward torque is responsible for maintaining the robot along the desired motion as soon

as the error has vanished (see some examples on the tracking of square paths in [VIDEO 136](#)).

Using full-state feedback, two possible controllers of this kind are

$$\begin{aligned} \boldsymbol{\tau} = & \boldsymbol{\tau}_d + \mathbf{K}_{P,\theta}(\boldsymbol{\theta}_d - \boldsymbol{\theta}) + \mathbf{K}_{D,\theta}(\dot{\boldsymbol{\theta}}_d - \dot{\boldsymbol{\theta}}) \\ & + \mathbf{K}_{P,q}(\mathbf{q}_d - \mathbf{q}) + \mathbf{K}_{D,q}(\dot{\mathbf{q}}_d - \dot{\mathbf{q}}) \end{aligned} \quad (11.53)$$

and

$$\begin{aligned} \boldsymbol{\tau} = & \boldsymbol{\tau}_d + \mathbf{K}_{P,\theta}(\boldsymbol{\theta}_d - \boldsymbol{\theta}) + \mathbf{K}_{D,\theta}(\dot{\boldsymbol{\theta}}_d - \dot{\boldsymbol{\theta}}) \\ & + \mathbf{K}_{P,J}(\boldsymbol{\tau}_{J,d} - \boldsymbol{\tau}_J) + \mathbf{K}_{D,J}(\dot{\boldsymbol{\tau}}_{J,d} - \dot{\boldsymbol{\tau}}_J). \end{aligned} \quad (11.54)$$

These trajectory tracking schemes are the most common in the control practice for robots with elastic joints. In the absence of full-state measurements, they can be combined with an observer of the unmeasurable quantities. An even simpler realization is

$$\boldsymbol{\tau} = \boldsymbol{\tau}_d + \mathbf{K}_P(\boldsymbol{\theta}_d - \boldsymbol{\theta}) + \mathbf{K}_D(\dot{\boldsymbol{\theta}}_d - \dot{\boldsymbol{\theta}}), \quad (11.55)$$

which uses only motor measurements and relies on the results obtained for the regulation case.

The different gain matrices used in (11.53)–(11.55) have to be tuned using a linear approximation of the robot system. This approximation may be obtained at a fixed equilibrium point or around the actual reference trajectory, leading respectively to a linear time-invariant or to a linear time-varying system. While the existence of (possibly time-varying) stabilizing feedback matrices is guaranteed by the controllability of these linear approximations, the validity of the approach is only *local* in nature and the region of convergence will depend both on the given trajectory and on the robustness of the designed linear feedback.

It should be mentioned that such a control approach to trajectory tracking problems can be used also for robots with flexible links. Once the inverse dynamics problem has been solved (for the case of link flexibility, this typically results in a noncausal solution), a controller of the form (11.55) (or (11.53), with link deflection $\boldsymbol{\delta}$ and deflection rate $\dot{\boldsymbol{\delta}}$ replacing, respectively, \mathbf{q} and $\dot{\mathbf{q}}$), can be directly applied.

11.1.5 Further Reading

This section contains the main references for the part of this chapter on robots with joint flexibility. In addition, we point out to a larger bibliography for topics that have not been included here.

Early interest in problems arising from the presence of flexible transmissions in industrial robots dates back to [11.1, 2], with first experimental findings on the

GE P-50 arm. Relevant mechanical considerations involved in the design of robot arms and in the evaluation of their compliant elements can be found in [11.3].

One of the first studies on the inclusion of joint elasticity in the dynamic modeling of robot arms is due to [11.4]. The detailed analysis of the model structure presented in Sect. 11.1.1 comes from [11.5], with some updates from [11.6]. The simplifying assumption leading to the reduced model was introduced in [11.7]. The special case of motors mounted on the driven links is considered in [11.8]. The observation that joints with limited elasticity lead to a singularly perturbed dynamic model was first recognized in [11.9]. Symbolic manipulation programs for the automatic generation of dynamic models of robots with elastic joints were also developed very early [11.10].

The inverse dynamics computations in Sect. 11.1.2 can be traced back to [11.11, 12]. The use of programs such as Modelica for the numerical evaluation of inverse dynamics is highlighted in [11.6]. An efficient Newton–Euler inverse dynamics algorithm for robots with elastic joints has been proposed in [11.12].

The first specific control designs were based on decentralized linear controllers, see, e.g., [11.13] and [11.14], where a fourth-order dynamics local to each elastic joint was used. However, schemes with proved global convergence characteristics appeared only later.


In Sect. 11.1.3, the PD controller with constant gravity compensation is a contribution of [11.15]. This was also extended to the case of robots with flexible links in [11.16]. The first two versions of regulation control with online gravity compensation are due, respectively, to [11.17] and [11.18]. Both these control laws were extended to Cartesian compliance schemes in [11.19–21]. The PD-like controller (11.38), with perfect cancellation of gravity effects on link motion, is a result of [11.22]. A general regulation framework based on energy shaping has been proposed in [11.23]. In the absence of any information on gravity, a proportional–integral–derivative (PID) regulator with semiglobal stability properties has been presented in [11.24], while a global learning scheme was proposed in [11.25].

The presentation of a full-state feedback design for regulation (and tracking) follows the idea used in [11.26]. Special interest has been devoted over the years to joint torque feedback, from the placement of torque sensors on transmission shafts [11.27] or within harmonic drives [11.28] to their use for achieving robust control performance [11.29].

The fact that the reduced model of robots with elastic joints can always be feedback linearized via static state feedback was shown for the first time in [11.7]. A previous similar result for a specific robot kinematics

can be found in [11.30]. The discrete-time implementation of the feedback linearization approach has been studied in [11.31], while its robustness properties were analyzed in [11.32]. Feedback linearization and input–output decoupling were also considered for the case of viscoelastic joints in [11.33], and for robots with joints of mixed type, some rigid and some elastic, in [11.34]. The same idea of inversion control, leading to input–output decoupling and linearization, has also been successfully applied to the tracking problem of joint-level trajectories in robots with flexible links [11.35].

For the general model of robots with elastic joints, the use of dynamic state feedback was first proposed in [11.36]. A comparative study of the errors induced by neglecting the motor–link inertia couplings (thus, for robots that are not linearizable by static state feedback) was carried out in [11.37]. The general algorithm for constructing the dynamic linearizing feedback is presented in [11.38, 39].

The benefit of combining a stabilizing feedback with a feedforward command in robots with flexible joints was experimentally shown for the first time in [11.39] (see also the  VIDEO 770) and then formalized in [11.11].

Other control design methodologies available for trajectory tracking, which were not discussed in Sect. 11.1.4, are based on singular perturbation, backstepping, or passivity. Nonlinear controllers based on the two-time scale separation property were proposed by [11.40] and [11.41]. These corrective controllers are an outcome of the singular perturbation model form and should be preferred in the case of very stiff joints, as they do not generate high-gain laws in the limit. Backstepping is based on the idea of considering the joint elastic torque [11.42] or the motor position [11.43] as an intermediate fictitious input to be used to control the link equations, and then to design the actual torque input in the motor equations so as to follow the reference behavior for the previous intermediate input. The main advantage is that this design may be easier to be transformed into an adaptive version. Adaptive control results for robots with elastic joints include the high-gain (approximate) schemes [11.44] and [11.45], as well as the global (but very complex) solution obtained in [11.46], both analyzed using only the reduced dynamic model. Moreover, robust control schemes have been proposed in [11.47], based on sliding mode techniques, and in [11.48–52], using iterative learning on repetitive tasks.

As for optimal control results, the intrinsic fourth-order dynamics associated to flexible joints has barred so far the derivation of analytical or numerically efficient results. Finding the time-optimal velocity profile

on a constrained geometric path is a solved problem in the rigid case, but only an approximate solution is available for robots with elastic joints [11.49]. A useful generalization from the rigid to the elastic case is the dynamic trajectory scaling algorithm of [11.50], which provides a closed-form expression to the uniform time scaling that recovers feasibility of commanded torques w.r.t. their bounds. Selected optimal control problems for single viscoelastic joints, involving either the maximization of stored potential energy or the minimization of rest-to-rest motion time, have been tackled and solved in [11.51] and [11.52], respectively.

Different state observers have been presented, starting from an approximate one [11.53] up to the exact ones in [11.5, 54], in which a tracking controller based on the estimated state was also tested. In all cases, link position or link position and velocity measurements are

assumed. On the other hand, the use of motor position and link acceleration has been shown to be a feasible alternative for robust state reconstruction [11.55].

Finally, the force control problem in constrained tasks for robots with elastic joints has been tackled following a singular perturbation technique [11.56, 57], an inverse dynamics approach [11.58], or an adaptive strategy [11.59].

A unified passivity-based approach has been presented in [11.60], where an inner torque feedback loop is incorporated for shaping (viz., reducing) the motor inertia. This enables approximate gravity compensation (as done in Sect. 11.1.3), as well as to assign a desired Cartesian stiffness relation for the link positions, mimicking the impedance control of the rigid case for handling interactions and contacts with the environment.

11.2 Robots with Flexible Links

Arm flexibility is a dynamic behavior in which kinetic energy interacts with elastic potential energy. Kinetic energy is stored in moving inertia, and potential energy is stored in compliant members. Flexible links provide both the inertia and compliance distributed throughout the member. Flexibility manifests itself as mechanical oscillations and static deflections, greatly complicating the motion control of a mechanical arm. If the time to settle the oscillations is significant relative to the cycle time of the overall task, flexibility will be a major consideration in the arm design.

11.2.1 Design Issues

We will deal with these issues in a modular way, separating link flexibility and joint flexibility. The first topic of link flexibility deals with the inherent spatial distribution of compliance and inertia, perhaps with both effects existing in the same element of material. The links of a manipulator arm can usually be stiffened by adding structural mass or by improving the material properties or distribution over the links. At some points, the links may be treated as rigid. The designer must realize that an arm with heavy rigid links and flexible joints may be more flexible dynamically than a lighter arm with more link flexibility and less inertia. The consequences are predicted by the natural frequency of the first flexible mode of motion, with the joint actuators locked, which can be approximated by

$$\omega_1 = \sqrt{\frac{k_{\text{eff}}}{I_{\text{eff}}}}, \quad (11.56)$$

where k_{eff} is the effective spring constant and I_{eff} is the effective inertia. For the elastic joint case, k_{eff} and I_{eff} are directly available from the elastic joint parameters and mass properties of the arm. The *effective* values applicable to a simple beam in bending, for example, would result from boundary conditions that are clamped at one end and free at the other and would be selected to yield a good approximation to the natural frequency. This natural frequency is readily available from handbooks on vibration in this case as $\omega_1 = 3.52 \sqrt{EI/ml^4}$. (The variables are used in (11.57) and (11.58) and defined below.) More complex geometries can be evaluated by various means, including the transfer matrix method discussed in Sect. 11.2.2 on modeling. The arm should be considered flexible when this frequency is low enough to interfere with the design of controllers based on rigid assumptions. The common PD control of a single joint on a flexible link can only achieve adequate damping of a closed-loop design when the magnitude of the closed loop poles is less than about 1/3 of ω_1 [11.61].

A distillation of the key aspects of the mechanics of materials is now in order. In some cases static compliance effects represent a member sufficiently, whereas in other cases the true distributed nature of compliance and mass and its dynamics must be modeled. A long structural member with forces f and moments M perpendicular to its long axis is subject to bending. Static bending relates the moment at the axial location x to the displacement w

$$M(x) = EI(x) \frac{\partial^2 w}{\partial x^2}, \quad (11.57)$$

where E is the elastic modulus of the material, and $I(x)$ is the area moment of inertia about the neutral axis of the cross section. The deflection at any point is obtained by integrating this equation from a reference point to a desired point, such as the end of the link.

This is a description of compliance that can be used when mass is isolated from elasticity. If mass is distributed throughout the beam with material mass density per unit volume ρ , the time t must be incorporated so that

$$m(x) \frac{\partial^2 w(x, t)}{\partial t^2} + \frac{\partial^2}{\partial x^2} \left(EI(x) \frac{\partial^2 w(x, t)}{\partial x^2} \right) = 0. \quad (11.58)$$

Here $m(x)$ is the mass density per unit length, incorporating the material properties and the cross-sectional area at x . Assumptions implicit in this equation, which is called the Bernoulli–Euler equation, include the minimal impact of shear distortion and rotational inertia of the cross section of the beam, which is valid for long beams. The Timoshenko beam model relaxes these assumptions but is not included here.

Torsional deflection of an angle θ results if a twisting moment T about the long beam axis occurs, such that, in the static case

$$\theta = \frac{Tl}{JG} = \alpha_{\theta T} T, \quad (11.59)$$

where G is the shear modulus of the material, and J is the polar area moment of inertia about the neutral axis of the beam. Again, the addition of a distributed mass and considering the dynamics produces a partial differential equation with independent variables in space and time

$$\mu(x) \frac{\partial^2 \theta}{\partial t^2} = GJ \frac{\partial^2 \theta}{\partial x^2}, \quad (11.60)$$

where $\mu(x)$ is the rotary mass moment of inertia per unit length of the shaft. While (11.60) is potentially appropriate for links, the smaller rotational mass moment of inertia of a long slender shaft relative to the links it drives results in the static compliance effects of torsion given by (11.59) being of most importance.

Tension and compression effects should also be acknowledged, although they tend to be the least significant. Here deflection δ in the x -direction (the long axis of the member) results from axial force F_a and is calculated as $\delta = \frac{F_a L}{AE}$

$$\delta = \frac{F_a L}{AE} = \alpha_{\delta F} F_a, \quad (11.61)$$

where L is the element length and A is its cross sectional area. In the dynamic case, with mass density ρ and displacement ξ , the axial motion is described by

$$\rho \frac{\partial^2 \xi}{\partial t^2} = E \frac{\partial^2 \xi}{\partial x^2}. \quad (11.62)$$

Note that these effects are special cases of the more general elastic behavior of a member subject to acceleration and external loading, specialized to the member with one long axis. The same general phenomena apply to joint structures (e.g., bearings and couplings) and drive-train components (e.g., gears and cables). The functional constraints on the structural design of these members may be more severe and limit the designer's ability to make them more rigid by adding more material. Under this constraint, the combined compliance of the flexible joint design and the rigidized link design results in inferior performance of the combination. A less rigid link with less inertia will raise the lowest natural frequency. Thus the design of the link and the joint must be coordinated.

Flexibility is only one of several link design constraints. Static compliance is obviously another based on the above discussion. Buckling and strength are two more considerations that constrain some of the same design parameters. While it has been shown that flexibility is a dominant constraint for typical arm design regimes [11.62], a simple optimization of bending stiffness of a beam with a tubular geometry illustrates the fallacy of ignoring buckling. If the radius of the tube is varied to maximize bending stiffness with constrained total mass, the radius increases without bound, producing a thin shell of infinitesimal thickness and infinite radius that lacks robustness. The true constraint becomes local buckling of the tube under slight perturbations of the applied load. A thin metal can illustrates this behavior as it crushes. Strength is another applicable constraint. Various materials differ in their strength, typically represented by their elastic limit or endurance limit on the stress at a point in the member. A sufficiently stiff member may fail due to stress, particularly at points of stress concentration.

In this presentation of options to overcome flexibility, and link flexibility in particular, radically different operational and design strategies should be recognized even though they are not the core of the treatment. The elastic modulus relates stress to strain, but physically the strain rate is sometimes a relevant term, providing structural damping to augment the joint or control-based damping. Composite materials have substantially more damping inherent in their behavior. Damping can be enhanced with passive damping treatments, with constrained layer damping having particularly pronounced effects [11.63]. Smart materials can also be

configured to enhance damping [11.64]. An operational strategy known as *bracing* can be combined with redundant actuation to achieve a large workspace for a flexible arm that provides gross motion and a smaller precision workspace after docking the large arm with a stationary structure, as described in [11.65].

The implication above is that flexibility was always due to the moving parts of the arm. However, the arm base itself may be a source of significant flexibility. If the base is stationary, the analysis may be almost identical to that of the flexible links of an arm. However, if the arm is mounted on a vehicle, tires or tracks may be the source of flexibility and empirical evaluation of these new elements might be the best solution. The vehicle could be a boat, aircraft, or space vehicle. Here there is no elastic connection to an inertial reference frame and some fundamental changes in approach will be needed. These changes are not unexplored and in some cases are simple extensions of the following approaches.

11.2.2 Modeling of Flexible Link Arms

Mathematical models of link flexibility trade accuracy for ease of use. It is therefore key to determine the effects that are important to represent accurately. The techniques presented here will assume linear elasticity with light damping. Rotational motions must be of modest angular rate so that centrifugal stiffening can be ignored. Small deflections will generally be assumed. These are reasonable assumptions for most robotic devices, but can be violated in more exotic applications, requiring reevaluation of the assumptions and more tortuous modeling approaches.

Four model types will be examined:

1. Lumped-element models having compliance or inertia but not both in a given member.
2. Finite-element models, which will be only briefly addressed.
3. Assumed mode models which readily include nonlinear dynamic behavior.
4. Transfer matrix models that incorporate the true distributed intermingling of compliance and inertia and consequently the infinite-dimensional nature of flexible link arms.

With the limited space available here, the discussion will be preliminary but should enable the reader to pursue one or more alternatives knowledgeably.

For lumped elements, one may build on the rigid kinematics presented in the section on fundamentals of kinematics (Chap. 2) that establishes rigid transformation matrices \mathbf{A}_i . The 4×4 homogenous transformations that describe position can be used to describe deflection

as well. Assuming small motions and static behavior (or negligible member mass), the transformation produced by elastic bending, torsion, and compression is

$$\mathbf{E}_i = \begin{pmatrix} 1 & -\alpha_{\theta Fi} F_{Yi}^i - \alpha_{\theta Mi} M_{Zi}^i & 0 & 0 \\ \alpha_{\theta Fi} F_{Yi}^i + \alpha_{\theta Mi} M_{Zi}^i & 1 & 0 & 0 \\ \alpha_{\theta Fi} F_{Zi}^i - \alpha_{\theta Mi} M_{Yi}^i & \alpha_{Ti} M_{Xi}^i & 0 & 0 \\ 0 & 0 & -\alpha_{\theta Fi} F_{Zi}^i + \alpha_{\theta Mi} M_{Yi}^i & \alpha_{Ci} F_{Xi}^i \\ -\alpha_{\theta Fi} F_{Zi}^i + \alpha_{\theta Mi} M_{Yi}^i & \alpha_{Ci} F_{Xi}^i & \alpha_{XFi} F_{Yi}^i + \alpha_{XMi} M_{Zi}^i & 0 \\ -\alpha_{Ti} M_{Xi}^i & \alpha_{XFi} F_{Yi}^i + \alpha_{XMi} M_{Zi}^i & \alpha_{XFi} F_{Zi}^i + \alpha_{XMi} M_{Yi}^i & 1 \\ 1 & \alpha_{XFi} F_{Zi}^i + \alpha_{XMi} M_{Yi}^i & 0 & 0 \\ 0 & 0 & 1 & 0 \end{pmatrix}, \quad (11.63)$$

where

α_{Ci} = coefficient in compression, displacement/force ,

α_{Ti} = coefficient in torsion, angle/moment ,

$\alpha_{\theta Fi}$ = coefficient in bending, angle/force ,

$\alpha_{\theta Mi}$ = coefficient in bending, angle/moment ,

α_{XFi} = coefficient in bending, displacement/force ,

α_{XMi} = coefficient in bending, displacement/moment ,

F_{Xi}^j = the force at the end of link i in the X direction of coordinate frame j ,

F_{Yi}^j = the force at the end of link i in the Y direction of coordinate frame j ,

F_{Zi}^j = the force at the end of link i in the Z direction of coordinate frame j ,

M_{Xi}^j = the moment at the end of link i in the X direction of coordinate frame j ,

M_{Yi}^j = the moment at the end of link i in the Y direction of coordinate frame j ,

M_{Zi}^j = the moment at the end of link i in the Z direction of coordinate frame j .

The listed coefficients depend on the construction of the element and are readily found for a slender beam from simple strength of materials. In other cases, a finite-element model or empirical measurements may be more readily used.

Alternating transformations for the undeformed and deformed aspects of N members (links or joints) produces the position vector of the end of arm (EOA)

$$\mathbf{p}^0 = (\mathbf{A}_1 \mathbf{E}_1 \mathbf{A}_2 \mathbf{E}_2 \dots \mathbf{A}_i \mathbf{E}_i \mathbf{A}_{i+1} \mathbf{E}_{i+1} \dots \mathbf{A}_N \mathbf{E}_N) \begin{pmatrix} 0 \\ 0 \\ 0 \\ 1 \end{pmatrix}. \quad (11.64)$$

If the massless elements connect rigid lumped masses, a linear spatial model is readily obtained, as described in [11.66]. Servo-controlled joints can also be inserted into this model. This analysis proceeds by examining the deflection of the elastic members produced by joint motion and the resulting forces and moments on the rigid inertias at the ends of the chain of links. The reference concentrates on the special case of only two inertias at each end of the chain but the technique is easily extended to inertias in the middle of the chain as well. The results are six linear second-order equations for each inertia and one first-order equation for each joint.

If the compliance and inertia properties are both to be treated as distributed throughout the same element, the partial differential equations (PDEs) introduced in the previous section for bending, torsion, and compression must be employed. Still insisting on a linear treatment, the general solution of these equations can be found in terms of each element with adjoining elements, i.e., the boundary conditions on the PDE. The convenient approach of Laplace transformation of these linear equations into the frequency domain, followed by factoring out the boundary conditions into a matrix–vector product, results in a technique known as the transfer matrix method (TMM) [11.67]. This method has been applied productively to general elastomechanics problems as well as specifically to flexible arms [11.68].

The transfer matrix relates variables at two stations along the arm with the number of variables depending on the model complexity. For the planar bending, deflection of the beam is shown in Fig. 11.9

$$\mathbf{z}_1 = \begin{pmatrix} -W \\ \psi \\ M \\ V \end{pmatrix}_1 = \begin{pmatrix} \text{--displacement} \\ \text{angle} \\ \text{moment} \\ \text{shear force} \end{pmatrix}_{\text{at station 1}}, \quad \mathbf{z}_0 = \mathbf{T}\mathbf{z}_1, \quad (11.65)$$

where T is the appropriate element transfer matrix.

If the element is a simple rotary spring with constant k and a damper with constant b , then the angle of rotation θ is related to the moment by a differential

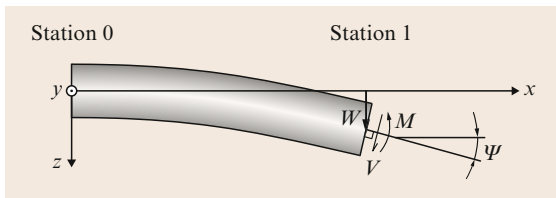


Fig. 11.9 State vector for the bending transfer matrix

equation with the following Laplace-domain representation

$$M = -L(k\theta + b\dot{\theta}) \Rightarrow k\Theta(s) + bs\Theta(s) = M_0 = M_1,$$

$$W_0 = W_1,$$

$$V_0 = V_1,$$

$$\Psi_0 = \Psi_1 - \Theta(s) = \Psi_1 - \frac{1}{k + bs}M_1.$$

Note that the only variable changed across the element is the angle related to the moment. The transfer matrix representation conventionally uses zero initial conditions and converts to the Fourier representation with $s = i\omega$. This leads to the transfer function

$$\mathbf{T} = \mathbf{C}(i\omega) = \begin{pmatrix} 1 & 0 & 0 & 0 \\ 0 & 1 & \frac{1}{k + b(i\omega)} & 0 \\ 0 & 0 & 1 & 0 \\ 0 & 0 & 0 & 1 \end{pmatrix},$$

which has the same form of the joint controller as shown in (11.69).

The beam model is much more complex, and the Euler–Bernoulli model gives

$$\mathbf{B} = \begin{pmatrix} c_0 & lc_1 & ac_2 & alc_3 \\ \frac{\beta^4 c_3}{l} & c_0 & \frac{ac_1}{l} & ac_2 \\ \frac{\beta^4 c_2}{a} & \frac{\beta^4 lc_3}{a} & c_0 & lc_1 \\ \frac{\beta^4 c_1}{al} & \frac{\beta^4 c_2}{a} & \frac{\beta^4 c_3}{l} & c_0 \end{pmatrix}, \quad (11.66)$$

where

$$\begin{aligned} \beta^4 &= \omega^2 l^4 \mu / (EI); \quad a = l^2 / (EI), \\ c_0 &= (\cosh \beta + \cos \beta) / 2, \\ c_1 &= (\sinh \beta + \sin \beta) / (2\beta), \\ c_2 &= (\cosh \beta - \cos \beta) / (2\beta^2), \\ c_3 &= (\sinh \beta - \sin \beta) / (2\beta^3), \\ \mu &= \text{density/unit length}, \\ \omega &= \text{circular frequency of vibration}, \\ E &= \text{elastic modulus}, \\ I &= \text{cross-sectional area moment of inertia}. \end{aligned}$$

The spatial variable has been transformed to the spatial Laplace variable but no longer appears explicitly. The Laplace time variable remains and is designated by s or by the frequency variable $\omega = -is$, where $i = \sqrt{-1}$.

The other transfer matrices needed for a simple planar model are as follows.

For a rotation in the plane of angle φ

$$\mathbf{A} = \begin{pmatrix} \frac{1}{\cos \varphi} & 0 & 0 & 0 \\ 0 & 1 & 0 & 0 \\ 0 & 0 & 0 & 0 \\ m_s \omega^2 \sin \varphi \tan \varphi & 0 & 0 & \cos \varphi \end{pmatrix}, \quad (11.67)$$

where m_s is the sum of all outboard masses from the angle to the end of the arm. This is an approximation resulting from ignoring compression elasticity. These elements appear as an additional mass to the extent they are translated with beam compression.

For a rigid mass, simply applying Newton's laws and collecting term yields

$$\mathbf{R} = \begin{pmatrix} 1 & l & 0 & 0 \\ 0 & 1 & 0 & 0 \\ -\frac{m\omega^2 l}{2} & I_m \omega^2 - \frac{m\omega^2 l^2}{2} & 1 & l \\ m\omega^2 & -\frac{m\omega^2 l}{2} & 0 & 1 \end{pmatrix}, \quad (11.68)$$

where m is the mass of the body, I_m is the mass moment of inertia about an axis through the center of mass and perpendicular to the plane of the arm, l is the length of the mass (the distance between the points of attachment at stations i and $i+1$), and $l/2$ is the distance to the center of mass from station i .

For a controlled joint with the controller transfer function (joint torque/joint angle) = $k(i\omega)$

$$\mathbf{C} = \begin{pmatrix} 1 & 0 & 0 & 0 \\ 0 & 1 & \frac{1}{k(i\omega)} & 0 \\ 0 & 0 & 1 & 0 \\ 0 & 0 & 0 & 1 \end{pmatrix}. \quad (11.69)$$

When combined to represent the planar arm with two joints as shown in Fig. 11.10, this analysis yields a composite transfer matrix that relates the four state variables at the two ends of the arm. Further analysis results from imposing the known boundary conditions at these ends.

The transfer matrix representation of an arm presented in [11.69] and pictured in Fig. 11.10 is shown in (11.70).

$$\begin{pmatrix} -W \\ \Psi \\ M \\ V \end{pmatrix}_0 = \mathbf{R}_1 \mathbf{B}_2 \mathbf{R}_3 \mathbf{A}_4 \mathbf{C}_5 \mathbf{B}_6 \mathbf{R}_7 \begin{pmatrix} -W \\ \Psi \\ M \\ V \end{pmatrix}_7. \quad (11.70)$$

In the example, the left end is pinned and the right end is free, yielding

$$\mathbf{z}_0 = \begin{pmatrix} -W \\ \Psi \\ M \\ V \end{pmatrix}_0 = \begin{pmatrix} u_{11} & u_{12} & u_{13} & u_{14} \\ u_{21} & u_{22} & u_{23} & u_{24} \\ u_{31} & u_{32} & u_{33} & u_{34} \\ u_{41} & u_{42} & u_{43} & u_{44} \end{pmatrix} \begin{pmatrix} -W \\ \Psi \\ M \\ V \end{pmatrix}_7, \quad (11.71)$$

$$\begin{pmatrix} u_{11} & u_{12} \\ u_{31} & u_{32} \end{pmatrix} \begin{pmatrix} -W \\ \Psi \end{pmatrix}_7 = \begin{pmatrix} 0 \\ 0 \end{pmatrix}.$$

The determinant of the 2×2 matrix must be zero when ω is a natural frequency, or a system eigenvalue if it is complex. This can be found by a numerical search. Evaluating variables (position, angle, shear, and moment) along the length of the arm with the eigenvalues used for the values of ω yields the eigenfunctions. If boundary conditions are not zero but known for given frequencies, the frequency response of the system can be obtained. Hence Bode plots are readily obtained for boundary condition forcing. Interior forcing can be handled using an extended state vector as described in [11.67], which was applied to arms in [11.61] and most recently updated with modern programming techniques in [11.68]. Inverse fast Fourier transform (FFT) will produce a time-domain response from the frequency response.

The creation of a state-space model in the time domain is attractive because it enables the use of powerful state-space design techniques and is compatible with the nonlinear behavior of arms undergoing large motion and experiencing centrifugal and Coriolis forces. The assumed modes method allows such a model to be constructed efficiently. The presentation here follows the early introduction of a recursive manner to calculate these equations introduced in [11.70]. The flexible kinematics of the links must be expressed as a sum of basis functions also known as assumed modes (shapes) $\varphi_i(x)$ with time-variable amplitudes $\delta_i(t)$

$$w(x, t) = \sum_{i=1}^{\infty} \delta_i(t) \varphi_i(x). \quad (11.72)$$

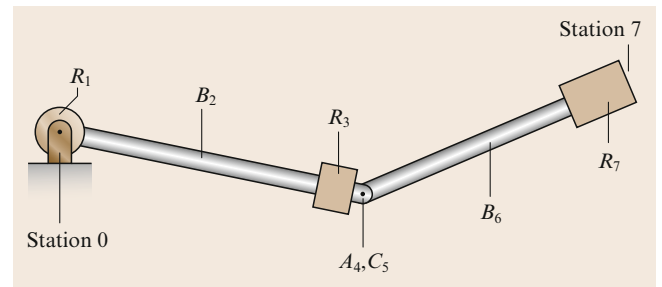


Fig. 11.10 Transfer matrix representation of an arm

The amplitudes and their derivatives become the states of the model. Compatible joint angle variables and their derivatives are also included as the rigid state variables. Joint angles tangent to the ends of the flexible links are compatible with mode shapes based on the clamped boundary conditions at one end and free boundary conditions at the other. This choice is generally chosen for simulation and the rigid coordinates are directly measured by standard joint angle transducers. If rigid coordinates are angles measured between lines connecting successive joint axes, the end of arm is known in terms of rigid coordinates alone and pinned–pinned boundary conditions are consistent. This produces advantages for inverse dynamics calculations as seen shortly.

The flexible and rigid kinematics combined describes the position and velocity of every point on the arm and can be used to express the kinetic energy \mathcal{T} and the potential energy \mathcal{V} . These expressions are used in the conservative form of Lagrange's equation

$$\frac{d}{dt} \frac{\partial \mathcal{T}}{\partial \dot{q}_i} - \frac{\partial \mathcal{T}}{\partial q_i} + \frac{\partial \mathcal{V}}{\partial q_i} = F_i, \quad (11.73)$$

where F_i is the force that does work as q_i is varied.

The kinematics of the deflection are again described by 4×4 transformation matrices, but this time the assumed mode shapes j are summed to give the position of link i

$$\mathbf{h}_i^j(\eta) = \begin{pmatrix} \eta \\ 0 \\ 0 \\ 1 \end{pmatrix} + \sum_{j=i}^{m_i} \delta_{ij} \begin{pmatrix} x_{ij}(\eta) \\ y_{ij}(\eta) \\ z_{ij}(\eta) \\ 0 \end{pmatrix}, \quad (11.74)$$

where x_{ij} , y_{ij} , and z_{ij} are the x_i , y_i , and z_i displacement components of mode j of link i 's deflection, respectively, δ_{ij} is the time-varying amplitude of mode j of link i , and m_i is the number of modes used to describe the deflection of link i

$$\mathbf{E}_i = \left(\mathbf{H}_i + \sum_{j=i}^{m_i} \delta_{ij} \mathbf{M}_{ij} \right), \quad (11.75)$$

where

$$\mathbf{H}_i = \begin{pmatrix} 1 & 0 & 0 & l_i \\ 0 & 1 & 0 & 0 \\ 0 & 0 & 1 & 0 \\ 0 & 0 & 0 & 1 \end{pmatrix} \quad (11.76)$$

and

$$\mathbf{M}_{ij} = \begin{pmatrix} 0 & -\theta_{zij} & \theta_{yij} & x_{ij} \\ \theta_{zij} & 0 & -\theta_{xij} & y_{ij} \\ -\theta_{yij} & \theta_{xij} & 0 & z_{ij} \\ 0 & 0 & 0 & 0 \end{pmatrix}. \quad (11.77)$$

This description is used in the formation of the potential and kinetic energy contributions of each element of mass. The integral over the link accumulates the total energy for that link and the sum over all links gives the energy of the arm system. Interchanging the order of integration and summation allows key invariant parameters to be identified, such as the *modal mass* that multiplies the second derivative of modal amplitude and the *modal stiffness* that multiplies the amplitude itself. The intermediate steps are aimed at the evaluation of Lagrange's equations, which separate into derivatives related to the rigid variables and the flexible variables. If the rigid variables θ are the joint variables, two groups of equations result

$$1. \quad \frac{d}{dt} \left(\frac{\partial \mathcal{T}}{\partial \dot{\theta}_j} \right) - \frac{\partial \mathcal{T}}{\partial \theta_j} + \frac{\partial \mathcal{V}_e}{\partial \theta_j} + \frac{\partial \mathcal{V}_g}{\partial \theta_j} = F_j \quad (11.78)$$

$$2. \quad \frac{d}{dt} \left(\frac{\partial \mathcal{T}}{\partial \dot{\delta}_{jf}} \right) - \frac{\partial \mathcal{T}}{\partial \delta_{jf}} + \frac{\partial \mathcal{V}_e}{\partial \delta_{jf}} + \frac{\partial \mathcal{V}_g}{\partial \delta_{jf}} = 0, \quad (11.79)$$

where the subscript e indicates elasticity, subscript g indicates gravity, and δ indicates the amplitude of a mode shape.

The simulation form of the equations is achieved by grouping all second derivatives of the rigid and flexible coordinates, which yields

$$\begin{pmatrix} \mathbf{M}_{rr}(\mathbf{q}) & \mathbf{M}_{rf}(\mathbf{q}) \\ \mathbf{M}_{fr}(\mathbf{q}) & \mathbf{M}_{ff}(\mathbf{q}) \end{pmatrix} \begin{pmatrix} \ddot{\theta} \\ \ddot{\delta} \end{pmatrix} = - \begin{pmatrix} 0 & 0 \\ 0 & \mathbf{K}_s \end{pmatrix} \begin{pmatrix} \theta \\ \delta \end{pmatrix} + \mathbf{N}(\mathbf{q}, \dot{\mathbf{q}}) + \mathbf{G}(\mathbf{q}) + \mathbf{R}(\mathbf{q}, \dot{\mathbf{q}}, \mathbf{Q}), \quad (11.80)$$

where θ is a vector of rigid coordinates, usually the joint variables, δ is the vector of flexible coordinates, $\mathbf{q} = [\theta^T \delta^T]^T$, \mathbf{M}_{ij} is the *mass* matrix for rigid and flexible coordinates corresponding to the rigid ($i, j = r$) or flexible ($i, j = f$) coordinates and equations, $\mathbf{N}(\mathbf{q}, \dot{\mathbf{q}})$ contains the nonlinear Coriolis and centrifugal terms, $\mathbf{G}(\mathbf{q})$ captures gravity effects, \mathbf{Q} represents the externally applied forces, and \mathbf{R} captures the effect of external forces and all other nonconservative forces including friction.

On the other hand, the inverse dynamics form of the equations is (assuming negligible friction)

$$\mathbf{Q} = \begin{pmatrix} \mathbf{M}_{rr}(\mathbf{q}) & \mathbf{M}_{rf}(\mathbf{q}) \\ \mathbf{M}_{fr}(\mathbf{q}) & \mathbf{M}_{ff}(\mathbf{q}) \end{pmatrix} \begin{pmatrix} \ddot{\theta} \\ \ddot{\delta} \end{pmatrix} + \begin{pmatrix} 0 & 0 \\ 0 & \mathbf{K}_s \end{pmatrix} \begin{pmatrix} \theta \\ \delta \end{pmatrix} - \mathbf{N}(\mathbf{q}, \dot{\mathbf{q}}) - \mathbf{G}(\mathbf{q}). \quad (11.81)$$

In general, Q is dependent on the vector T of motor torques or forces at the joints, and the distribution of these effects is such that

$$Q = \begin{pmatrix} B_r \\ B_f \end{pmatrix} T, \quad (11.82)$$

where T has the same dimensionality as q_r . By rearranging the inverse dynamics equation, we obtain

$$\begin{pmatrix} B_r & -M_{rf} \\ B_f & -M_{ff} \end{pmatrix} \begin{pmatrix} T \\ \ddot{\delta} \end{pmatrix} = \begin{pmatrix} M_{rr} \\ M_{rf} \end{pmatrix} \ddot{\theta} + N(q, \dot{q}) + G(q), \quad (11.83)$$

which is arranged with a vector of unknowns on the left-hand side of the equation and the prespecified rigid and solvable flexible coordinates on the right. This is at least approximately true, with the caveat that the nonlinear and gravity terms have a weak influence on the immediate flexible coordinates, which are not simultaneously known but which can be estimated for the next time step.

One consequence of the distributed flexibility is non-minimum-phase behavior. This can occur for other cases where the excitation is separated from the output point by mass and flexibility, a condition known as non-collocation. These systems are characterized by a step response in which the initial movement is opposite in sign from the final movement. This is simply characterized for linear systems as a transfer function zero in the right half-plane. As will be shown in the section on Command Generation, it may be possible to overcome this problem by redefining the output.

11.2.3 Control

Appropriate reaction to flexible dynamics requires appropriate sensors. While a Kalman filter can theoretically observe flexible link states from joint measurements, it is based on back driving the joint from the various modes of flexible dynamics. More reliable indications of flexibility include strain gauges, accelerometers, and optical sensors.

Sensors for Flexibility Control

The strain of a beam element is a direct indication of curvature, which is the second spatial derivative of beam deflection, as indicated in (11.57). Modern semiconductor strain gauges have high gauge factors producing a good signal-to-noise ratio. The second spatial derivative relationship means that a slight change in location can result in a large change in the reading, but once affixed to the arm this is not a problem. More of a problem is the relatively short lifetime of a strain gauge subject to wear and tear if not carefully protected.

By suitably placing strain gauges, good measurements of multiple assumed modes are possible.

Optical measurement of deflection can be very versatile but is subject to interference between a target measurement point and the sensor, particularly if the sensor is stationary. If the sensor is mounted on the link, this difficulty is reduced but optical measurements are then usually a complex combination of the rotation of the optical axis of the sensor and the deflection of the target. Machine vision senses a wide field of view but typically with less precision. Multiple points can be detected, which is attractive in measuring multiple modes. Machine vision requires considerable processing and, even for enhanced targets or retroreflective fiducials, sample rates can be slow relative to some modes of control interest.

Accelerometers are attractive transducers in that they do not require explicit grounding to a fixed frame. Microelectromechanical systems (MEMSs) accelerometers provide the required low-frequency sensitivity and are very inexpensive. However, they are subject to orientation in a gravity field, which must be compensated for by knowing the orientation of the sensor. If one is interested in position, accelerometers require two integrations and are consequently subject to drift in position measurement. Consequently, the combined use of sensors is appealing. For example, vision sensors, which are relatively slow but give direct position information for the end of a flexible member, can be combined with accelerometers, which give information about the same point at high sample rates but with noise and drift problems. The two sensor readings can be combined with a Kalman filter or other fusion scheme.

Issues Related to Model Order

Realizing that the theoretical order of a flexible arm is infinite, one should be prepared to deal with certain issues related to model order. The first of these is possible aliasing problems arising from finite sampling rates. Antialiasing filters should be employed, and even more effective is the use of analog damping by materials, damping treatments, or the back electromotive force (emf) of actuators to provide an inherent damping of the system under digital control. A more subtle problem is that of measurement and control spill over.

Control of Special Configurations: Macro/Micro Redundancy

Several special configurations have been proposed to enable improved controlled performance of flexible link arms. The problem with noncollocation noted above is a case in point. In some cases, a large range of motion and high accuracy cannot be achieved with a single set of actuators. Redundant degrees of freedom can then

be employed with the macro degrees of freedom that provide large range of motion but with inherent lack of precision or accuracy. Vibrations are particularly difficult to eliminate with a long arm, and construction accuracy and even thermal drift can exceed the tolerance limits. If the gross motion is completed quickly, residual vibrations may remain and be very lightly damped. Actuators constructed for gross motions of large axes do not have the bandwidth capabilities to damp these vibrations actively, but small motion axes typically do. This has been illustrated in several instances for long-reach manipulators when exploring nuclear waste cleanup solutions [11.71–74]. Using the inertial forces generated at the end of the arm also has the advantage of creating forces collocated with the measurements being used for control, assuming the base of the micro arm is at the end of the macro arm and the location of sensors. *Book and Loper* [11.73] and *George and Book* [11.75] have shown that this control is possible based on accelerometers in multiple degrees of freedom. It is also possible to excite undesired modes which have not been accounted for. If the full six degrees of freedom are used it is possible to argue stability based on a simple passive analogy. Generating prescribed forces at the base of an articulated micromanipulator is a challenging task, requiring the solution of a new type of inverse dynamics problem, which solves for motions or joint torques to produce the prescribed base forces and moments.

Command Generation for Flexible Link Arms via Command Shaping

The trajectory undertaken by a flexible arm can dramatically affect the consequences of flexibility. Purely

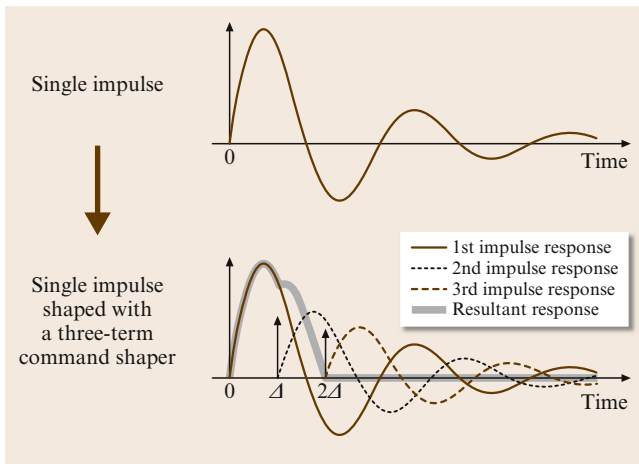


Fig. 11.11 Impulse response of a shaper and the effect on a vibratory system. Time is normalized by the intersample time T_s and T_d , chosen such that $\Delta = T_d/T_s$ is an integer

open-loop anticipation of the flexible dynamics has been used to create motion profiles wherein the motion cancels the incipient oscillation that had been created by earlier motions. This strategy is referred to as command shaping. A more complicated strategy to implement is a true inverse-dynamics-based trajectory wherein the rigid and flexible states are all orchestrated to arrive at the desired point in state space, typically at a static equilibrium. The high order of the flexible model is further complicated by the non-minimum-phase nature of the noncollocated system and noncausal inverse is necessary to produce a physically realizable trajectory (VIDEO 778).

Time delay command shaping is a variation of the deadbeat control introduced by [11.76, 77]. It can be couched in terms of a finite impulse response filter with a simple impulse response as depicted in Fig. 11.11 with a single input impulse producing a small number (typically two to four) of output impulses with appropriate time spacing and amplitudes. Extensions by *Singer and Seering* [11.78] and *Singhose et al.* [11.79] have produced more robust varieties under the trademark Input Shaping. The robustness is enhanced by using more output impulses and appropriate selection of the impulse spacing. The optimal arbitrary time-delay (OAT) filter [11.80, 81] reduces this selection to a simple formula for linear vibrations that depends on the natural frequency and damping ratio of those modes to be eliminated from the response. The simplicity of implementation is illustrated in Fig. 11.12, where the relationships between the filter parameters and the mode parameters are

$$\begin{aligned}\text{coefficient 1} &= \frac{1}{M} \\ \text{coefficient 2} &= \frac{-(2 \cos(\omega_d T_d) e^{-\zeta \omega_n T_d})}{M} \\ \text{coefficient 3} &= \frac{e^{-2\zeta \omega_n T_d}}{M} \\ M &= 1 - 2 \cos(\omega_d T_d) e^{-\zeta \omega_n T_d} + e^{-2\zeta \omega_n T_d}\end{aligned}$$

$$\omega_d = \omega_n \sqrt{1 - \zeta^2} = \text{damped natural frequency}$$

$$\omega_n = \text{undamped natural frequency}$$

$$\zeta = \text{damping ratio}$$

$$T_d = \text{time delay selected, an integer number of samples.}$$

(11.84)

Note that the formulation here is oriented toward digital systems with fixed sampling intervals such that the time delay of the filter is adjusted to an integer

number of sampling intervals. Command shaping has been applied to a wide range of flexible systems including disk drives, cranes, and large robot arms, such as the example by CAMotion (📺 VIDEO 777) as shown in Fig. 11.13. Note that this example contains a flexible drive belt, effectively a flexible joint, as well as flexible links that contribute to the compliance of the lowest mode that is quenched with an OAT filter.

Adaptive versions of command shaping have also been demonstrated. A version oriented toward repetitive motion applications is presented in [11.82].

Command Generation for Flexible Link Arms via Inverse Dynamics

In contrast to the scant system knowledge required for command shaping, the inverse dynamics of a flexible arm requires a great deal of knowledge about the system. The creation of an appropriate model was discussed above. An assumed modes model, for example, is well adapted to inverse dynamics if the rigid coordinates are not the joint angles, but the angles between lines connecting the joint axes (where it is assumed that joints are rotational). In this case, the desired end-of-arm motion can be expressed solely in terms of rigid variables, that is, the same variables q_d used in the flexible joint case, and the desired flexible variables are found from the second-order equations driven by the known rigid positions and velocities. The remaining difficulty is the unstable zero dynamics of the system.

For the purposes of introduction, only the linear situation will be treated here in the fashion of [11.83]. First, the rigid coordinates and their derivatives are found from the desired end-of-arm motion profile. The flexible equations are separated into causal stable zeros and anticausal unstable zeros, and the stable inverse is solved forward in time. Physically the motion response responds after the torque inputs. The computational input however is the response and the torque is calculated as an output, so no physical laws are violated in solving the anticausal portion beginning at the final time when flexible coordinates are specified to be zero and proceeding to the initial time and beyond. In fact, the exact solution extends from negative infinity (where the anticausal solution decays) to positive infinity (where the causal solution decays). For realistic dynamics, the necessary time for the input is only slightly more than the motion time for the end of the arm because the zeros are often quite far from the origin in both directions. If the end-of-arm motion begins at time zero, shortly before that, the joint torques begin to *pre-shape* the flexible links without moving the end of arm. Similarly, when the end of the arm reaches its final position, the joint torques must release the arm deflection in a manner that is not seen from the

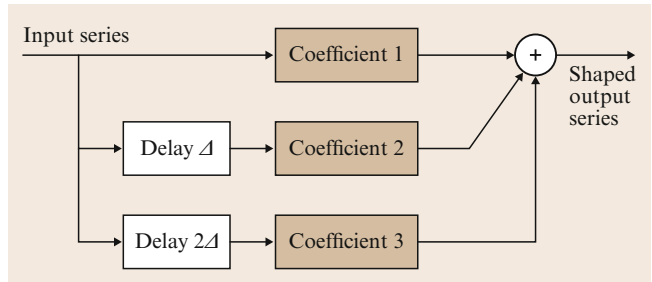


Fig. 11.12 Block diagram representation of the command shaping algorithm

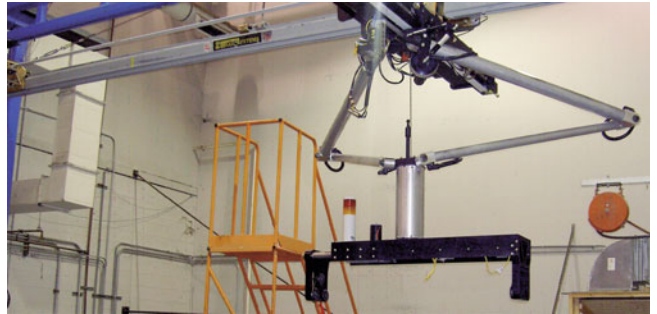


Fig. 11.13 A large flexible linking arm with command shaping

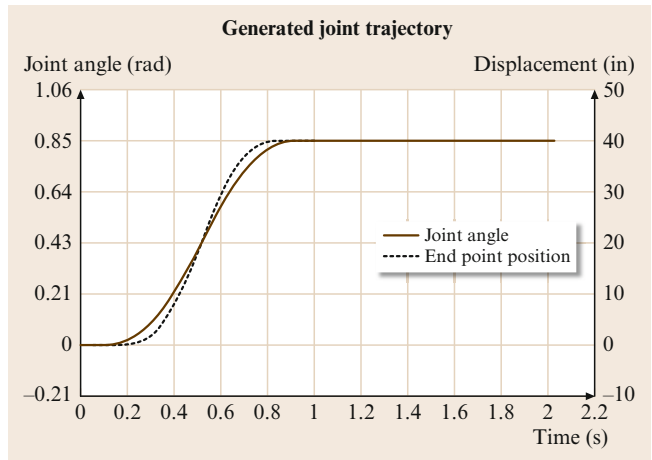


Fig. 11.14 Inverse dynamics driven motion of a single-link flexible arm

end of arm (or any other chosen output location). Figure 11.14 shows the example from Kwon [11.84] for a single-link arm and the 📺 VIDEO 778 shows the behavior improvement.

Since inversion of the flexible plant as described earlier containing nonminimum phase or *unstable* zeros can result in an anticausal input torque to achieve an arbitrary trajectory, it is appropriate to look for other trajectories with special characteristics that avoid these

problems. The location of zeros are dependent on where on the flexible link the trajectory is specified. *De Luca* et al. studied the one flexible link rotational arm and the migration of zeros as the point of interest is shifted from tip to joint. They utilize a point where zeros are nonexistent as the output point, a point that enables inversion to proceed without the causality problem [11.85–87]. When this point reaches the desired angle with zero deflection, the end point will also be at the desired angle. Joint velocity and deflection velocities must also be brought to zero resulting in a rest-to-rest motion completed in specified time and with no residual oscillations. The cited references show the equivalence of this development in the time or frequency domain for linear systems. For a two link arm (only the forearm is flexible), the nonlinear behavior demanded a time domain approach [11.86].

De Luca and *Di Giovanni* [11.85] address rest-to-rest motion of a single flexible link and carries through an example for a single flexible mode. The later reference [11.87] also provides experimental results for which a brief video (VIDEO 779) is available. The strength of this approach is its relative simplicity in achieving the desired final position described by a single polynomial. The degree of the single polynomial required to meet all the boundary conditions is $4n_c + 3$ where n_c is the number of flexible modes. One difficulty is the inability to efficiently constrain the peak torque required. Torque profiles developed in this simplest of strategies have high peaks but for most of the trajectory (at start and end) are relatively low. Hence the peak torque capabilities of the actuator may not be efficiently used. It is not necessary for a single polynomial to describe the entire trajectory, of course, but the complexity of developing the response without zeros becomes more challenging for piece wise polynomials, and arises from meeting all the boundary conditions on polynomial segments. The nonlinear case arising from a two link arm with the forearm flexible [11.86] provides further exploration of the inversion approach for flexible arms.

The model employed by *De Luca* varies slightly since deflection is measured from an axis passing through the dynamic center of mass of the flexible arm as shown in Fig. 11.15, not the tangent to the neutral axis of the beam at the rotary actuator. This modifies the boundary conditions on the shape equation and hence the mode shapes. For an introduction, a single flexible link is considered here. Variables are defined as follows:

- J_0, J_p : rotary inertia of the rotary actuator, tip payload, respectively
- m_p : mass of the tip payload

- $\theta, \theta_c, \theta_t$: angles through center of mass, tangent to actuated end, and through tip, respectively
- x : axis through the center of mass (COM)
- y : deflection perpendicular to x .

Consider the case with no damping on the modes. While modal damping is readily incorporated, its typically low values justify an abbreviated treatment here for the sake of space and simplicity. The output y specified is the sum of the angle (to the center of mass), the angular velocity, deflections and deflection rate, each times appropriate gains. These gains are found by specifying the transfer function from joint torque to y to be of maximum relative degree, i. e., it has no zeros. Equivalently, the successive derivatives of y do not explicitly involve the torque until the $(2n_c + 1)$ -th derivative. Note that these characteristics ascribed to differentially flat systems may yield a more complete understanding of this approach [11.88, 89],

$$\frac{y(s)}{\tau(s)} = \frac{K}{s^2 \prod_{i=1}^{n_c} (s^2 + \omega_i^2)},$$

$$K = \frac{1}{J} \prod_{i=1}^{n_c} \omega_i^2.$$

When transformed to the time domain, the resulting form of the torque based on derivatives of the desired output will be

$$\tau_d(t) = \frac{J}{\prod_{i=1}^{n_c} \omega_i^2} \left[y_d^{(2(n_c+1))}(t) + \sum_{i=0}^{2n_c-1} \alpha_i y_d^{(i+2)}(t) \right].$$

The α_i values are readily found from the convolution of the polynomial or expansion of the denominator of $y(s)/\tau(s)$. But what must be used for y_d ? With the given definition of y , the desired value of y_d for the rest-to-rest trajectory will be achieved by creating an interpolating trajectory with the desired initial and final values of y_d

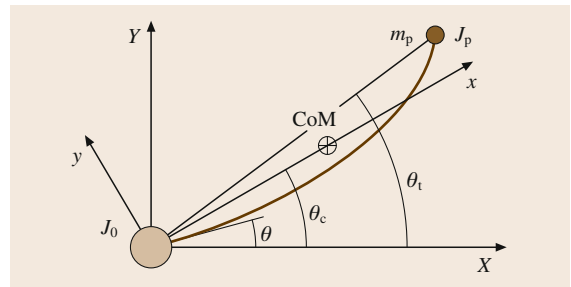


Fig. 11.15 A definition of variables for the causal inversion of *De Luca*

and derivatives of y_d at the initial and final times that are zero. The number of derivatives to set equal to zero are at least $2n_e + 1$, but it may be preferred to set additional derivatives equal to zero to obtain a smoother torque at the ends of the trajectory. As explained in [11.85] this is a transformation of states that results also in the desired rest-to-rest behavior of the joint angle, the deflection and their derivatives. For more robustness, the feedforward command should be supplemented with feedback control, for example a simple PD or PID control of the joint angle to follow y_d .

Shown in Fig. 11.16 are the torque and resulting bending deflection for a 2.2 s move using this combination on a single link flexible arm [11.87].

To best comprehend these results, some details of the flexible arm in the experiment are needed. The desired trajectory was defined by a polynomial of degree 19. The arm length was 0.655 m, of sheet steel 2 mm thick and 51 mm wide, directly driven by a DC motor with inertia of $1.888 \times 10^{-3} \text{ kg m}^2$ and no tip mass. The resulting natural frequencies were 14.4, 13.2 and 69.3 Hz with damping ratios of 0.0001, 0.001, and 0.008, respectively. Frequency errors of the model were less than 1%. Friction compensation was applied based on static and viscous models of the friction under continuous rotation.

Feedback Control of Flexible Links

Flexibility in the links is in some cases controlled in the same way as concentrated flexibility in joints. Herein the focus is on approaches that apply specifically to link flexibility; consequently the use of Kalman filtering to estimate tip position and other broadly used techniques are not reexamined. A long history of research

on this topic exists. *Cannon and Schmitz* [11.90], *Truckenbrodt* [11.91], and others showed that these techniques work for flexible link arms and that the noncollocated nature of the system aggravates the sensitivity to modeling errors.

Strain measurements provide a valuable indication of the state of a flexible link, and strain rate, obtained from filtered differentiation of the typically noisy strain signal, was shown by *Hastings and Book* [11.92] to be an appropriate way of overcoming the limitations imposed by purely joint feedback control. *Yuan et al.* [11.93] produced an adaptive version of strain-rate feedback.

Strain measurements readily lend themselves to calculation of the modal amplitudes, and the number of appropriately placed strain gage measurements N can be equal to the number of mode amplitudes to be evaluated. In this case, no estimation algorithm is necessary, although filtering is usually needed. If the mode shape φ_i of a beam is known, strain is proportional to the second derivative of φ_i

$$\alpha_{ij} = \left. \frac{\partial^2 \varphi_i}{\partial x^2} \right|_{x_j} \quad (11.85)$$

By inverting the coefficient matrix thus formed, it is simple to obtain the amplitude of N modes as

$$\begin{pmatrix} \delta_1 \\ \delta_2 \\ \vdots \\ \delta_N \end{pmatrix} = \begin{pmatrix} \alpha_{11} & \alpha_{12} & \dots & \alpha_{1N} \\ \alpha_{21} & \alpha_{22} & \dots & \alpha_{2N} \\ \vdots & \vdots & \ddots & \vdots \\ \alpha_{N1} & \alpha_{N2} & \dots & \alpha_{NN} \end{pmatrix}^{-1} \begin{pmatrix} \varepsilon_1 \\ \varepsilon_2 \\ \vdots \\ \varepsilon_N \end{pmatrix} \quad (11.86)$$

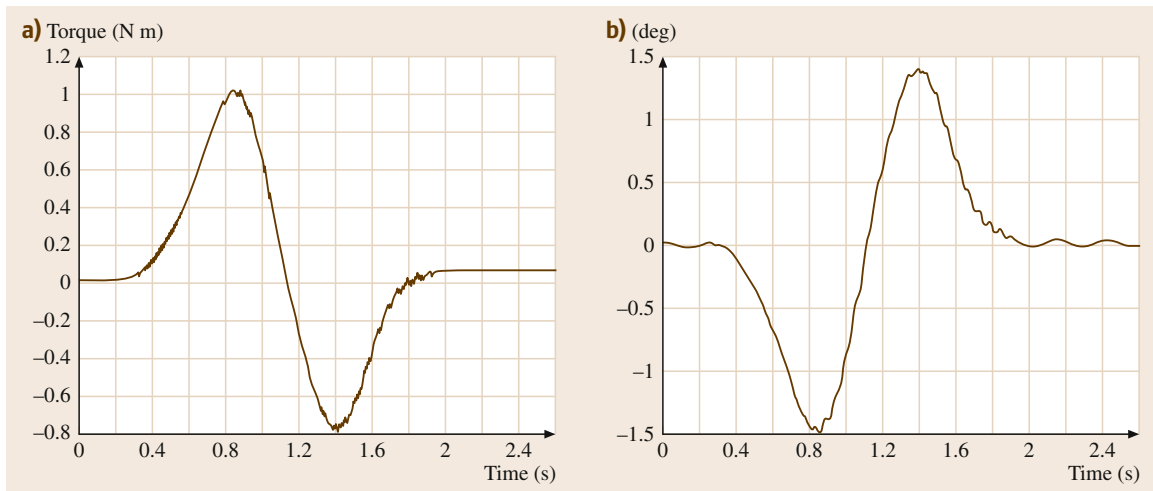


Fig. 11.16 (a) Applied torque for rest to rest motion with PD control. (b) Bending deformation at the tip

Additional attention is necessary if beam torsion is a significant part of the mode deflection, but the principle still applies. Active control of high-frequency modes may not be warranted, and feedback of the one or two lowest-frequency modes can be managed by classical or state-space design techniques to increase the damping of that mode.

The use of the measurement of the end-of-arm position has perpetual appeal and is very effective for rigid arms for the elimination of variability due to arm distortion and the change over time of arm calibration. Machine vision can eliminate uncertainty in the target position as well as the arm position. These approaches are plagued by the noncollocated and hence non-minimum-phase dynamics of link flexibility, however, and may require particular caution. Wang and Vidyasagar [11.94] proposed an alternative formulation of EOA measurements in the control formulation that he called the reflected tip position. For a rotating link of angle θ and length l , the deflected position is $l\theta + \delta$ while the reflected tip position $l\theta - \delta$ is minimum phase. This combination of joint and tip measure-

ments produced the desired undeflected position but would not serve for EOA tracking control. Obergfell and Book [11.95] synthesized an output based on strain feedback combined with EOA position that allowed tracking control as well. They first produced a passive system with deflection feedback obtained from optical measurements of the link deflection, and then devised a traditional feedback control of the tip position measured by machine vision of the large two link arm shown in Fig. 11.17 for the experimental robot RALF (robot arm long and flexible). Figures 11.18 and 11.19 compare the path for a large square traced in a plane with only the deflection feedback and with both deflection and EOA position feedback.

Robust Estimation for Flexible Link Systems

The state feedback algorithms readily designed for linear flexible link systems are dependent on information about states that cannot be directly measured and are theoretically infinite in number. Truncation of the states to represent the most dominant low frequency modes is a ready solution to the second problem and state estimators or observers present a viable approach to the first problem. (Estimator and observer are commonly used interchangeably, but the term observer is more common will be used in this section.) For linear systems a Luenberger observer or the stochastically based Kalman filter are commonly used. Unfortunately, observers require an accurate system model or the estimates may be poor and the observer, a dynamic system



Fig. 11.17 Robotic arm large and flexible (RALF) used in EOA feedback experiments

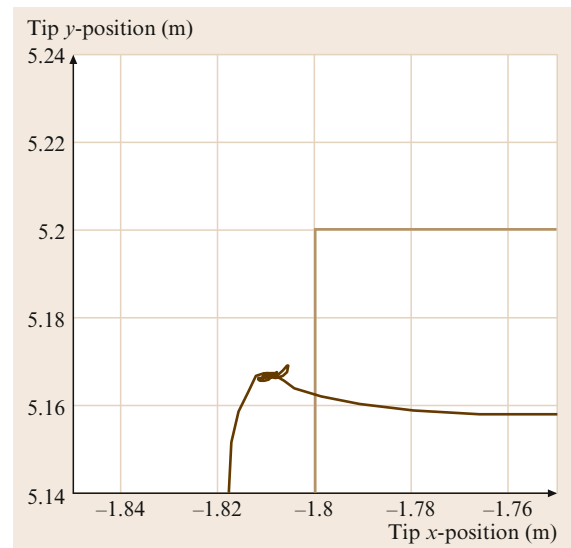


Fig. 11.18 Path followed without EOA position feedback. (Commanded trajectory is a square partially shown in light brown. Actual trajectory shown in dark brown)

of order as high as the order of the system itself, may even be unstable. Hence the robustness of the state observer is a critical subject for the control of flexible link systems. The quality of the control is ultimately the best measure of the quality of the estimator. Robust observer design has been the subject of considerable research and, in large part, mirrors the development of robust controllers. This is natural since an observer is a dynamic system which, like the plant itself, can be controlled to achieve a desired outcome. *Control effort* of the observer is utilized to drive convergence of the estimated outputs of the observer to the measured outputs of the real system. Hence research on estimators based on H-infinity, fuzzy logic, neural network, sliding mode, adaptive, and other design techniques abound. In this chapter, two types of observers will be discussed: sliding mode observers and multiple model observers.

For all observers the placement of sensors is crucial and for estimation of multiple modes it is desirable, although not theoretically essential, to use multiple sensors. Joint sensors (position and velocity) are typically available for general pose (joint) control, but for deflection sensing strain gages and accelerometers are currently most appropriate. The MEMS accelerometers now readily available and inexpensive will be the principle choice here. Strain gages are more fragile and generally provide more complex readings of the mode behavior. Accelerometers are complicated by the fact that acceleration is not dependent on just states z which include the mode amplitudes and their derivatives, but also on the input u creating the link motion. Acceleration measurement of a point p on the link is affected by both the states z and the input u as follows,

$$\ddot{x}_p = \left\{ -\beta(p)[\Phi][\omega^2] - \beta(p)[\Phi][\hat{C}] \right\} z + \left\{ \beta(p)[\Phi][\Phi]^T Q \right\} u,$$

where \ddot{x}_p is the acceleration in the direction perpendicular to the beam axis, Φ is the matrix of eigenvectors, z is the state vector, composed of joint motion as well as beam deflections, p is the location of the sensor along the beam axis, ω^2 is the diagonal matrix of natural frequencies squared, \hat{C} is the modal damping matrix, $\beta(p)$ expresses the sensor motion in terms of the modal states variables, and Q relates the input to the system states.

As Post [11.96] has explained, the ability of a given sensor to detect a mode depends on the amplitude of the mode at the sensor location. Overall the singular values of the observability grammian, also used for testing the system observability, is a reasonable but not perfect

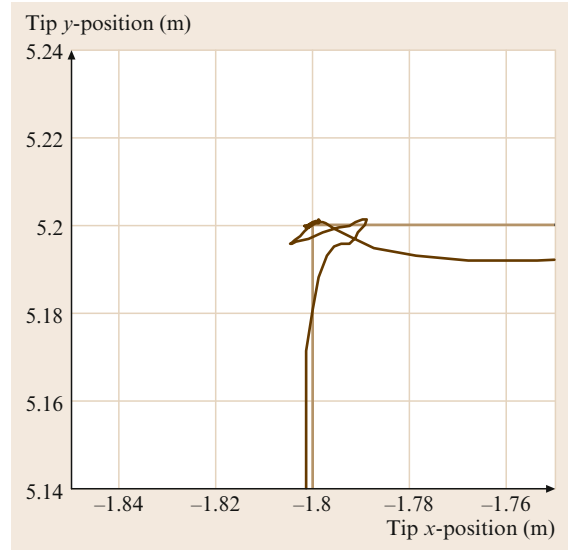


Fig. 11.19 Path followed with EOA feedback from camera. (Commanded trajectory is a square partially shown in light brown. Actual trajectory shown in dark brown)

metric. A robust measurement requires the placement of sensors so as to avoid nodes (zero crossings) of the modes to be sensed even when parameters of the system change or are inaccurate. A single sensor (strain gage or accelerometer) is much more likely to have this problem than multiple sensors. The next sections depend on suitably placed sensors. For those modes not being controlled, one should minimize their influence by placing sensors near the node of those modes. This helps to avoid spillover of these modes that interferes with the system as approximated.

Parametric Errors in System Model

Parametric errors are inaccuracies in the parameters of a model with an accurate representation of the system structure. For flexible link systems this might arise from inaccurate payload mass, stiffness values, stiffness distribution, boundary conditions, etc., all of which lead to inaccurate mode shapes, natural frequencies and input coefficients. Errors are inevitable to some degree. As a consequence of parametric errors, one of the most powerful results of linear feedback control of estimated states, the separation principle which says the design of the observer does not change the eigenvalues of the controlled system and vice versa, is compromised. The rapid convergence of observer error to zero will in general not occur with parametric error. The net effect is a major blow to the effectiveness of the classical Luenberger observer. The Kalman filter, which optimizes observer gains under conditions of Gaussian process and measurement noise, is likewise

compromised. Without good state estimates the effectiveness of the powerful state feedback approaches are in jeopardy.

One currently popular tack to improve the robustness of observers is the sliding mode observer. There are several variations of this approach, and the technique by *Wallcot* and *Zak* [11.97, 98] was followed by *Post* [11.96] in exploring the consequences of parametric error. As typical, a sliding surface is defined which is intended to guide the estimate error to zero. The reaching phase moves from the initial error state to the sliding surface and when that surface is crossed the sign on the control changes. This rapid switching may be modified by establishing a *boundary layer* near the switching surface that substitutes a linear behavior.

In this section, we will use z as the state vector, \hat{z} as its estimate, L as the feedback of the observer, y as the measurement and K_s as the sliding mode gain. The *hat* on a variable will generally denote its estimate and an over dot its time derivative. The symbol Δ preceding a symbol indicates the variation of the true system parameter from its model. The linear plant model is thus

$$\dot{z} = Az + Bu; \quad y = Cz + Du.$$

The equation approaching the switching surface is

$$\dot{\hat{z}} = A\hat{z} + Bu + L(y - \hat{y}) + K_s \text{sgn}(y - \hat{y}).$$

When the boundary layer is included, the control is changed in a region near the switching surface where the design is essentially a conventional linear observer. For present purposes we will not employ a boundary layer but examine the pure sliding mode case, for which the error equation is

$$\dot{e} = A_0 e - K_s \text{sgn}(Ce) + \Delta Az + \Delta Bu,$$

which clearly has a steady state error solution that is not zero except in the case that $\Delta Az = -\Delta Bu$ which tends to occur when the overall system comes to rest. Thus the convergence of the sliding mode observer has similar issues found with the conventional linear observers. They can be stable but can converge to the wrong steady state value leading to error, particularly after the observer's state estimates should have converged to the slower changing system state. However, when the overall plant reaches steady state and $z = 0$, $u = 0$, the observer error will also converge to zero. In contrast, the usual intent is to design the observer to quickly converge to the true state estimate in order to appropriately control the plant.

Successful Estimation with Model Parameter Uncertainty

Models are seldom, if ever, exact in their representation of a physical system. In addition to error in parameter identification, parameters can change with time and operating conditions. For example, robots acquire and release payloads and move to different poses which may change parameters. As reported before, convergence of state observers is adversely affected by these changes which can lead to poor performance and even instability. In a recent work, *Post* [11.96] described a multiple model estimation scheme that successfully overcomes these limitations for a flexible link robot in both simulation and experiment. Other authors, e.g., *Chalhoub* and *Kfoury* [11.99] have used fuzzy logic techniques to address the needs for improving sliding mode observers.

Since the true state of the system is not known, the steady state estimation error cannot be calculated, but if it is known to exist, *Post* has shown it to be proportional to parameter error. Hence multiple models based on a different set of sensors can be used to establish which is most accurate. The difference in estimated states based on two sensor selections $\delta_z(t) = \hat{z}_{s_1} - \hat{z}_{s_2}$ is then a metric for choosing between alternative observers in an array of observers with different assumed parameters.

The observers themselves (conventional Luenberger observers or Kalman filters) have the form

$$\dot{\hat{z}}_{s_1}(t) = A\hat{z}_{s_1}(t) + Bu(t) + L_{s_1}[y_{s_1}(t) - \hat{y}_{s_1}(t)],$$

where \hat{z}_{s_1} is the estimate of the state vector z using the sensor array 1, A is the plant matrix, B is the input matrix, L_{s_1} is the gain matrix to be designed, y_{s_1} is the sensor measurement of sensor array 1, and \hat{y}_{s_1} estimate of sensor measurement of sensor array 1, and similarly for sensor s_2 . The difference between states and their estimates converges rapidly (relative to the states themselves) to steady state and hence $\hat{z}_{s_1} - \hat{z}_{s_2}$ converges to zero and hence

$$\begin{aligned} \delta_z(t) = & \chi_1[\Delta Az(t) + \Delta Bu] \\ & + \chi_2[\Delta C_{s_1}z(t) + \Delta D_{s_1}u(t)] \\ & + \chi_3[\Delta C_{s_2}z(t) + \Delta D_{s_2}u(t)] \end{aligned}$$

is found to be the *steady state* slowly changing (relative to the observer dynamics) difference in the two observers based on sensors s_1 and s_2 . Here, the χ_i are constant matrices based on the model parameters and not the true values of the system. Δ indicates the deviation of the true matrices from the model's matrices following that symbol. Note that subscripts s_1 and s_2 indicate different sensors involved in the measurement

and feed through matrices C and D , respectively. Also note that this equation is somewhat complicated by the feedthrough matrices occurring due to the use of accelerometers to sense the motion.

Incorporating the specific representation of a linear flexible manipulator, the equations are

$$\dot{z} = \begin{pmatrix} 0_{(n \times n)} & I_{(n \times n)} \\ -\omega_{(n \times n)}^2 & -\hat{C}_{(n \times n)} \end{pmatrix} z + \begin{pmatrix} 0_{(n \times m)} \\ \hat{Q}_{(n \times m)} \end{pmatrix} u,$$

where \hat{C} denotes modal damping and \hat{Q} denotes the modal forcing coefficient. The sensor's output is

$$y_{Si} = \left\{ -[1, \psi_1(p_{Si}), \dots, \psi_n(p_{Si})] \Phi_{(n \times n)} \omega_{(n \times n)}^2 \right. \\ \left. - [1, \psi_1(p_{Si}), \dots, \psi_n(p_{Si})] \Phi_{(n \times n)} \hat{C}_{(n \times n)} \right\} z \\ + [1, \psi_1(p_{Si}), \dots, \psi_n(p_{Si})] \Phi_{(n \times n)} \hat{Q}_{(n \times n)} u.$$

Let $\beta_{Si} = [1, \psi_1(p_{Si}), \dots, \psi_n(p_{Si})]$ and one can attribute to the sub-matrices the parametric change matrices

$$(\Delta A z(t) + \Delta B u) = \\ \begin{pmatrix} 0_{(n \times n)} \\ I_{(n \times n)} \end{pmatrix} \left[(-\Delta \omega^2 - \Delta \hat{C}) z(t) + \Delta \hat{Q} u(t) \right], \\ (\Delta C_{Si} z(t) + \Delta D_{Si} u) = \\ \beta_{Si} \Phi \left[(-\Delta \omega^2 - \Delta \hat{C}) z(t) + \Delta \hat{Q} u(t) \right], \\ \delta_z(t) = \left[\chi_1 \begin{pmatrix} 0_{(n \times n)} \\ I_{(n \times n)} \end{pmatrix} + \chi_2 \beta_{s1} \Phi + \chi_3 \beta_{s2} \Phi \right] \\ \times \left[(-\Delta \omega^2 - \Delta \hat{C}) z(t) + \Delta \hat{Q} u \right],$$

which will be coalesced to give

$$\delta_z(t) = \Lambda_{(2n \times n)} \gamma(t),$$

where it can be seen that Λ consists of known model parameters and γ is an unknown metric of parameter errors that can't be solved from this equation. However, using the pseudo inverse we can produce a least squares metric $\gamma_m(t)$ which evaluates the relative accuracy of two observers based on different models

$$(\Lambda^T \Lambda)^{-1} \Lambda^T \delta_z^*(t) = \gamma_m(t).$$

The smaller the norm of $\gamma_m(t)$, the more accurate the observer based on a given model is expected to be.

While various methods of using $\gamma_m(t)$ can be contrived, *Post* [11.96] utilized a switching approach he referred to as the multiple model switching adaptive estimator (MMSAE), visualized in Fig. 11.20. The weighting value w_i is based on $\gamma_{mi}(t)$ for the observer

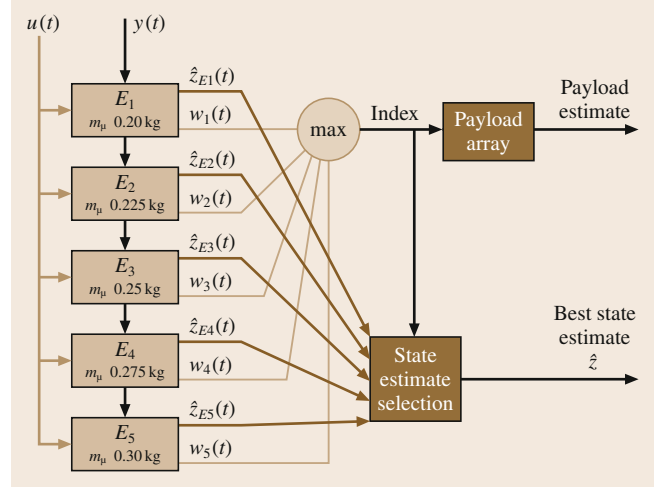


Fig. 11.20 Flow chart for the multiple model switching adaptive estimator (MMSAE)

based on a given model, then the estimate \hat{z}_i from that observer was used. Figure 11.21 shows schematically the flow inside the estimator blocks E_1 through E_5 . The parameter varied in Post's experiments was arm payload. Multiple parameters could be varied but would lead to a higher dimensional formulation and poten-

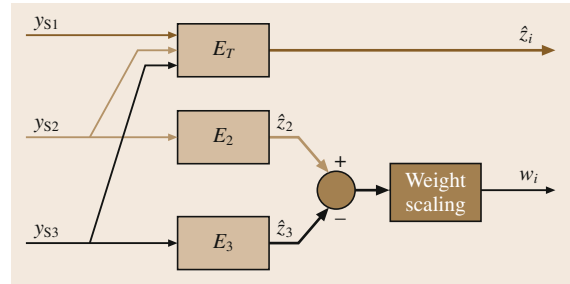


Fig. 11.21 Estimation module with weight scaling

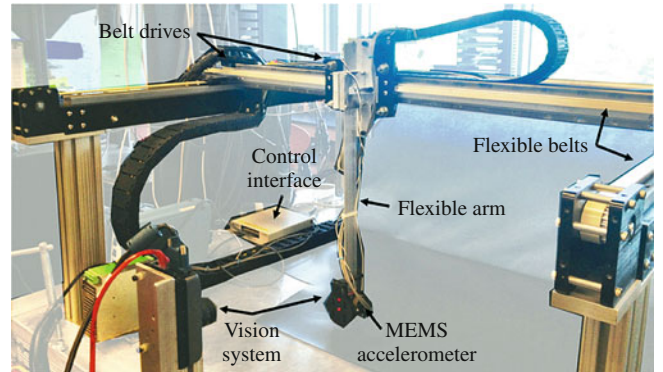


Fig. 11.22 Gantry robot used in MMSAE experiments (after *Post* [11.96])

tially many estimators numbering $N_T = N_1 N_2 \cdots N_p$ for the variation of p parameters, each with N_i values represented.

Post [11.96] conducted experiments with a linear model of the gantry robot as illustrated in Fig. 11.22 and schematically modeled in Fig. 11.23, with the parameters given in Table 11.1 and sensor placements at 0.015, 0.25, and 0.42 m from the actuated end of the beam. He compared:

- Conventional PID (VIDEO 780).
- Fixed gain linear-quadratic regulator (LQR) plus Luenberger state space designs (VIDEO 781).
- MMSAE design observers and LQR controls. Five potential payloads were chosen with spacing in even increments between 0.2 and 0.3 kg, i.e., an end-point mass between 0.35 and 0.55.

The penalty matrices were kept the same for the LQR controls but the resulting gains changed based on the model employed by the MMSAE selection. While various measures of performance could be demonstrated involving somewhat arbitrary selection of con-

troller types, controller gains and metrics, the following characteristics are considered most critical:

- Stability with various payloads.
- Cycle completion time, with requirements for settling of vibration amplitude at prescribed stops.
- Variation of cycle times with changing payloads.

Since reasonable work cycles often pick up and drop off payloads, the test included these operations. Cycle times are graphed in Fig. 11.24. The light bars show the cycle times for the complete cycle with segments of the task carrying the payload and others with the gripper empty. The dark bars show operation with no payload carried and only the gripper mass present for the entire cycle. In addition to the pair of bars labeled PID and MMSAE (with obvious meanings) are pairs labeled SS 0.25 through SS 0.40. These latter labels refer to the *designed-for* tip mass (payload plus gripper). The most obvious message from this figure is that the state space control is a vast improvement over PID, reducing cycle time by about 90%. What is not obvious from this figure is that some means of gain change is needed to accommodate the payload variations. With a designed-for tip mass of 0.45 kg and above, the operation without payload was unstable. This is still below the actual tip mass of 0.5 kg. Hence MMSAE was essential for a successful completion of the task with these design criteria (i.e., LQR penalty matrices and resulting gains). The exact tip mass does not need to be known, only the range of masses. The near identical cycle times with and without the additional payload seen on the chart for MMSAE is also a practical advantage.

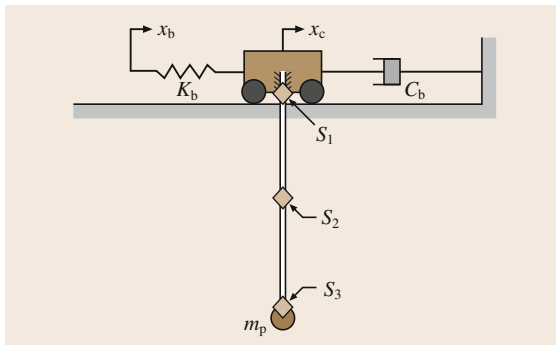


Fig. 11.23 Schematic of gantry robot model

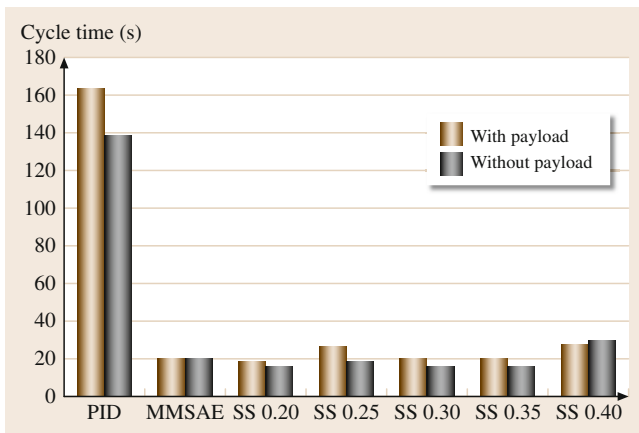


Fig. 11.24 Cycle times with implemented control methods

11.2.4 Further Reading

The topic of flexible link robot control is widely covered with papers on modeling and control. The reader wishing to probe further may want to begin with a paper giving some perspective on the nature of the problem. This was the goal of Book in [11.100]. Progress to date in this field from the theoretical perspective is signifi-

Table 11.1 Parameters of the gantry robot model











Parameter	Value	Unit
Payload (m_t)	0.281	kg
Cart mass (m_c)	10	kg
Arm length (L)	0.42	m
Elastic modulus (E)	7×10^{-10}	N/m
Density (ρ)	2700	kg/m ³
Area moment (I)	1.0114×10^{-10}	m ⁴
Belt stiffness (K_b)	2.1814×10^5	N/m
Cart damper (C_d)	100	N s/m
Structural damping coefficient (γ)	0.0005	N s/m

cant and has been collected by *Canudas de Witt* et al. in [11.101]; this reference includes a wide range of research approaches, but the examples of the practical application of this theory are more limited. The German Aerospace Center has produced lightweight space arms [11.102] and deployed them in space. The startup CAMotion, Inc. [11.103] has produced large lightweight industrial robots using the command-shaping approach to improve cycle time. High-speed arms such as the FlexPicker [11.104] achieve a light weight and avoid flexibility because of their parallel structure, but suffer the usual disadvantages of parallel actuation: restricted workspace considering the space occupied by the robot structure.

Trautt and *Bayo*'s early exploration of non-minimum-phase inverses is described in [11.105]. This is a particularly interesting variation of the work by

Kwon [11.83, 84] in that it uses the frequency domain and deals with nonzero initial conditions. The concept of using two time scales, a fast time scale for the flexible dynamics and a slow time scale for the rigid dynamics, can be found in *Siciliano* and *Book* [11.106]. The singular perturbation approach was used earlier by *Spong* for elastic joint arms. *Ghorbel* and *Spong* also consider flexible links and contact with a rigid environment in [11.107]. Achieving robustness is a problem, particularly with end-point sensors. Sliding mode control [11.108] and passivity-based control [11.109] address this problem in effective but widely varying ways. While these seem to be the more promising methods of control, one will find many more approaches to this challenging control problem. H_∞ , adaptive, fuzzy, and other controllers have all been applied with varying degrees of success.

Video-References

-  VIDEO 133 Cartesian impedance control with damping off available from <http://handbookofrobotics.org/view-chapter/11/videodetails/133>
-  VIDEO 134 Cartesian impedance control with damping on available from <http://handbookofrobotics.org/view-chapter/11/videodetails/134>
-  VIDEO 135 Control laws for a single-link arm with an elastic joint available from <http://handbookofrobotics.org/view-chapter/11/videodetails/135>
-  VIDEO 136 Feedforward/feedback law for path tracking with a KUKA KR15/2 robot available from <http://handbookofrobotics.org/view-chapter/11/videodetails/136>
-  VIDEO 770 Trajectory generation and control for a KUKA IR 161/60 robot available from <http://handbookofrobotics.org/view-chapter/11/videodetails/770>
-  VIDEO 777 Input shaping on a lightweight gantry robot available from <http://handbookofrobotics.org/view-chapter/11/videodetails/777>
-  VIDEO 778 Inverse dynamics control for a flexible link available from <http://handbookofrobotics.org/view-chapter/11/videodetails/778>
-  VIDEO 779 Rest-to-rest motion for a flexible link available from <http://handbookofrobotics.org/view-chapter/11/videodetails/779>
-  VIDEO 780 PID response to impulse in presence of link flexibility available from <http://handbookofrobotics.org/view-chapter/11/videodetails/780>
-  VIDEO 781 State feedback response to impulse in presence of link flexibility available from <http://handbookofrobotics.org/view-chapter/11/videodetails/781>

References

- | | |
|--|---|
| <p>11.1 L.M. Sweet, M.C. Good: Redefinition of the robot motion control problem, <i>IEEE Control Syst. Mag.</i> 5(3), 18–24 (1985)</p> <p>11.2 M.C. Good, L.M. Sweet, K.L. Strobel: Dynamic models for control system design of integrated robot and drive systems, <i>ASME J. Dyn. Syst. Meas. Control</i> 107, 53–59 (1985)</p> <p>11.3 E. Rivin: <i>Mechanical Design of Robots</i> (McGraw-Hill, New York 1988)</p> <p>11.4 S. Nicosia, F. Nicolò, D. Lentini: Dynamical control of industrial robots with elastic and dissipative joints, 8th IFAC World Congr., Kyoto (1981) pp. 1933–1939</p> | <p>11.5 P. Tomei: An observer for flexible joint robots, <i>IEEE Trans. Autom. Control</i> 35(6), 739–743 (1990)</p> <p>11.6 R. Höppler, M. Thümmel: Symbolic computation of the inverse dynamics of elastic joint robots, <i>IEEE Int. Conf. Robotics Autom. (ICRA)</i>, New Orleans (2004) pp. 4314–4319</p> <p>11.7 M.W. Spong: Modeling and control of elastic joint robots, <i>ASME J. Dyn. Syst. Meas. Control</i> 109, 310–319 (1987)</p> <p>11.8 S.H. Murphy, J.T. Wen, G.N. Saridis: Simulation and analysis of flexibly jointed manipulators, 29th IEEE Conf. Decis. Control, Honolulu (1990) pp. 545–550</p> |
|--|---|

- 11.9 R. Marino, S. Nicosia: *On the Feedback Control of Industrial Robots with Elastic Joints: A Singular Perturbation Approach* (Dipartimento di Ingegneria Elettronica, Univ. Rome Tor Vergata, Rome 1984), Rep. R-84.01
- 11.10 G. Cesaro, F. Nicolò, S. Nicosia: DYMR: A code for generating dynamic model of robots, IEEE Int. Conf. Robotics Autom. (ICRA), Atlanta (1984) pp. 115–120
- 11.11 A. De Luca: Feedforward/feedback laws for the control of flexible robots, IEEE Int. Conf. Robotics Autom. (ICRA), San Francisco (2000) pp. 233–240
- 11.12 G. Buondonno, A. De Luca: A recursive Newton–Euler algorithm for robots with elastic joints and its application to control, IEEE/RSJ Int. Conf. Intell. Robots Syst., Hamburg (2015) pp. 5526–5532
- 11.13 H.B. Kuntze, A.H.K. Jacobasch: Control algorithms for stiffening an elastic industrial robot, IEEE J. Robotics Autom. **1**(2), 71–78 (1985)
- 11.14 S.H. Lin, S. Tosunoglu, D. Tesar: Control of a six-degree-of-freedom flexible industrial manipulator, IEEE Control Syst. Mag. **11**(2), 24–30 (1991)
- 11.15 P. Tomei: A simple PD controller for robots with elastic joints, IEEE Trans. Autom. Control **36**(10), 1208–1213 (1991)
- 11.16 A. De Luca, B. Siciliano: Regulation of flexible arms under gravity, IEEE Trans. Robotics Autom. **9**(4), 463–467 (1993)
- 11.17 A. De Luca, B. Siciliano, L. Zollo: PD control with on-line gravity compensation for robots with elastic joints: Theory and experiments, Automatica **41**(10), 1809–1819 (2005)
- 11.18 C. Ott, A. Albu-Schäffer, A. Kugi, S. Stramigioli, G. Hirzinger: A passivity based Cartesian impedance controller for flexible joint robots – Part I: Torque feedback and gravity compensation, IEEE Int. Conf. Robotics Autom. (ICRA), New Orleans (2004) pp. 2659–2665
- 11.19 L. Zollo, B. Siciliano, A. De Luca, E. Guglielmelli, P. Dario: Compliance control for an anthropomorphic robot with elastic joints: Theory and experiments, ASME J. Dyn. Syst. Meas. Control **127**(3), 321–328 (2005)
- 11.20 A. Albu-Schäffer, C. Ott, G. Hirzinger: A passivity based Cartesian impedance controller for flexible joint robots – Part II: Full state feedback, impedance design and experiments, IEEE Int. Conf. Robotics Autom. (ICRA), New Orleans (2004) pp. 2666–2672
- 11.21 C. Ott, A. Albu-Schäffer, A. Kugi, G. Hirzinger: On the passivity-based impedance control of flexible joint robots, IEEE Trans. Robotics **24**(2), 416–429 (2008)
- 11.22 A. De Luca, F. Flacco: A PD-type regulator with exact gravity cancellation for robots with flexible joints, IEEE Int. Conf. Robotics Autom. (ICRA), Shanghai (2011) pp. 317–323
- 11.23 R. Kelly, V. Santibanez: Global regulation of elastic joint robots based on energy shaping, IEEE Trans. Autom. Control **43**(10), 1451–1456 (1998)
- 11.24 J. Alvarez-Ramirez, I. Cervantes: PID regulation of robot manipulators with elastic joints, Asian J. Control **5**(1), 32–38 (2003)
- 11.25 A. De Luca, S. Panzieri: Learning gravity compensation in robots: Rigid arms, elastic joints, flexible links, Int. J. Adapt. Control Signal Process. **7**(5), 417–433 (1993)
- 11.26 A. Albu-Schäffer, G. Hirzinger: A globally stable state feedback controller for flexible joint robots, Adv. Robotics **15**(8), 799–814 (2001)
- 11.27 L.E. Pfeffer, O. Khatib, J. Hake: Joint torque sensory feedback in the control of a PUMA manipulator, IEEE Trans. Robotics Autom. **5**(4), 418–425 (1989)
- 11.28 M. Hashimoto, Y. Kiyosawa, R.P. Paul: A torque sensing technique for robots with harmonic drives, IEEE Trans. Robotics Autom. **9**(1), 108–116 (1993)
- 11.29 T. Lin, A.A. Goldenberg: Robust adaptive control of flexible joint robots with joint torque feedback, IEEE Int. Conf. Robotics Autom. (ICRA), Nagoya (1995) pp. 1229–1234
- 11.30 M.G. Forrest-Barlach, S.M. Babcock: Inverse dynamics position control of a compliant manipulator, IEEE J. Robotics Autom. **3**(1), 75–83 (1987)
- 11.31 K.P. Jankowski, H. Van Brussel: An approach to discrete inverse dynamics control of flexible-joint robots, IEEE Trans. Robotics Autom. **8**(5), 651–658 (1992)
- 11.32 W.M. Grimm: Robustness analysis of nonlinear decoupling for elastic-joint robots, IEEE Trans. Robotics Autom. **6**(3), 373–377 (1990)
- 11.33 A. De Luca, R. Farina, P. Lucibello: On the control of robots with visco-elastic joints, IEEE Int. Conf. Robotics Autom. (ICRA), Barcelona (2005) pp. 4297–4302
- 11.34 A. De Luca: Decoupling and feedback linearization of robots with mixed rigid/elastic joints, Int. J. Robust Nonlin. Control **8**(11), 965–977 (1998)
- 11.35 A. De Luca, B. Siciliano: Inversion-based nonlinear control of robot arms with flexible links, AIAA J. Guid. Control Dyn. **16**(6), 1169–1176 (1993)
- 11.36 A. De Luca: Dynamic control of robots with joint elasticity, IEEE Int. Conf. Robotics Autom. (ICRA), Philadelphia (1988) pp. 152–158
- 11.37 S. Nicosia, P. Tomei: On the feedback linearization of robots with elastic joints, 27th IEEE Conf. Decis. Control, Austin (1988) pp. 180–185
- 11.38 A. De Luca, P. Lucibello: A general algorithm for dynamic feedback linearization of robots with elastic joints, IEEE Int. Conf. Robotics Autom. (ICRA), Leuven (1998) pp. 504–510
- 11.39 J. Swevers, D. Torfs, M. Adams, J. De Schutter, H. Van Brussel: Comparison of control algorithms for flexible joint robots implemented on a KUKA IR 161/60 industrial robot, 5th Int. Conf. Adv. Robotics, Pisa (1991) pp. 120–125
- 11.40 K. Khorasani, P.V. Kokotovic: Feedback linearization of a flexible manipulator near its rigid body manifold, Syst. Control Lett. **6**, 187–192 (1985)
- 11.41 M.W. Spong, K. Khorasani, P.V. Kokotovic: An integral manifold approach to the feedback control of

- flexible joint robots, IEEE J. Robotics Autom. **3**(4), 291–300 (1987)
- 11.42 S. Nicosia, P. Tomei: Design of global tracking controllers for flexible-joint robots, J. Robot. Syst. **10**(6), 835–846 (1993)
- 11.43 B. Brogliato, R. Ortega, R. Lozano: Global tracking controllers for flexible-joint manipulators: A comparative study, Automatica **31**(7), 941–956 (1995)
- 11.44 M.W. Spong: Adaptive control of flexible joint manipulators, Syst. Control Lett. **13**(1), 15–21 (1989)
- 11.45 F. Ghorbel, J.Y. Hung, M.W. Spong: Adaptive control of flexible-joint manipulators, IEEE Control Syst. Mag. **9**(7), 9–13 (1989)
- 11.46 R. Lozano, B. Brogliato: Adaptive control of robot manipulators with flexible joints, IEEE Trans. Autom. Control **37**(2), 174–181 (1992)
- 11.47 H. Sira-Ramirez, M.W. Spong: Variable structure control of flexible joint manipulators, Int. Robotics Autom. **3**(2), 57–64 (1988)
- 11.48 A. De Luca, G. Ulivi: Iterative learning control of robots with elastic joints, IEEE Int. Conf. Robotics Autom. (ICRA), Nice (1992) pp. 1920–1926
- 11.49 O. Dahl: Path constrained motion optimization for rigid and flexible joint robots, IEEE Int. Conf. Robotics Autom. (ICRA), Atlanta (1993) pp. 223–229
- 11.50 A. De Luca, L. Farina: Dynamic scaling of trajectories for robots with elastic joints, IEEE Int. Conf. Robotics Autom. (ICRA), Washington (2002) pp. 2436–2442
- 11.51 S. Haddadin, M. Özparpucu, A. Albu-Schäffer: Optimal control for maximizing potential energy in a variable stiffness joint, IEEE 51st Conf. Decis. Control, Maui (2012) pp. 1199–1206
- 11.52 M. Özparpucu, S. Haddadin: Optimal control of elastic joints with variable damping, 13th European Control Conf., Strasbourg (2014) pp. 2526–2533
- 11.53 S. Nicosia, P. Tomei, A. Tornambè: A nonlinear observer for elastic robots, IEEE J. Robotics Autom. **4**(1), 45–52 (1988)
- 11.54 S. Nicosia, P. Tomei: A method for the state estimation of elastic joint robots by global position measurements, Int. J. Adapt. Control Signal Process. **4**(6), 475–486 (1990)
- 11.55 A. De Luca, D. Schröder, M. Thümmel: An acceleration-based state observer for robot manipulators with elastic joints, IEEE Int. Conf. Robotics Autom. (ICRA), Rome (2007) pp. 3817–3823
- 11.56 M.W. Spong: On the force control problem for flexible joint manipulators, IEEE Trans. Autom. Control **34**(1), 107–111 (1989)
- 11.57 J.K. Mills: Stability and control of elastic-joint robotic manipulators during constrained-motion tasks, IEEE Trans. Robotics Autom. **8**(1), 119–126 (1992)
- 11.58 K.P. Jankowski, H.A. El Maraghy: Dynamic decoupling for hybrid control of rigid-/flexible-joint robots interacting with the environment, IEEE Trans. Robotics Autom. **8**(5), 519–534 (1992)
- 11.59 T. Lin, A.A. Goldenberg: A unified approach to motion and force control of flexible joint robots, IEEE Int. Conf. Robotics Autom. (ICRA), Minneapolis (1996) pp. 1115–1120
- 11.60 A. Albu-Schäffer, C. Ott, G. Hirzinger: A unified passivity-based control framework for position, torque and impedance control of flexible joint robots, Int. J. Robotics Res. **26**(1), 23–39 (2007)
- 11.61 W. Book, O. Maizza-Neto, D.E. Whitney: Feed-back control of two beam, two joint systems with distributed flexibility, ASME J. Dyn. Syst. Meas. Control **97**(4), 424–431 (1975)
- 11.62 W. Book: Characterization of strength and stiffness constraints on manipulator control. In: *Theory and Practice of Robots and Manipulators*, ed. by W. Book (Elsevier, Amsterdam 1977) pp. 37–45
- 11.63 T.E. Alberts, W. Book, S. Dickerson: Experiments in augmenting active control of a flexible structure with passive damping, AIAA 24th Aerosp. Sci. Meet., Reno (1986)
- 11.64 T. Bailey, J.E. Hubbard Jr.: Distributed piezoelectric-polymer active vibration control of a cantilever beam, J. Guid. Control Dyn. **8**(5), 605–611 (1985)
- 11.65 W. Book, V. Sangveraphunsiri, S. Le: The Bracing Strategy for Robot Operation, Jt. IFToMM-CISM Symp. Theory Robots Manip. (RoManSy), Udine (1984)
- 11.66 W. Book: Analysis of massless elastic chains with servo controlled joints, ASME J. Dyn. Syst. Meas. Control **101**(3), 187–192 (1979)
- 11.67 E.C. Pestel, F.A. Leckie: *Matrix Methods in Elastomechanics* (McGraw-Hill, New York 1963)
- 11.68 R. Krauss: Transfer Matrix Modeling, Ph.D. Thesis (School of Mechanical Engineering, Georgia Institute of Technology, Atlanta 2006)
- 11.69 W.J. Book: Modeling, Design and Control of Flexible Manipulator Arms, Ph.D. Thesis (Department of Mechanical Engineering, Massachusetts Institute of Technology, Cambridge 1974)
- 11.70 W. Book: Recursive lagrangian dynamics of flexible manipulators, Int. J. Robotics Res. **3**(3), 87–106 (1984)
- 11.71 W.J. Book, S.H. Lee: Vibration control of a large flexible manipulator by a small robotic arm, Proc. Am. Control Conf., Pittsburgh (1989) pp. 1377–1380
- 11.72 J. Lew, S.-M. Moon: A simple active damping control for compliant base manipulators, IEEE/ASME Trans. Mechatron. **2**, 707–714 (1995)
- 11.73 W.J. Book, J.C. Loper: Inverse dynamics for commanding micromanipulator inertial forces to damp macromanipulator vibration, IEEE, Robot Soc. Int. Conf. Intell. Robots Syst., Kyongju (1999)
- 11.74 I. Sharf: Active damping of a large flexible manipulator with a short-reach robot, Proc. Am. Control Conf., Seattle (1995) pp. 3329–3333
- 11.75 L. George, W.J. Book: Inertial vibration damping control of a flexible base manipulator, IEEE/ASME Trans. Mechatron. **8**(2), 268–271 (2003)
- 11.76 J.F. Calvert, D.J. Gimpel: Method and apparatus for control of system output in response to system input, U.S. Patent 280 1351 (1957)
- 11.77 O.J.M. Smith: *Feedback Control Systems* (McGraw-Hill, New York 1958)

- 11.78 N. Singer, W.P. Seering: Preshaping command inputs to reduce system vibration, *ASME J. Dyn. Syst. Meas. Control* **112**(1), 76–82 (1990)
- 11.79 W. Singhose, W. Seering, N. Singer: Residual vibration reduction using vector diagrams to generate shaped inputs, *J. Mech. Des.* **2**, 654–659 (1994)
- 11.80 D.P. Magee, W.J. Book: The Application of Input Shaping to a System with Varying Parameters, *Proc. 1992 Japan–USA Symp. Flex. Autom.*, San Francisco (1992) pp. 519–526
- 11.81 D.P. Magee, W.J. Book: Optimal arbitrary time-delay (OAT) filter and method to minimize unwanted system dynamics, U.S. Patent 6078844 (2000)
- 11.82 S. Rhim, W.J. Book: Noise effect on time-domain adaptive command shaping methods for flexible manipulator control, *IEEE Trans. Control Syst. Technol.* **9**(1), 84–92 (2001)
- 11.83 D.-S. Kwon, W.J. Book: A time-domain inverse dynamic tracking control of a single-link flexible manipulator, *J. Dyn. Syst. Meas. Control* **116**, 193–200 (1994)
- 11.84 D.S. Kwon: An Inverse Dynamic Tracking Control for a Bracing Flexible Manipulator, Ph.D. Thesis (School of Mechanical Engineering, Georgia Institute of Technology, Atlanta 1991)
- 11.85 A. De Luca, G. Di Giovanni: Rest-to-rest motion of a one-link flexible arm, *Proc. IEEE/ASME Int. Conf. Adv. Intell. Mechatron.*, Como (2001) pp. 923–928
- 11.86 A. De Luca, G. Di Giovanni: Rest-to-rest motion of a two-link robot with a flexible forearm, *Proc. IEEE/ASME Int. Conf. Adv. Intell. Mechatron.*, Como (2001) pp. 929–935
- 11.87 A. De Luca, V. Caiano, D. Del Vecovo: Experiments on rest-to-rest motion of a flexible arm. In: *Experimental Robotics VIII*, Springer Tracts in Advanced Robotics, Vol. 5, ed. by B. Siciliano, P. Dario (Springer, Berlin, Heidelberg 2003) pp. 338–349
- 11.88 R.M. Murray, M. Rathinam, W. Sluis: Differential flatness of mechanical control systems: A catalog of prototype systems, *Proc. ASME Int. Mech. Engr. Congr.*, San Francisco (1995)
- 11.89 M. Fliess, P. Martin, P. Rouchon: Flatness and defect of nonlinear systems: Introductory theory and examples, *Int. J. Control* **61**(6), 1327–1361 (1995)
- 11.90 R.H. Cannon, E. Schmitz: Initial experiments on the end-point control of a flexible one-link robot, *Int. J. Robotics Res.* **3**(3), 62–75 (1984)
- 11.91 A. Truckenbrot: Modeling and control of flexible manipulator structures, *Proc. 4th CISM–IFTOMM Symp. Theory Robots Manip. (RoManSy)*, Zaborow (1981) pp. 90–101
- 11.92 G.G. Hastings, W.J. Book: Reconstruction and robust reduced-order observation of flexible variables, *ASME Winter Ann. Meet.*, Anaheim (1986)
- 11.93 B.S. Yuan, J.D. Huggins, W.J. Book: Small motion experiments with a large flexible arm with strain feedback, *Proceedings of the 1989 Am. Control Conf.*, Pittsburgh (1989) pp. 2091–2095
- 11.94 D. Wang, M. Vidyasagar: Passive control of a stiff flexible link, *Int. J. Robotics Res.* **11**, 572–578 (1992)
- 11.95 K. Obergfell, W.J. Book: Control of flexible manipulators using vision and modal feedback, *Proc. Int. Conf. Risk Assess. Manag. (ICRAM)*, Istanbul (1995)
- 11.96 B. Post: Robust State Estimation for the Control of Flexible Robotic Manipulators, Ph.D. Thesis (School of Mechanical Engineering, Georgia Institute of Technology, Atlanta 2013)
- 11.97 B. Walcott, S. Zak: State observation of nonlinear uncertain dynamical system, *IEEE Trans. Autom. Control* **32**, 166–170 (1987)
- 11.98 B. Walcott, S. Zak: Observation of dynamical systems in the presence of bounded nonlinearities/uncertainties, *Proc. IEEE Conf. Dec. Control* **25**, 961–966 (1986)
- 11.99 N.G. Chalhoub, G.A. Kfoury: Development of a robust nonlinear observer for a single-link, flexible manipulator, *Nonlin. Dyn.* **39**(3), 217–233 (2005)
- 11.100 W.J. Book: Controlled motion in an elastic world, *ASME J. Dyn. Syst. Meas. Control* **2B**, 252–261 (1993)
- 11.101 C. Canudas-de-Wit, B. Siciliano, G. Bastin (Eds.): *Theory of Robot Control* (Springer, Berlin, Heidelberg 1996)
- 11.102 G. Hirzinger, N. Sporer, J. Butterfass, M. Grebenstein: Torque-controlled lightweight arms and articulated hands: Do we reach technological limits now?, *Int. J. Robotics Res.* **23**(4/5), 331–340 (2004)
- 11.103 Camotion Inc.: <http://www.camotion.com> (Camotion Inc., Atlanta 2007)
- 11.104 B. Rooks: High speed delivery and low cost from new ABB packaging robot, *Ind. Robotics Int. J.* **26**(4), 267–275 (1999)
- 11.105 T. Trautt, E. Bayo: Inverse dynamics of non-minimum phase systems with non-zero initial conditions, *Dyn. Control* **7**(1), 49–71 (1997)
- 11.106 B. Siciliano, W. Book: A singular perturbation approach to control of lightweight flexible manipulators, *Int. J. Robotics Res.* **7**(4), 79–90 (1988)
- 11.107 F. Ghorbel, M.W. Spong: Singular perturbation model of robots with elastic joints and elastic links constrained by a rigid environment, *J. Intell. Robotics Syst.* **22**(2), 143–152 (1998)
- 11.108 J. Guldner, J. Shi, V. Utkin: *Sliding Mode Control in Electromechanical Systems* (Taylor, London 1999)
- 11.109 J.-H. Ryu, D.-S. Kwon, B. Hannaford: Control of a flexible manipulator with noncollocated feedback: Time-domain passivity approach, *IEEE Trans. Robotics* **20**(4), 776–780 (2004)